

PLUME RISE AND DISPERSION--
EFFECTS OF EXIT VELOCITY
AND ATMOSPHERIC STABILITY

by

R. L. Petersen,* J. E. Cermak**
and R. N. Meroney***

Prepared under Contract to
North American Weather Consultants

Fluid Dynamics and Diffusion Laboratory
Department of Civil Engineering
Colorado State University
Fort Collins, Colorado

June 1977

*Graduate Research Assistant

**Professor-in-charge and Director, Fluid Dynamics and
Diffusion Laboratory

***Professor

CER76-77RLP-JEC-RNM59

TA7.C6

CFR 76/77-59
APR 1977

ABSTRACT

Plume rise and dispersion was studied under stable and neutral stratification in an environmentally controlled wind tunnel. A 1:300 model of a power plant stack was constructed and positioned in the wind tunnel to assess the effect of exit velocity and temperature on plume rise and dispersion. The complete test scenario for each stability included five exit velocities (from 12.5 to 250 m/s), three exit temperatures (200, 366 and 422°K) and three stratifications (D, E and F). The exit velocity was varied by adding nozzles of different diameter to the stack top while maintaining a constant volume flow. Exit temperature variations were simulated by mixing equivalent density mixtures of helium and air.

For each test case plume dispersion was assessed by traversing the plume at incremental altitudes and three downwind locations. Concentrations of the helium tracer gas were measured continuously with a Thermal Conductivity Gas Chromatograph. Plume rise was assessed using photographic techniques and by analyzing the concentration data.

The results show the expected tendency for increased plume rise with increased exit velocity. More significant is the decrease in maximum centerline concentration at a given downwind distance when exit velocity increases. Curves comparing the standard plume dispersion model with the wind tunnel results are presented. Also present are the plume centerline trajectories for each case studied.

ACKNOWLEDGEMENTS

Mr. James A. Garrison supervised the photographic recording of the flow visualization. Mr. James Maxton supervised the concentration measurements. Processing of the photographic data was coordinated by Mr. Samir Ayad. The authors also acknowledge the assistance of the following students: Messrs. John Elmer, Thatcher Harvey, and Mike Allen. The report was typed by Mrs. Susan Kuehl.

TABLE OF CONTENTS

	<u>Page</u>
Abstract	ii
Acknowledgements	iii
Table of Contents	iv
List of Tables	v
List of Figures	vi
List of Symbols	ix
1.0 INTRODUCTION	1
2.0 SIMULATION OF ATMOSPHERIC MOTION	3
3.0 EXPERIMENTAL PROGRAM	9
3.1 Wind Tunnel	9
3.2 Model	9
3.3 Flow Visualization Techniques	10
3.4 Gas Tracer Techniques	11
3.5 Velocity and Temperature Measurements	15
4.0 RESULTS	16
4.1 Plume Rise	16
4.2 Concentration Measurements	18
5.0 SUMMARY	21
References	22
Tables	24
Figures	38

LIST OF TABLES

Table		Page
3.2-1	General Model and Prototype Parameters	24
3.2-2	Model and Prototype Parameters for the Pasquill D Wind Tunnel Tests	25
3.2-3	Model and Prototype Parameters for the Pasquill E Wind Tunnel Tests	27
3.2-4	Model and Prototype Parameters for the Pasquill F Wind Tunnel Tests	28
4.2-1	Summary of Concentration Measurement Results for the Pasquill D Wind Tunnel Tests	29
4.2-2	Summary of Concentration Measurement Results for the Pasquill E Wind Tunnel Tests	32
4.2-3	Summary of Concentration Measurement Results for the Pasquill F Wind Tunnel Tests	35

LIST OF FIGURES

Figure		Page
3.1-1	The Meteorological Wind Tunnel	38
3.2-2	Photograph of Model Stack with the Five Nozzel Attachments	39
3.3-1	Schematic of Plume Visualization System	40
3.3-2	Plan and Top View of Camera Set-up for Photographing the Wind Tunnel Plumes	41
3.4-1	Schematic of Gas Sampling System	42
3.4-2	Gas Chromotograph Calibration Curve	43
3.5-1	Schematic of Velocity and Temperature Measurement System	44
3.5-2	Velocity Profiles for Neutral Conditions	45
3.5-3	Velocity Profiles for E-stability	46
3.5-4	Velocity Profiles for F-stability	47
3.5-5	Temperature Profiles for Stable Conditions	48
4.1-1	Plume Visualization for Neutral Stability, A Stack Height Wind Speed of 2 m/s, a 388°K Exit Temperature and Exit Velocities of a) 12.5 m/s, b) 30 m/s, c) 60 m/s, d) 120 m/s and e) 240 m/s	49
4.1-2	Plume Visualization for Neutral Stability, A Stack Height Wind Speed of 4 m/s, a 388°K Exit Temperature, and Exit Velocities of a) 12.5 m/s, b) 30 m/s, c) 60 m/s, d) 120 m/s and e) 240 m/s	50
4.1-3	Plume Visualization for Neutral Stability, A Stack Height Wind Speed of 8 m/s, a 388°K Exit Temperature, and Exit Velocities of a) 12.5 m/s, b) 30 m/s, c) 60 m/s, d) 120 m/s and e) 240 m/s	51
4.1-4	Plume Visualization for Neutral Stability, A Stack Height Wind Speed of 16 m/s, a 388°K Exit Temperature, and Exit Velocities of a) 12.5 m/s, b) 30 m/s, c) 60 m/s, d) 120 m/s and e) 240 m/s	52
4.1-5	Plume Centerline Trajectories for D-stability, A 388°K Exit Temperature, Various Exit Velocities and a Stack Height Wind Speed of a) 2 m/s, b) 4 m/s, c) 8 m/s and d) 16 m/s	53

Figure		Page
4.1-6	Plume Centerline Trajectories for D-stability, A 30 m/s Exit Velocity, Three Exit Temperatures and a Stack Height Wind Speed of a) 2 m/s and b) 8 m/s	57
4.1-7	Plume Centerline Trajectories for D-stability, A 60 m/s Exit Velocity, Three Exit Temperatures and a Stack Height Wind Speed of a) 2 m/s and b) 8 m/s	59
4.1-8	Plume Visualization for E-stability, A Stack Height Wind Speed of 5.9 m/s, a 366°K Exit Temperature and Exit Velocities of a) 12.5 m/s, b) 30 m/s, c) 60 m/s, d) 120 m/s and e) 240 m/s	61
4.1-9	Plume Visualization for E-stability, A Stack Height Wind Speed of 5.9 m/s, a 388°K Exit Temperature and Exit Velocities of a) 12.5 m/s, b) 30 m/s, c) 60 m/s, d) 120 m/s and e) 240 m/s	62
4.1-10	Plume Visualization for E-stability, A Stack Height Wind Speed of 5.9 m/s, a 422°K Exit Temperature and Exit Velocities of a) 12.5 m/s, b) 30 m/s, c) 60 m/s, d) 120 m/s and e) 240 m/s	63
4.1-11	Plume Centerline Trajectories for E-stability, A Stack Height Wind Speed of 5.9 m/s, Various Exit Velocities and an Exit Temperature of a) 366°K, b) 388°K and c) 422°K	64
4.1-12	Plume Centerline Trajectories for E-stability, A Stack Height Wind Speed of 5.9 m/s, Three Exit Temperatures and an Exit Velocity of a) 30 m/s and b) 60 m/s	67
4.1-13	Plume Visualization for F-stability, A Stack Height Wind Speed of 3.0 m/s, a 366°K Exit Temperature and Exit Velocities of a) 12.5 m/s, b) 30 m/s, c) 60 m/s, d) 120 m/s and e) 240 m/s	69
4.1-14	Plume Visualization for F-stability, A Stack Height Wind Speed of 3.0 m/s, a 388°K Exit Temperature and Exit Velocities of a) 12.5 m/s, b) 30 m/s, c) 60 m/s, d) 120 m/s and e) 240 m/s	70
4.1-15	Plume Visualization for F-stability, A Stack Height Wind Speed of 3.0 m/s, a 422°K Exit Temperature and Exit Velocities of a) 12.5 m/s, b) 30 m/s, c) 60 m/s, d) 120 m/s and e) 240 m/s	71
4.1-16	Plume Centerline Trajectories for F-stability, A Stack Height Wind Speed of 3.0 m/s, Various Exit Velocities and an Exit Temperature of a) 366°K, b) 388°K and c) 422°K	72

Figure		Page
4.1-17	Plume Centerline Trajectories for F-stability, A Stack Height Wind Speed of 3.0 m/s, Three Exit Temperatures and an Exit Velocity of a) 30 m/s and b) 60 m/s	75
4.2-1	Plume Dilution ($\chi u/Q$) versus Downwind Distance for D-stability, a 388°K Exit Temperature, Various Exit Speeds and a Stack Top Wind Speed of a) 4 m/s, b) 8 m/s and c) 16 m/s	77
4.2-2	Plume Dilution ($\chi u/Q$) versus Trajectory Distance for D-stability, a 388°K Exit Temperature, Various Exit Speeds and a Stack Top Wind Speed of a) 4 m/s, b) 8 m/s and c) 16 m/s	80
4.2-3	Plume Dilution ($\chi u/Q$) versus Downwind Distance for E-stability, a Stack Top Wind Speed of 5.9 m/s, Various Exit Velocities and Exit Temperatures of a) 366°K, b) 388°K and c) 422°K	83
4.2-4	Plume Dilution ($\chi u/Q$) versus Trajectory Distance for E-stability, a Stack Top Wind Speed of 5.9 m/s, Various Exit Velocities and Exit Temperatures of a) 366°K, b) 388°K and c) 422°K	86
4.2-5	Plume Dilution ($\chi u/Q$) versus Downwind Distance for F-stability, a Stack Top Wind Speed of 3.0 m/s, Various Exit Velocities and Exit Temperatures of a) 366°K, b) 388°K and c) 422°K	89
4.2-6	Plume Dilution ($\chi u/Q$) versus Trajectory Distance for F-stability, a Stack Top Wind Speed of 3.0 m/s, Various Exit Velocities and Exit Temperatures of a) 366°K, b) 388°K and c) 422°K	92

LIST OF SYMBOLS

<u>Symbol</u>	<u>Definition</u>	
D	Stack diameter	(L)
E	Gas Chromotograph Response	(mvs)
Fr	Froude number	(-)
g	Gravitational constant	(L/T ²)
h	Stack height	(L)
L	Length scale	(L)
P	Pressure	(F/L ²)
Q	Source strength	(ppm)
R	Exhaust velocity ratio (u_s/u_a)	(-)
Re	Reynolds number	(-)
t	Time	(T)
T	Temperature	(θ)
u	Flow velocity	(L/T)
x,y,z	General coordinates--downwind, lateral, upward	(L)
z_0	Surface roughness parameter	(L)

Greek Symbols

χ	Local concentration	(ppm)
t	Time	(T)
ν	Kinematic viscosity	(L ² /T)
ρ	Density	(M/L ³)
δ	Kronecker delta	(-)
ϵ_{ijk}	Tensor permutation symbol	(-)
Ω	Angular velocity	(T ⁻¹)
ϕ	Dissipation term	

Greek SymbolsDefinition

γ	Density ration $(\frac{\rho_a - \rho_s}{\rho_s})$	(-)
Γ	Adiabatic lapse rate	(θ/L)
θ	Potential temperature	($^{\circ}K$)

Subscripts and Superscripts

*	Dimensionless quantity
a,r	Ambient reference height (stack top)
b	Bulk
i,j,k	Tensor indices
m	Model
o	General reference height
p	Prototype
s	Stack
'	Turbulence quantity

1.0 INTRODUCTION

The design or modification of a power plant stack may be optimized so as to meet ambient air quality standards (Petersen, et al., 1975). Predictions of plume rise may be made using equations such as outlined in Briggs (1969) or Hewett et al. (1970). Concentration patterns may then be estimated using the "Gaussian model" as described in Turner (1969).

The basic drawback to the plume rise models is the method employed to close the system of governing equations. Typically, the ambient air entrainment rate is set proportional to the plume centerline velocity (Chan and Kennedy, 1972; Fox, 1970; Hault, et al., 1969). Most of the theoretical investigators have assumed that the ambient flow is a steady, horizontal, laminar crosswind with no variation of temperature or wind with altitude. The atmosphere, on the other hand, is seldom laminar with no vertical variations of wind or temperature. Hence, to obtain more realistic estimates of plume rise and plume dispersion, physical modeling in the wind tunnel is an advantageous alternative. A scale model of a stack and surrounding topography or roughness positioned in a long test section wind tunnel would allow for measurements of plume rise and dispersion in a turbulent cross flow with vertically varying temperature and wind speed.

The purpose of this study is to determine the effect of stack-gas emission temperature and velocity on the trajectory and concentration patterns of the resulting plume under varying atmospheric stratifications. The intent being to provide a data base that will establish the feasibility of increasing stack gas emission speed or temperature to achieve greater plume rise and lower concentrations through enhanced dispersion.

Neutral thermal stratification and ground-level inversions were simulated in the Colorado State University (CSU) Meteorological Wind Tunnel (MWT). A 1:300 scale model of a 60.8 m stack was placed in the wind tunnel. Plume rise was assessed by photographing a visual simulation of the plume. The concentration patterns were determined by traversing the plume at various locations and measuring the concentrations of tracer gas (He) released from the stack. While the exit velocity and temperature varied during the study, the volume of gas flow remained a constant for all tests. A summary of the test scenario follows:

Test Scenario

Stability	Stack-Gas Temperature (°K)	Reference Wind Speed (m/s)	Stack-Gas Exit Speed (m/s)
D	388	2, 4, 8, 16	12.5, 30, 60 120, 240
	366, 422	2, 4, 8, 16	30, 60
E(F)	366, 388, 422	5.9 (3)	12.5, 30, 60, 120, 240

Included in this report are a complete description of similarity requirements for wind tunnel modeling, the experimental program, the results and conclusions. A complete set of color slides and motion pictures supplement this report.

2.0 SIMULATION OF ATMOSPHERIC MOTION

The basic equations governing atmospheric motion (conservation of mass, momentum and energy) may be expressed in the following dimensionless form (Cermak, 1974):

$$\frac{\partial \rho^*}{\partial t^*} + \frac{\partial (\rho^* u^*)}{\partial x^*} = 0, \quad (1)$$

$$\begin{aligned} \frac{\partial u_i^*}{\partial t^*} + u_j^* \frac{\partial u_i^*}{\partial x_j^*} + \left[\frac{L_o \Omega_o}{u_o} \right] 2\epsilon_{ijk} \Omega_j^* u_k^* = \\ - \frac{\partial P^*}{\partial x_i^*} - \left[\frac{\Delta T_o L_o g_o}{T_o u_o^2} \right] \Delta T^* g^* \delta_{i3} \\ + \left[\frac{v_o}{u_o L_o} \right] \frac{\partial^2 u_i^*}{\partial x_k^* \partial x_k^*} + \frac{\partial \overline{-u_i^* u_j^*}}{\partial x_j^*}, \end{aligned} \quad (2)$$

and

$$\begin{aligned} \frac{\partial T^*}{\partial t^*} + u_i^* \frac{\partial T^*}{\partial x_i^*} = \left[\frac{k_o}{\rho_o C_p v_o} \right] \left[\frac{v_o}{L_o u_o} \right] \frac{\partial^2 T^*}{\partial x_k^* \partial x_k^*} \\ + \frac{\partial}{\partial x_i^*} \overline{\theta^* u_i^*} + \left[\frac{v_o}{u_o L_o} \right] \left[\frac{u_o^2}{C_p (\Delta T)_o} \right] \phi^* \end{aligned}$$

The dependent and independent variables have been made dimensionless (indicated by an asterisk) by choosing appropriate reference values.

For exact similarity, the bracketted quantities and boundary conditions must be the same in the wind tunnel and for the corresponding atmospheric flow. The complete set of requirements for similarity is

1) Undistorted geometry

2) Equal Rossby number: $Ro = u_o / (L_o \Omega_o)$

3) Equal gross Richardson number: $Ri = \frac{\Delta T_o g_o L_o}{T_o u_o^2}$

- 4) Equal Reynolds number: $Re = u_o L_o / \nu_o$
- 5) Equal Prandtl number: $Pr = (\nu_o \rho_o C_{p_o}) / k_o$
- 6) Equal Eckert number: $Ec = u_o^2 / [C_{p_o} (\Delta T)_o]$
- 7) Surface-boundary conditions
- 8) Approach-flow characteristics

All of the above requirements cannot be simultaneously satisfied in the wind tunnel and atmosphere. However, some of the quantities are not important for the simulation of many flow conditions. The parameters which can be neglected and those which are important to this study will now be discussed in detail.

● Neglected Parameters

Equal Reynolds number for model and prototype is not possible for this study, since the viscosity of air is nearly the same and the length scaling is 1:300. This inequality is not a serious limitation. The Reynolds number related to the plume trajectory is defined by

$$Re_s = \frac{u_s D}{\nu_s} .$$

Weil (1968) reported that plume trajectories are independent of stack Reynolds number, provided the plume is turbulent at the stack exit. Weil suggested a lower limit for Re_s of 300 for laboratory simulation. For this study, all stack Reynolds numbers exceeded this value. Consequently, similarity of plume trajectories is assured.

Similarity of concentration fields is dependent on the bulk Reynolds number which is defined by

$$Re_h = \frac{u_a h}{\nu_a} .$$

Golden, as cited by Halitsky (1963), found that for flow about a cube there was no change in concentration patterns at the cube surface for Re_b greater than 11,000. Additionally, Golden found that in the wake region the concentration patterns were invariant for Re_b down to at least 3000. In this study concentration patterns in the wake of a building or at the building surface are not of interest. However, Golden's results suggest qualitatively that bulk Reynolds number independence does occur near $Re_b = 3000$. For this study, Re_b was greater than 3000 (except for one case).

A second factor confirming Re_b independence are the posteriori results of this study. When the plume centerline dilution ($\chi u/Q$) was plotted versus trajectory distance for different wind speeds and stabilities, the values fell along a straight line for each stability. Since the D-stability cases were taken over four different tunnel speeds (hence four bulk Reynolds numbers) and the $\chi u/Q$ values fell along the expected curve, similarity of concentration patterns is inferred.

The Rossby number, Ro , is a quantity which indicates the effect of the earth's rotation on the flow field. In the wind tunnel equal Rossby numbers between model and prototype cannot be achieved. The effect of the earth's rotation becomes significant if the distance scale is large. For this particular study, relatively small distance scales are involved (< 5000 m). Hence, neglecting the term with Ro is justified.

When equal Richardson numbers are achieved, equality of the Eckert number between model and prototype cannot be attained. This is not a serious compromise since the Eckert number is equivalent to a Mach number squared. Consequently, the Eckert number is small compared to unity for laboratory and atmospheric flows.

● Relevant Parameters

Since air is the transport medium in the wind tunnel and the atmosphere, near equality of the Prandtl number is assured.

The Froude number, Fr, is defined by

$$Fr = \frac{u_a^2}{g \gamma D}$$

where

$$\gamma = \frac{\rho_a - \rho_s}{\rho_a}$$

Although Fr does not specifically appear in the list of similarity parameters, it can be thought of as a modified Richardson number (the inverse of the Richardson number) for the stack gas. Dimensional analysis reveals that the parameter γ is also important for simulating plume motion. Thus, if Fr and γ are set equal for model and prototype, the following relation between model and prototype velocity is obtained

$$\frac{(u_a)_m}{(u_a)_p} = \left(\frac{D_m}{D_p} \right)^{1/2}$$

Since $D_m/D_p = 300$,

$$(u_a)_m = 0.058 (u_a)_p$$

To properly scale the stack exit velocity with the approaching ambient velocity, the ratio $R = u_s/u_a$ is set equal for model and prototype.

For simulating stable atmospheric conditions, equality of the Richardson number between model and prototype is required. The bulk Richardson number is defined by

$$Ri_b = \frac{\frac{g}{T} \left[\frac{\Delta T}{\Delta z} + \Gamma \right]}{\left(\frac{\Delta u}{\Delta z} \right)^2} = \frac{\frac{g}{T} \Delta \theta}{\left(\frac{\Delta u}{\Delta z} \right)^2}$$

For this study, Pasquill E and F (Turner, 1969) stratification were to be simulated using the criteria outlined in Atomic Energy Safety Guide #23. Accordingly, $\frac{\Delta\theta}{\Delta z} = 0.01^\circ\text{C/m}$ for E stability and 0.03°C/m for F stability. Hence, if $Ri_m = Ri_p$ the following relation results

$$\left(\frac{\Delta T}{\Delta z}\right)_m^1 = \left(\frac{\Delta\theta}{\Delta z}\right)_p \frac{\left(\frac{\Delta u}{\Delta z}\right)_m^2}{\left(\frac{\Delta u}{\Delta z}\right)_p^2}$$

or substituting for Δu_m

$$\left(\frac{\Delta T}{\Delta z}\right)_m = \left(\frac{\Delta\theta}{\Delta z}\right)_p \frac{\Delta z_p}{\Delta z_m} = 300 \left(\frac{\Delta\theta}{\Delta z}\right)_p$$

Finally, to simulate Pasquill E and F conditions in the wind tunnel, the respective $\Delta T/\Delta z$ values are 3 and 9°C/m .

The region of interest for plume dispersion is from 0.2 to 0.5 m (61 to 161 m - prototype) in the wind tunnel. Thus, the ΔT values are 0.99°C and 2.97°C for E and F stability, respectively.

Since no specific location was being studied, the surface of the tunnel was not roughened. The surface roughness factor, z_0 , for the wind tunnel was calculated from the velocity profiles to be 1.14×10^{-4} cm.

To summarize, the following scaling criteria were applied for the neutral and stable boundary layer simulations.

$$1) \quad Fr = \frac{u_a^2}{g \gamma D}; \quad (Fr)_m = (Fr)_p$$

$$2) \quad R = \frac{u_s}{u_a}; \quad R_m = R_p$$

$$3) \quad \gamma = \frac{\rho_a - \rho_s}{\rho_s}; \quad \gamma_m = \gamma_p$$

1) Since $\frac{\Delta T}{\Delta z}_m$ is usually on the order of 1 and Γ is .01, the term Γ can be neglected for model calculations.

$$4) \text{ Ri} = \frac{g \left(\frac{\Delta \theta}{\Delta z} \right)}{T \left(\frac{\Delta u}{\Delta z} \right)^2}; (\text{Ri})_m = (\text{Ri})_p$$

5) Similar geometric dimensions

6) Sufficiently high Re_b and Re_s to insure Reynolds number independence.

The parameters for each test considered are summarized in Tables 3.2-1, 3.2-2, 3.2-3, and 3.2-4.

3.0 EXPERIMENTAL PROGRAM

3.1 Wind Tunnel

The meteorological wind tunnel (MWT) shown in Figure 3.1-1 was used for this study. This wind tunnel, especially designed to study atmospheric flow phenomena, incorporates special features such as an adjustable ceiling, a rotating turntable, temperature controlled boundary walls, and a long test section to permit adequate reproduction of micro-meteorological behavior. Mean wind speeds of 0.06 to 39.6 m/s in the MWT can be obtained. Boundary-layer thicknesses up to 1.2 m can be developed "naturally" over the downstream 6.1 m of the MWT test section. Thermal stratification in the MWT is provided by the heating and cooling systems in the section passage and the test section floor.

A set of vortex generators was installed 0.6 m downwind of the entrance to give the simulated boundary an initial impulse of growth. From 1.8 to 6.1 m a set of 12 roll-band aluminum panels were placed on the tunnel floor. These panels were connected to the facility refrigeration system and cooled to approximately 0°C for F stability tests and 14°C for E stability tests. The free stream air was maintained at about 24°C for both tests. For neutral condition, no heating or cooling to the facility was supplied.

3.2 Model

The power plant stack was simulated by constructing a 1:300 model. To simulate various exit velocities while maintaining a constant volume flow, five nozzles were constructed for positioning on top of the model stack. A photograph of the stack and nozzles is shown in Figure 3.2-1. The stack parameters relevant to all cases studied are given in Table

3.2-1. Those parameters which changed for each test case are tabulated for D, E and F stability in Tables 3.2-2, 3.2-3 and 3.2-4, respectively.

Metered quantities of gas were allowed to flow from the model stack. Helium (the tracer) and compressed air were mixed in the appropriate proportion to simulate the densities associated with prototype exit temperatures of 366, 388 and 422°K. Fischer-Porter flow meter settings were adjusted for pressure, temperature, and molecular weight effects as necessary. When a visible plume was required, the gas was bubbled through titanium tetrachloride before emission.

3.3 Flow Visualization Techniques

Smoke was used to define plume behavior from the model stack. The smoke was produced by passing the air mixture through a container of titanium tetrachloride located outside the wind tunnel and transported through the tunnel wall by means of a tygon tube terminating at the stack inlet. A schematic of the process is shown in Figure 3.3-1.

The plume was illuminated with arc-lamp beams and a visible record was obtained by means of pictures taken with a Speed Graphic camera. Additional still pictures were obtained with a Hasselblad camera. Stills were taken with a camera speed of one second to identify mean plume boundaries. A plan and top view of the camera set-up is shown in Figure 3.3-2. A series of 16 mm color motion pictures were also taken with a Bolex motion-picture camera.

The color slides of the plume visualization were used to identify the plume centerline trajectory. To determine the centerline trajectory the color slides were projected onto a blank-gridded sheet of paper. Thereafter, the plume centerline was traced onto the paper; after which, the centerline coordinates were key-punched for subsequent analysis. Using

trigonometric relations, the photo-coordinates were corrected for optical distortion according to Halitsky (1961).

3.4 Gas Tracer Techniques

After the desired wind tunnel conditions were obtained, a mixture of helium and air of predetermined concentration was released from the model stack at the required rate to simulate prototype plume rise. The flow rate of the helium mixture was controlled by a pressure regulator at the supply cylinder outlet and monitored by a Fisher-Porter precision flow meter. A schematic of the system is shown in Figure 3.4-1.

Gas samples of the plumes were obtained by drawing the gas through a sampling train which ended at the outlet of a Carle Model 1800 thermal-conductivity gas chromatograph (TCGC). A 40 cm telescoping brass tube (0.16 cm ID) was mounted on a traversing mechanism in the wind tunnel (shown in Figure 3.4-2). PVC tubing connected the probe and the TCGC. The sampling probe was positioned at 10, 41 and 203 cm downwind of the stack. At each downwind position horizontal traverses through the plume were made at incremental heights above the tunnel floor. The horizontal traverse speed was approximately 4.7 cm/min. This traverse speed was determined by experimentation to be slow enough to prevent smoothing of the peak values.

Concentrations of the tracer gas (He) were determined by using the TCGC. The TCGC was modified so that continuous sample analysis was possible. The flow rate through the TCGC was maintained at 2.5 cc/min and the carrier gas was ambient air.

The TCGC detector is based on the principle that a hot body will lose heat at a rate which is dependent upon the composition of the

surrounding gas (McNair and Boudli, 1969). The gas concentrations are detected by measuring changes in the resistance of a heated thermistor which has a constant current flowing through it. When ambient tunnel air flows through the detector, the resistance remains essentially constant. When air mixed with various percentages of helium flows through, the heat transfer from the thermistor changes as does the resistance. If various known concentrations of helium in the air are run through the analyzer and the voltage output due to maintaining a constant resistance is recorded, a calibration of the analyzer is obtained. Figure 3.4-3 shows a calibration curve of helium in N_2 versus voltage output. Since the calibration was nearly linear, 100 percent helium was used to record changes in the calibration curve during the course of the study.

The voltage output readings from the TCGC were transformed into a helium concentration using the relation

$$\chi(\text{ppm}) = C(\text{ppm/mvs}) E(\text{mvs})$$

where C was determined from the daily calibrations with 100 percent helium.

The values of the concentration parameter initially determined apply to the model and it is desirable to express these values in terms of the field. The simplest and most straight-forward procedure is to make this transformation using the scaling factor of the model. Since

$$1\text{m}|_m = 300\text{m}|_p ,$$

one can write

$$\frac{\chi u}{Q} |_p (\text{m}^{-2}) = \frac{1}{300^2} \frac{\chi u}{Q} |_m (\text{m}^{-2}) .$$

The value for u was determined at the height of the maximum concentration from the velocity power law relation for E and F stability. For D-stability the stack-top wind speed was used since the velocity profiles were nearly uniform. Prototype concentrations were then calculated using the relation

$$x_p \text{ (ppm)} = \left(\frac{x}{Q} \right)_m \cdot \frac{1}{300^2} \left(\frac{Q}{u} \right)_p$$

When interpreting model concentration measurements, it is important to remember that there can be considerable difference between the instantaneous concentration in a plume and the average concentration due to horizontal meandering. In the wind tunnel, a plume does not generally meander due to the absence of large-scale eddies. Thus, it is found that field measurements of peak concentrations which effectively eliminate horizontal meandering should correlate with the wind tunnel data (Hino, 1968). In order to compare downwind measurements of dispersion to predict average field concentrations, it is necessary to use data on peak-to-mean concentration ratios as gathered by Singer, et al. (1953, 1963). Their data is correlated in terms of the gustiness categories suggested by Pasquill for a variety of terrain conditions. It is possible to determine the frequency of different gustiness categories for a specific site. Direct use of wind tunnel data at points removed from the building cavity region may underestimate the dilution capacity of a site by a factor of four unless these adjustments are considered (Martin, 1965).

To estimate the equivalent prototype sampling time, another dimensionless variable was derived by including time as one of the pertinent parameters. The relation then exists

$$\left(\frac{tu_a}{L_o}\right)_m = \left(\frac{tu_a}{L_o}\right)_p \quad \text{or}$$

$$t_p = t_m \left(\frac{L_p}{L_m}\right) \left(\frac{u_{a_m}}{u_{a_p}}\right) .$$

Since the model sampling time was approximately instantaneous, it is reasonable to assume that the prototype sampling time is on the order of 10 min. A comparison of the concentration results of this study with the predicted 10 min. values using the Pasquill-Gifford relations as presented in Turner (1969) also supports this assumption. Consequently, no correction for sampling time is presented herein since all model comparisons are with respect to a 10 min. sampling time.

A total system error can be evaluated by considering the mean deviation found for a set of measurements where a precalibrated gas mixture is monitored. For a gas of 100 percent helium, the average mean deviation from the TCGC was three percent. Since the source gas was premixed to the appropriate molecular weight and repetitive measurements were made of its source strength, the confidence in source strength concentration is similar. The flow rate of the source gas was monitored by Fischer-Porter flow meters which are accurate to 2 percent, including calibration and scale fraction error. The wind tunnel velocity was constant to ± 10 percent at such low settings. Hence, the cumulative confidence in the measured values of the dilution factor $\left(\frac{\chi u}{Q}\right)_m$ will be a mean deviation of about ± 9 percent, whereas the worst cumulative scenario suggests an error of no more than ± 20 percent.

The lower limit of measurement (approximately 200 ppm) is imposed by the instrument sensitivity and the background concentrations of helium in

the air within the wind tunnel. Background concentrations were measured and subtracted from all measurements quoted herein.

3.5 Velocity and Temperature Measurements

A schematic of the velocity and temperature sensor arrangement for the wind tunnel tests is shown in Figure 3.5-1. The velocity probe is a Datametrics Model 800-LV linearized hot-wire anemometer with a range capability of 0.03 to 5.1 m/s and an accuracy of 2 percent of the reading or 0.03 m/s whichever is greatest. A calibration of the anemometer before conducting the tests gave the following relation

$$u(\text{m/s}) = 5.91 R + 0.09$$

where R is the anemometer output reading.

The velocity probe was positioned upwind of the stack, a height of 0.2 m to set and monitor tunnel flow conditions. The same probe was used to measure velocity profiles at the stack location. The probe was attached to a vertically traversing carriage and average velocities (60 sec) were obtained at incremental altitudes. The profiles for D, E and F stability are shown in Figures 3.5-2, 3.5-3 and 3.5-4. The low wind speed neutral velocity profiles show a nearly uniform velocity distribution. The velocity power law relations over a height from 0.2 to 0.6 m are shown for E and F stability in the figures.

The temperature conditions in the wind tunnel were set using a rack of twelve thermistors (positioned at incremental altitudes) placed upwind of the stack. The rack was taken out of the tunnel once the desired condition stabilized. Figure 3.5-4 shows the temperature profiles obtained for E and F stability.

4.0 RESULTS

4.1 Plume Rise

The assessment of the effects of exit velocity and exit temperature upon plume rise was completed using photographic techniques. A summary of the variables for each case studied is presented in Tables 3.2-2, 3.2-3 and 3.2-4 for D, E and F stability, respectively. The results for each stability class will be discussed separately.

● D-Stability

Photographs of the plume visualization are presented in Figures 4.1-1 through 4.1-4 for the four stack height wind speeds considered (2, 4, 8 and 16 m/s) and a 388°K exit temperature. The photographs show an increase in plume rise with increased exit velocity and an overall decrease in plume rise with increased ambient wind speed.

From an analysis of the photographs, plume centerline trajectories were plotted. Figure 4.1-5 shows the dependence of plume rise on exit velocity for each ambient wind speed considered. The most significant increase in plume rise occurs for the 16 m/s ambient wind case (Figure 4.1-5d). For the 12.5 m/s exit velocity, the plume rise is nearly zero while the rise ranges from 20 to 60 m for the 30 m/s and 240 m/s exit velocities, respectively.

The effect of exit temperature on plume rise is illustrated in Figures 4.1-6 and 4.1-7 for a 30 and 60 m/s exit velocity. The figures show a slight increase in plume rise with increased exit temperature. However, for the range of downwind distances considered, the added plume rise is small and within the range of experimental error.

● E-Stability

The plume visualization photographs for this stability are shown in Figures 4.1-8, 4.1-9 and 4.1-10 for 366, 388 and 422°K exit temperatures and five exit velocities. A qualitative analysis shows an increase in plume rise with exit velocity. The effect of exit temperature is difficult to ascertain from the photographs due to the small changes involved.

The plume centerline trajectories are plotted in Figures 4.1-11 and 4.2-12. Figure 4.1-11 shows the dependence of plume rise on exit speed for each exit temperature considered. In general, there seems to be little change in plume rise with exit speeds of 12.5, 30 and 60 m/s. However, with exit speeds of 120 and 240 m/s a significant increase in plume rise is observed.

Figure 4.1-12 shows the dependence of plume rise on exit temperature for a 30 and 60 m/s exit velocity. An insignificant change in plume rise with exit temperature is observed for the range of downwind distances considered.

● F-Stability

Photographs of the plume visualization for this stability are presented in Figures 4.1-13, 4.1-14 and 4.1-15 for the three exit temperatures and five exit speeds considered. The expected result of increased plume rise with exit speed is observed. The effect of exit temperature is difficult to ascertain from the figures because of the small changes.

Figure 4.1-16 shows the centerline plume trajectories versus exit speed for each exit temperature considered. The results show no significant increase in plume rise for exit speeds of 12.5, 30 and 60

m/s. For exit speeds of 120 and 240 m/s a significant increase in plume rise is observed.

Figure 4.1-17 shows the effect of exit temperature on plume rise for the 30 and 60 m/s exit speeds. For the 30 m/s exit speed it appears that a 422°K exit temperature gives approximately 20 m of additional rise over a 388°K exit temperature. The remaining results show little change in plume rise with exit temperature.

4.2 Concentration Measurements

The concentration data were analyzed to obtain peak concentration values for each downwind distance and atmospheric condition studied. The results of the analysis are presented in Tables 4.2-1, 4.2-2 and 4.2-3 for D, E and F stability, respectively. To quantitatively assess the dependence of maximum centerline concentration on exit temperature and exit velocity, the dilution $(xu/Q)_p$ was plotted versus downwind and trajectory distance. The trajectory distance was computed from the plume rise graphs in section 4.1. The plume travel distance (trajectory) to each downwind location was obtained for each exit velocity and temperature considered. The results of the analyses will be discussed by Pasquill stability class.

● D-Stability

Figure 4.2-1 shows the maximum centerline dilution versus downwind distance for ambient wind speeds of 4, 8 and 16 m/s, a 388°K exit temperature and the five exit velocities considered. The velocity used for calculating $(xu/Q)_p$ was the stack top wind velocity.

The figure shows that the dilution decreases with increased exit velocity. The greatest decrease is for the high exit velocities (120 and 240 m/s). This is to be expected since the plume travels

farther to each downwind location as the exit velocity increases. All of the dilution values fall below the Pasquill D dilution curve. This curve was obtained by using the Gaussian diffusion equation and techniques outlined in Turner (1969). Relatively close to a stack one would expect the observed dilution to be less than that predicted by using the Gaussian model. That is because the model assumes a point source emitted parallel to the wind whereas in reality the plume is emitted perpendicular to the wind. Hence, a bent over plume results.

In order to correct for the point source effect, the plume travel distance from the stack nozzle was calculated from the plume trajectories discussed in section 4.1. Figure 4.2-2 shows the dilution plotted versus plume trajectory distance. For all wind speeds considered the dilution values, when scaled in this manner, fall along the Pasquill D curve. The best fit was observed for the 4 m/s case. The best agreement for this case is to be expected, since the wind speed was nearly uniform with height. Consequently, no error would be introduced by using the stack top winds instead of the winds at plume altitude.

● E-Stability

The plume centerline dilution versus distance for this stability is shown in Figure 4.2-3. The trend of decreasing dilution with increased exit velocity at a given downwind distance is evident. No consistent change in dilution with exit temperature is apparent from the figures. All of the dilution values tend to approach the Pasquill E curve as the downwind distance increases.

To account for the point source effect, the dilution was plotted versus trajectory distance. These plots are shown in Figure 4.2-4 for

the exit temperatures and speeds considered. The dilution values scatter about the Pasquill E curve when plotted in this manner. This indicates that increased exit velocity or exit temperature does not affect plume dispersion.

● F-Stability

Figure 4.2-5 shows the plume centerline dilution versus distance for this stability and the various wind speeds and temperatures considered. Again, the trend of decreasing dilution with increased exit speed is evident at downwind distances of 30 and 120 m. At 600 m the dilution is nearly invariant with exit velocity. From the figure no consistent variation with exit temperature is apparent.

Figure 4.2-6 shows the plot of dilution versus trajectory distance. For this case all values scattered about a curve falling below the Pasquill F curve but close to the Pasquill E curve. This may be explained by referring to the Richardson number for this series of data. The Richardson number for the F-stability data was 0.31 while for the E-stability data it was 0.57. Thus, the F-case was actually less stable than the E-case. Consequently, if Richardson number were used to classify the stability instead of the lapse rate, both the E and F cases would be classified as E-stability. The plots of dilution versus trajectory distance also verify this conclusion.

5.0 SUMMARY

The results of the wind tunnel study show qualitatively and quantitatively the effect of exit temperature and exit velocity upon near field (less than 600 m) plume rise and dispersion under various simulated atmospheric conditions. The results can be summarized as follows.

- For exit velocities of 12.5, 30.0 and 60.0 m/s, small changes in plume rise were observed. A larger change in plume rise was observed for the 120 and 240 m/s exit speeds.
- Exit temperature changes (366, 388 and 422°K) produced little change in plume rise for the downwind distances considered.
- The plume centerline dilution ($\chi u/Q$) generally decreased with increasing exit velocity at downwind distances of 30 and 120 m. The greatest decrease was observed for the 120 and 240 m/s exit velocities.
- The dilution values, when plotted versus trajectory distance, fell along the Pasquill D and E curves for the respective simulated cases. The $\chi u/Q$ values for the F-stability cases fell along the Pasquill E curve, suggesting that lapse rate is not an effective method for determining Pasquill category. The Richardson number was more indicative of stability.

REFERENCES

1. Cermak, J. E., "Applications of Fluid Mechanics to Wind Engineering," 1974 Freeman Scholar Lecture, ASME Journal of Fluids Engineering, Vol. 97, Series 1, No. 1, March, 1975, CEP74-75JEC7.
2. Briggs, G. A., "Plume Rise," AEC Critical Review Series, USAEC Report TID-25075, November, 1969.
3. Chan, T. L. and J. Kennedy, "Turbulent Nonbuoyant or Buoyant Jets Discharged Into Flowing or Quiescent Fluids," U.S. Navy Contract No. NQ0014-68-0196-004, The University of Iowa, IIHR-140, August, 1972.
4. Fox, D. G., "Forest Plume in a Stratified Fluid," Journal of Geophysical Research, Vol. 75, pp. 6818-6831, November, 1970.
5. Halitsky, J., J. Golden, P. Halpern and P. Wu, "Wind Tunnel Tests of Gas Diffusion from a Leak in the Shell of a Nuclear Power Reactor and from a Nearby Stack," Geophysical Sciences Laboratory Report No. 63-2, New York University, April, 1963.
6. Halitsky, J., "Gas Diffusion near Buildings," Geophysical Sciences Laboratory Report No. 63-3, New York University, February, 1963.
7. Halitsky, J., "Single-Camera Measurement of Smoke Plumes," Int. J. Air and Water Poll., Vol. 4, pp. 185-198, 1961.
8. Hewett, T. A., "Model Experiments of Smokestack Plumes in a Stable Atmosphere," Ph.D. Thesis, Massachusetts Institute of Technology, 1970.
9. Hino, M., "Maximum Ground-Level Concentration and Sampling Time," Atmospheric Environment, Vol. 2, pp. 149-165, 1968.
10. Hoult, D. P., J. Fay, and L. Forney, "A Theory of Plume Rise Compared with Field Observations," Journal of the Air Pollution Control Association, Vol. 19, pp. 585-590, MIT, August, 1969.
11. Martin, J. E., "The Correlation of Wind Tunnel and Field Measurements of Gas Diffusion Using Kr-85 as a Tracer," Ph.D. Thesis, MMPP 272, University of Michigan, June, 1965.
12. McNair, H. M. and E. Bonelli, Basic Gas Chromatography, Consolidated Printers, Berkeley, California, 1968.
13. Petersen, R. L., E. Hovind and A. Petersen, "A Systematic Approach to Meet Air Quality Standards at an Existing Smelter Facility," Presented at the Air Pollution Control Association Meeting in Vancouver, British Columbia, November 19-21, 1975.
14. Singer, I. A. and M. E. Smith, "The Relation of Gustiness to Other Meteorological Parameters," Journal of Meteorology, Vol. 10, No. 2, 1953.

15. Singer, I. A., I. Kazukiko and G. Roman, "Peak to Mean Pollutant Concentration Ratios for Various Terrain and Vegetative Cover," Journal of APCA, Vol. 13, No. 1, p. 40, 1963.
16. Turner, P. B., "Workbook of Atmospheric Dispersion Estimates," U.S. Department of Health, Education and Welfare, Public Health Service, Cincinnati, Ohio, 1969.
17. Weil, J. C., "Model Experiments of High Stack Plumes," S.M. Thesis, Massachusetts Institute of Technology, Cambridge, Massachusetts, 1968.

Table 3.2-1 General Model and Prototype Parameters

Parameter	Prototype	Model
1. Stack Height (h)	60.8 m	0.2 m
2. Volumetric Emission Rate (V)	320 m ³ /s	2.14 x 10 ⁻⁴ m ³ /s
3. Ambient Density (ρ_a)	1.17 kg/m ³	1.17 kg/m ³
4. Viscosity of Air (ν_a)	1.82 x 10 ⁻⁵ kg m ⁻¹ s ⁻¹	1.82 x 10 ⁻⁵ kg m ⁻¹ s ⁻¹
5. Ambient Temperature (T _a)	293°K	293°K
6. Nozzle Height	8.57 m	2.86 cm
7. Roughness Length (z _o)	.03 cm	1.14 x 10 ⁻⁴ cm

Table 3.2-2 Model and Prototype Parameters for the Pasquill D Wind Tunnel Tests

Run #	u_p (m/s)	u_m (m/s)	$(Re_b)_p$	$(Re_b)_m$	γ	T_{s_p} (°K)	$Fr_{m=p}$	$R_{m=p}$	u_{s_p} (m/s)	D_p (m)	Re_{s_m}
1	2	.12	7.85×10^6	1.5×10^3	.245	388	.29	6.25	12.5	5.72	960
2							.45	15.0	30.0	3.69	1400
3							.64	30.0	60.0	2.61	1900
4							.91	60.0	120.0	1.83	2700
5							1.29	120.0	240.0	1.29	3800
6					.31	422	.36	15.0	30.0	3.69	1400
7							.51	30.0	60.0	2.61	1900
8					.20	366	.55	15.0	30.0	3.69	1400
9							.78	30.0	60.0	2.61	1900
10	4	.23	1.57×10^7	3×10^3	.245	388	1.28	3.75	12.5	5.72	960
11							1.81	7.5	30.0	3.69	1400
12							2.56	15.0	60.0	2.61	1900
13							3.64	30.0	120.0	1.83	2700
14							5.17	60.0	240.0	1.29	3800
15					.31	422	1.43	7.5	30.0	3.69	1400
16							2.02	15.0	60.0	2.61	1900
17					.20	366	2.21	7.5	30.0	3.69	1400
18							3.13	15.0	60.0	2.61	1900

Table 3.2-2 (continued)

Run #	u_p (m/s)	u_m (m/s)	$(Re_b)_p$	$(Re_b)_m$	γ	T_{sp} (°K)	$Fr_{m=p}$	$R_{m=p}$	u_{sp} (m/s)	D_p (m)	Re_{sm}
19	8	.46	3.1×10^7	6×10^3	.245	388	5.1	1.88	12.5	5.72	960
20							7.2	3.75	30.0	3.69	1400
21							10.2	7.50	60.0	2.61	1900
22							14.6	15.0	120.0	1.83	2700
23							20.7	30.0	240.0	1.29	3800
24					.31	422	5.71	3.75	30.0	3.69	1400
25							8.07	7.50	60.0	2.61	1900
26					.20	366	8.85	3.75	30.0	3.69	1400
27							12.51	7.50	60.0	2.61	1900
28	16	.92	6.2×10^7	1.2×10^4	.245	388	20.4	7.78	94	5.72	960
29							28.9	1.88	30.0	3.69	1400
30							40.9	3.75	60.0	2.61	1900
31							58.3	7.50	120.0	1.83	2700
32							82.7	15.0	240.0	1.29	3800
35					.31	422	22.8	1.88	30.0	3.69	1400
36							32.3	3.75	60.0	2.61	1900
37					.20	366	35.4	1.88	30.0	3.69	1400
38							50.1	3.75	60.0	2.61	1900

Table 3.2-3 Model and Prototype Parameters for the Pasquill E Wind Tunnel Tests

Run #	$Ri_{m=p}$	$\left(\frac{\Delta\theta}{\Delta z}\right)_p$ (°K/m)	u_p (m/s)	u_m (m/s)	$(Re_b)_p$	$(Re_b)_m$	γ	T_{s_p} (°K)	$Fr_{m=p}$	$R_{m=p}$	u_{s_p} (m/s)	D_p (m)	$(Re_s)_m$
49	.57	.01	5.9	.34	2.3×10^7	4.4×10^3	.20	366	3.1	2.1	12.5	5.72	875
50									4.8	5.1	30.0	3.69	1371
51									6.8	10.2	60.0	2.61	1940
52									9.7	20.3	120.0	1.83	2707
53									13.8	40.7	240.0	1.29	3825
54							.245	388	2.5	2.1	12.5	5.72	875
55									3.9	5.1	30.0	3.69	1371
56									5.6	10.2	60.0	2.61	1940
57									7.9	20.3	120.0	1.83	2707
58									11.2	40.7	240.0	1.29	3825
59							.31	422	2.0	2.1	12.5	5.72	875
60									3.1	5.1	30.0	3.69	1371
61									4.4	10.2	60.0	2.61	1940
62									6.3	20.3	120.0	1.83	2707
63									8.9	40.7	240.0	1.29	3825

Table 3.2-4 Model and Prototype Parameters for the Pasquill F Wind Tunnel Tests

Run #	$Ri_{m=p}$	$\left(\frac{\Delta\theta}{\Delta z}\right)_p$ (°K/m)	u_p (m/s)	u_m (m/s)	$(Re_b)_p$	$(Re_b)_m$	γ	Ts_p (°K)	$Fr_{m=p}$	$R_{m=p}$	u_{s_p} (m/s)	D_p (m)	$(Re_s)_m$
64	.31	.03	2.97	.17	1.2×10^7	2.2×10^3	.20	366	.79	4.2	12.5	5.72	825
65									1.22	10.1	30.0	3.69	1371
66									1.72	20.2	60.0	2.61	1940
67									2.46	40.4	120.0	1.83	2707
68									3.49	80.8	240.0	1.29	3825
69							.245	388	.64	4.2	12.5	5.72	875
70									1.00	10.1	30.0	3.69	1371
71									1.41	20.2	60.0	2.61	1940
72									2.01	40.4	120.0	1.83	2707
73									2.85	80.8	240.0	1.29	3825
74							.31	422	.51	4.2	12.5	5.72	875
75									.79	10.1	30.0	3.69	1371
76									1.11	20.2	60.0	2.61	1940
77									1.59	40.4	120.0	1.83	2707
78									2.25	80.8	240.0	1.29	3825

Table 4.2-1a. Summary of Concentration Measurement Results for the Pasquill D Wind Tunnel Tests

SOURCE STRENGTH OF PROTOTYPE = 385.00 (PPM)
 SOURCE STRENGTH OF MODEL = .33E+06 (PPM)
 WIND SPEED AT STACK TOP OF MODEL = .23 (M/S)
 WIND SPEED AT STACK TOP OF PROTOTYPE = 4.00 (M/S)
 VELOCITY PROFILE POWER LAW EXPONENT = *00
 CALIBRATION FACTOR = 2426.2 (PPM/MVS)

EXIT VELOCITY (M/S)	RUN NO.	DISTANCE (M) DOWNWIND/ TRAJECTORY	CONCM (PPM)	CONCP (PPM)	DILUTION (M ⁻²)	HGT MAX (M, AGL)	WIND SPEED (M/S)
12.5	10	30.5 / 110.0	38236.91	25.15	.145E-02	95.27	4.0
		122.0 / 260.0	12235.81	8.05	.464E-03	99.09	4.0
30.0	11	30.5 / 170.0	30589.53	20.12	.116E-02	95.27	4.0
		122.0 / 340.0	12331.40	8.11	.468E-03	121.95	4.0
60.0	12	30.5 / 250.0	20074.38	13.20	.762E-03	110.52	4.0
		122.0 / 430.0	8698.90	5.72	.330E-03	144.82	4.0
120.0	13	30.5 / 320.0	13956.47	9.16	.530E-03	129.57	4.0
		122.0 / 570.0	5831.13	3.84	.221E-03	163.87	4.0
240.0	14	30.5 / 390.0	9750.41	6.41	.370E-03	160.06	4.0
		122.0 / 690.0	3967.08	2.61	.151E-03	163.87	4.0

Table 4.2-1b. Summary of Concentration Measurement Results for the Pasquill D Wind Tunnel Tests

SOURCE STRENGTH OF PROTOTYPE = 385.00 (PPM)
 SOURCE STRENGTH OF MODEL = .33E+06 (PPM)
 WIND SPEED AT STACK TOP OF MODEL = .46 (M/S)
 WIND SPEED AT STACK TOP OF PROTOTYPE = 8.00 (M/S)
 VELOCITY PROFILE POWER LAW EXPONENT = *00
 CALIBRATION FACTOR = 2426.2 (PPM/MVS)

EXIT VELOCITY (M/S)	RUN NO.	DISTANCE (M) DOWNWIND/ TRAJECTORY	CONCM (PPM)	CONCP (PPM)	DILUTION (M-2)	HGT MAX (M.AGL)	WIND SPEED (M/S)
12.5	19	30.5 / 60.0	40148.76	26.41	.305E-02	76.22	8.0
		122.0 / 180.0	13850.88	9.12	.105E-02	80.03	8.0
		610.0 / 710.0	2198.62	1.45	.167E-03	124.81	8.0
30.0	20	30.5 / 110.0	35369.14	23.26	.269E-02	91.46	8.0
		122.0 / 220.0	13765.29	9.05	.105E-02	99.09	8.0
		610.0 / 730.0	1816.25	1.19	.138E-03	101.94	8.0
60.0	21	30.5 / 150.0	28677.68	18.86	.218E-02	91.46	8.0
		122.0 / 260.0	12331.40	8.11	.936E-03	106.71	8.0
		610.0 / 800.0	2342.01	1.54	.178E-03	115.28	8.0
120.0	22	30.5 / 220.0	15103.58	9.93	.115E-02	114.33	8.0
		122.0 / 340.0	7073.83	4.65	.537E-03	114.33	8.0
		610.0 / 860.0	2819.97	1.85	.214E-03	139.10	8.0
240.0	23	30.5 / 260.0	10993.11	7.23	.835E-03	121.95	8.0
		122.0 / 420.0	4875.21	3.21	.370E-03	137.20	8.0
		610.0 / 920.0	1290.50	.85	.980E-04	150.06	8.0

Table 4.2-1c. Summary of Concentration Measurement Results for the Pasquill D Wind Tunnel Tests

SOURCE STRENGTH OF PROTOTYPE = 385.00 (PPM)
 SOURCE STRENGTH OF MODEL = .33E+06 (PPM)
 WIND SPEED AT STACK TOP OF MODEL = .92 (M/S)
 WIND SPEED AT STACK TOP OF PHOTOTYPE = 16.00 (M/S)
 VELOCITY PROFILE POWER LAW EXPONENT = *00
 CALIBRATION FACTOR = 2426.2 (PPM/MVS)

EXIT VELOCITY (M/S)	RUN NO.	DISTANCE (M) DOWNWIND/ TRAJECTORY	CONCM (PPM)	CONCP (PPM)	DILUTION (M-2)	HGT MAX (M.AGL)	WIND SPEED (M/S)
12.5	28	30.5 / 40.0	40148.76	26.41	.610E-02	64.79	16.0
		122.0 / 130.0	8937.88	5.88	.136E-02	55.26	16.0
		610.0 / 630.0	1409.99	.93	.214E-03	60.98	16.0
30.0	29	30.5 / 60.0	35847.10	23.58	.544E-02	76.22	16.0
		122.0 / 130.0	11767.41	7.74	.179E-02	76.22	16.0
		610.0 / 650.0	1395.65	.92	.212E-03	80.03	16.0
60.0	30	30.5 / 80.0	30035.09	19.75	.456E-02	83.84	16.0
		122.0 / 180.0	11557.11	7.60	.175E-02	87.65	16.0
		610.0 / 680.0	1338.29	.88	.203E-03	100.99	16.0
120.0	31	30.5 / 130.0	18544.90	12.20	.282E-02	91.46	16.0
		122.0 / 220.0	8230.50	5.41	.125E-02	95.27	16.0
		610.0 / 730.0	1228.36	.81	.187E-03	104.33	16.0
240.0	32	30.5 / 160.0	11471.07	7.54	.174E-02	102.90	16.0
		122.0 / 260.0	5993.64	3.94	.910E-03	99.09	16.0
		610.0 / 780.0	955.92	.63	.145E-03	100.51	16.0

Table 4.2-2a. Summary of Concentration Measurement Results for the Pasquill E Wind Tunnel Tests

SOURCE STRENGTH OF PROTOTYPE = 385.00 (PPM)
 SOURCE STRENGTH OF MODEL = .23E+06 (PPM)
 WIND SPEED AT STACK TOP OF MODEL = .34 (M/S)
 WIND SPEED AT STACK TOP OF PROTOTYPE = 5.93 (M/S)
 VELOCITY PROFILE POWER LAW EXPONENT = .27
 CALIBRATION FACTOR = 2387.2 (PPM/MVS)

EXIT VELOCITY (M/S)	RUN NO.	DISTANCE (M) DOWNWIND/ TRAJECTORY	CONCM (PPM)	CONCP (PPM)	DILUTION (M-2)	HGT MAX (M.AGL)	WIND SPEED (M/S)
12.5	49	30.5 / 90.0	35808.00	33.69	.306E-02	76.22	6.3
		122.0 / 230.0	7877.76	7.41	.765E-03	121.95	7.1
		610.0 / 830.0	1312.96	1.24	.135E-03	152.44	7.6
30.0	50	30.5 / 160.0	26736.64	25.16	.243E-02	95.27	6.7
		122.0 / 300.0	8116.48	7.64	.774E-03	114.33	7.0
		610.0 / 800.0	1193.60	1.12	.125E-03	160.06	7.7
60.0	51	30.5 / 140.0	36285.44	34.14	.333E-02	99.09	6.8
		122.0 / 300.0	7639.04	7.19	.729E-03	114.33	7.0
		610.0 / 875.0	1193.60	1.12	.125E-03	163.87	7.7
120.0	52	30.5 / 275.0	10981.12	10.33	.107E-02	123.86	7.2
		122.0 / 430.0	4774.40	4.49	.478E-03	137.20	7.4
		610.0 / 960.0	1074.24	1.01	.116E-03	194.36	8.1
240.0	53	30.5 / 360.0	8593.92	8.09	.855E-03	133.38	7.3
		122.0 / 520.0	2984.00	2.81	.306E-03	148.63	7.5
		610.0 / 1040.0	895.20	.84	.103E-03	224.85	8.4

Table 4.2-2b. Summary of Concentration Measurement Results for the Pasquill E Wind Tunnel Tests

SOURCE STRENGTH OF PROTOTYPE = 385.00 (PPM)
 SOURCE STRENGTH OF MODEL = .29E+06 (PPM)
 WIND SPEED AT STACK TOP OF MODEL = .34 (M/S)
 WIND SPEED AT STACK TOP OF PROTOTYPE = 5.93 (M/S)
 VELOCITY PROFILE POWER LAW EXPONENT = .27
 CALIBRATION FACTOR = 2387.2 (PPM/MVS)

EXIT VELOCITY (M/S)	RUN NO.	DISTANCE (M) DOWNWIND/ TRAJECTORY	CONCM (PPM)	CONCP (PPM)	DILUTION (M ⁻²)	HGT MAX (M, AGL)	WIND SPEED (M/S)
12.5	54	30.5 / 90.0	34283.30	25.58	.236E-02	80.03	6.4
		122.0 / 240.0	13459.37	10.04	.959E-03	91.46	6.6
		610.0 / 830.0	1881.11	1.40	.152E-03	144.82	7.5
30.0	55	30.5 / 135.0	24157.26	21.76	.217E-02	106.71	6.9
		122.0 / 290.0	14860.80	11.09	.113E-02	118.14	7.1
		610.0 / 860.0	1881.11	1.40	.152E-03	144.82	7.5
60.0	56	30.5 / 210.0	25089.35	18.72	.192E-02	118.14	7.1
		122.0 / 335.0	11662.90	8.70	.898E-03	121.95	7.1
		610.0 / 885.0	2398.42	1.79	.207E-03	186.74	8.0
120.0	57	30.5 / 250.0	12424.76	9.27	.980E-03	133.38	7.3
		122.0 / 390.0	7242.29	5.40	.571E-03	133.38	7.3
		610.0 / 950.0	1598.95	1.19	.142E-03	205.79	8.2
240.0	58	30.5 / 300.0	8239.28	6.15	.645E-03	129.57	7.3
		122.0 / 500.0	4232.51	3.16	.341E-03	144.82	7.5
		610.0 / 1060.0	1363.81	1.02	.121E-03	205.79	8.2

Table 4.2-2c. Summary of Concentration Measurement Results for the Pasquill E Wind Tunnel Tests

SOURCE STRENGTH OF PROTOTYPE = 385.00 (PPM)
 SOURCE STRENGTH OF MODEL = .36E+06 (PPM)
 WIND SPEED AT STACK TOP OF MODEL = .34 (M/S)
 WIND SPEED AT STACK TOP OF PROTOTYPE = 5.93 (M/S)
 VELOCITY PROFILE POWER LAW EXPONENT = .27
 CALIBRATION FACTOR = 2387.2 (PPM/MVS)

EXIT VELOCITY (M/S)	RUN NO.	DISTANCE (M) DOWNWIND/ TRAJECTORY	CONCM (PPM)	CONCP (PPM)	DILUTION (M ⁻²)	HGT MAX (M.AGL)	WIND SPEED (M/S)
12.5	59	30.5 / 100.0	31511.04	18.94	.170E-02	72.41	6.2
		122.0 / 240.0	12413.44	7.46	.728E-03	99.09	6.8
		610.0 / 830.0	2029.12	1.22	.137E-03	167.68	7.8
30.0	60	30.5 / 170.0	15278.08	9.18	.856E-03	83.84	6.5
		122.0 / 310.0	15278.08	9.18	.931E-03	114.33	7.0
		610.0 / 870.0	2864.64	1.72	.194E-03	167.68	7.8
60.0	61	30.5 / 180.0	30556.16	18.37	.175E-02	91.46	6.6
		122.0 / 330.0	11458.56	6.89	.711E-03	121.95	7.1
		610.0 / 840.0	3103.36	1.87	.212E-03	175.30	7.9
120.0	62	30.5 / 235.0	17187.84	10.33	.105E-02	114.33	7.0
		122.0 / 420.0	7161.60	4.31	.451E-03	129.57	7.3
		610.0 / 990.0	1790.40	1.08	.125E-03	186.74	8.0
240.0	63	30.5 / 300.0	14323.20	8.61	.903E-03	129.57	7.3
		122.0 / 985.0	5251.84	3.16	.346E-03	152.44	7.6
		610.0 / 1045.0	1432.32	.86	.104E-03	219.51	8.4

Table 4.2-3a. Summary of Concentration Measurement Results for the Pasquill F Wind Tunnel Tests

SOURCE STRENGTH OF PROTOTYPE = 385.00 (PPM)
 SOURCE STRENGTH OF MODEL = .23E+06 (PPM)
 WIND SPEED AT STACK TOP OF MODEL = .17 (M/S)
 WIND SPEED AT STACK TOP OF PROTOTYPE = 2.97 (M/S)
 VELOCITY PROFILE POWER LAW EXPONENT = .83
 CALIBRATION FACTOR = 3519.2 (PPM/MVS)

EXIT VELOCITY (M/S)	RUN NO.	DISTANCE (M) DOWNWIND/ TRAJECTORY	CONCM (PPM)	CONCP (PPM)	DILUTION (M-2)	HGT MAX (M.AGL)	WIND SPEED (M/S)
12.5	64	30.5 / 90.0	33277.56	31.26	.174E-02	83.84	3.9
		122.0 / 210.0	10191.25	9.57	.574E-03	91.46	4.2
		610.0 / 690.0	2218.50	2.08	.125E-03	91.46	4.2
30.0	65	30.5 / 160.0	27731.30	26.05	.156E-02	91.46	4.2
		122.0 / 270.0	11785.80	11.07	.732E-03	102.90	4.6
		610.0 / 780.0	2426.49	2.28	.160E-03	110.52	4.9
60.0	66	30.5 / 90.0	19550.56	18.36	.125E-02	106.71	4.7
		122.0 / 325.0	10676.55	10.03	.724E-03	114.33	5.0
		610.0 / 830.0	2357.16	2.21	.186E-03	137.20	5.8
120.0	67	30.5 / 265.0	10399.24	9.77	.705E-03	114.33	5.0
		122.0 / 420.0	6378.20	5.99	.503E-03	137.20	5.8
		610.0 / 930.0	1663.88	1.56	.143E-03	152.44	6.4
240.0	68	30.5 / 300.0	10260.58	9.64	.809E-03	137.20	5.8
		122.0 / 480.0	4367.68	4.10	.368E-03	148.63	6.2
		610.0 / 1000.0	1594.55	1.50	0.	0.00	0.0

Table 4.2-3b. Summary of Concentration Measurement Results for the Pasquill F Wind Tunnel Tests

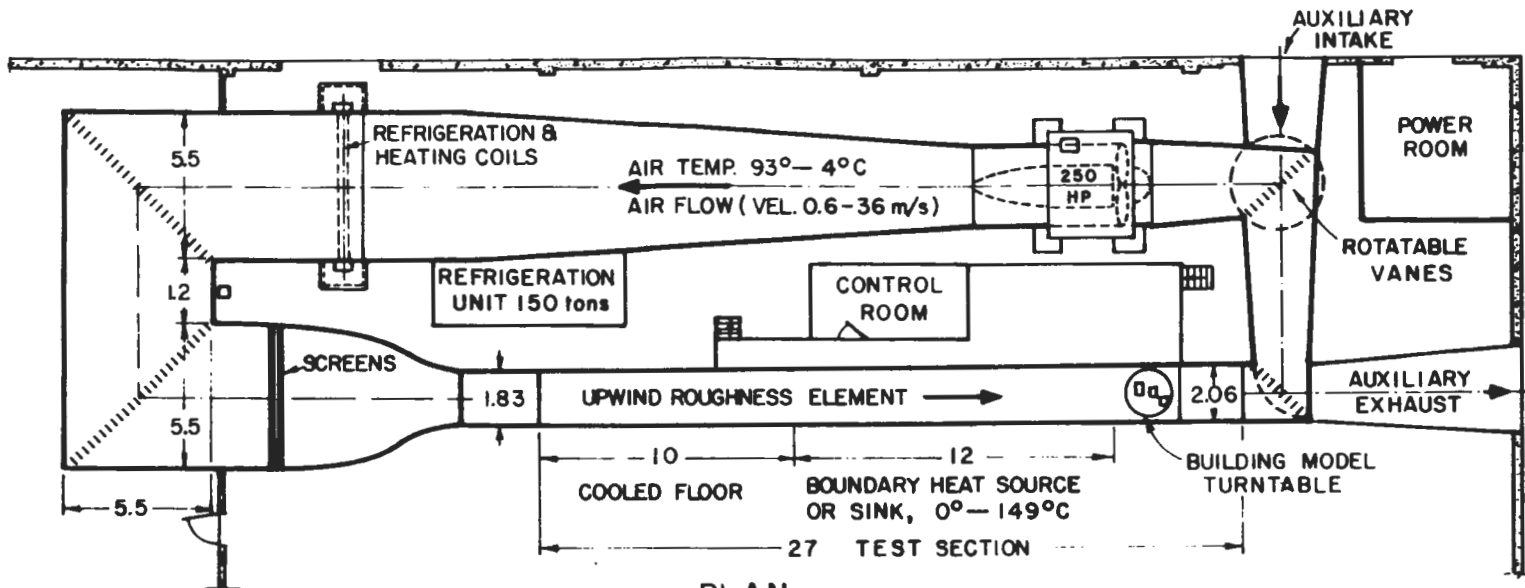
SOURCE STRENGTH OF PROTOTYPE = 385.00 (PPM)
 SOURCE STRENGTH OF MODEL = .29E+06 (PPM)
 WIND SPEED AT STACK TOP OF MODEL = .17 (M/S)
 WIND SPEED AT STACK TOP OF PROTOTYPE = 2.97 (M/S)
 VELOCITY PROFILE POWER LAW EXPONENT = .83
 CALIBRATION FACTOR = 3519.2 (PPM/MVS)

EXIT VELOCITY (M/S)	RUN NO.	DISTANCE (M) DOWNWIND/ TRAJECTORY	CONCM (PPM)	CONCP (PPM)	DILUTION (M ⁻²)	HGT MAX (M, AGL)	WIND SPEED (M/S)
12.5	69	30.5 / 80.0	65168.55	48.55	.271E-02	83.84	3.9
		122.0 / 200.0	15113.56	11.26	.652E-03	87.65	4.0
		610.0 / 660.0	3397.08	2.53	.173E-03	106.71	4.7
30.0	70	30.5 / 140.0	61702.13	45.97	.276E-02	91.46	4.2
		122.0 / 260.0	7764.76	5.78	.394E-03	106.71	4.7
		610.0 / 780.0	3605.07	2.69	.194E-03	114.33	5.0
60.0	71	30.5 / 190.0	45756.64	34.09	.219E-02	99.09	4.4
		122.0 / 300.0	15806.84	11.78	.850E-03	114.33	5.0
		610.0 / 830.0	3605.07	2.69	.205E-03	121.95	5.3
120.0	72	30.5 / 260.0	27038.01	20.14	.145E-02	114.33	5.0
		122.0 / 390.0	8735.36	6.51	.547E-03	137.20	5.8
		610.0 / 910.0	2634.47	1.96	.198E-03	171.49	7.0
240.0	73	30.5 / 380.0	14697.59	10.95	.920E-03	137.20	5.8
		122.0 / 470.0	6239.54	4.65	.426E-03	152.44	6.4
		610.0 / 960.0	1802.53	1.34	0.	0.00	0.0

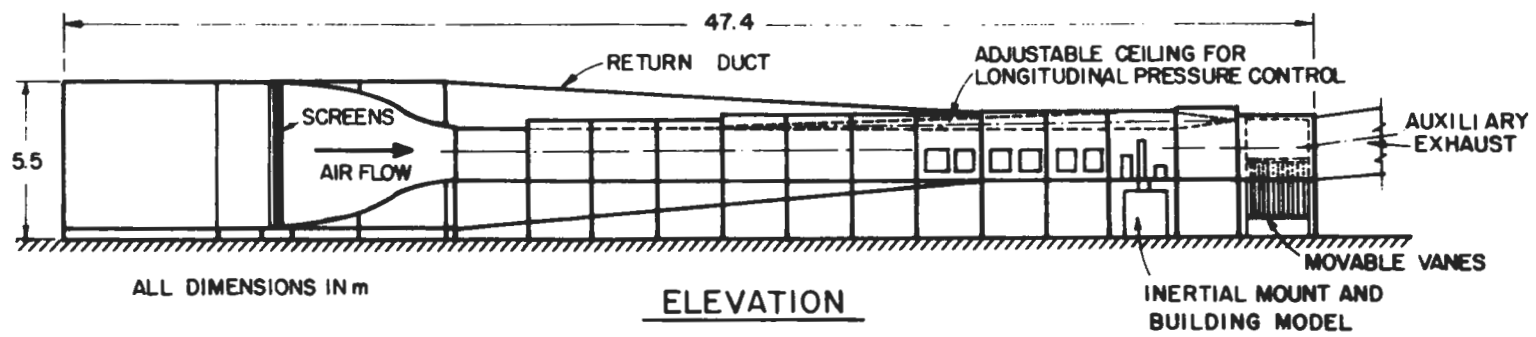
Table 4.2-3c. Summary of Concentration Measurement Results for the Pasquill F Wind Tunnel Tests

SOURCE STRENGTH OF PROTOTYPE = 385.00 (PPM)
 SOURCE STRENGTH OF MODEL = .36E+06 (PPM)
 WIND SPEED AT STACK TOP OF MODEL = .17 (M/S)
 WIND SPEED AT STACK TOP OF PROTOTYPE = 2.97 (M/S)
 VELOCITY PROFILE POWER LAW EXPONENT = .83
 CALIBRATION FACTOR = 3519.2 (PPM/MVS)

EXIT VELOCITY (M/S)	RUN NO.	DISTANCE (M) DOWNWIND/ TRAJECTORY	CONCM (PPM)	CONCP (PPM)	DILUTION (M ⁻²)	HGT MAX (M, AGL)	WIND SPEED (M/S)
12.5	74	30.5 / 70.0	91499.20	54.91	.283E-02	76.22	3.6
		122.0 / 210.0	12201.77	7.32	.424E-03	87.65	4.0
		610.0 / 740.0	1802.53	1.08	.737E-04	106.71	4.7
30.0	75	30.5 / 155.0	55462.59	33.29	.200E-02	91.46	4.2
		122.0 / 295.0	15529.53	9.32	.635E-03	106.71	4.7
		610.0 / 820.0	1871.86	1.12	.811E-04	114.33	5.0
60.0	76	30.5 / 200.0	39517.10	23.72	.152E-02	99.09	4.4
		122.0 / 330.0	13372.96	8.03	.579E-03	114.33	5.0
		610.0 / 840.0	2079.85	1.25	.112E-03	148.63	6.2
120.0	77	30.5 / 250.0	22878.32	13.73	.991E-03	114.33	5.0
		122.0 / 400.0	9359.31	5.62	.428E-03	121.95	5.3
		610.0 / 900.0	2079.85	1.25	.131E-03	179.12	7.3
240.0	78	30.5 / 300.0	20798.47	12.48	.926E-03	118.14	5.1
		122.0 / 460.0	9775.28	5.87	.470E-03	129.57	5.6
		610.0 / 980.0	901.27	.54	.616E-04	198.17	7.9



PLAN



ELEVATION

ALL DIMENSIONS IN m

METEOROLOGICAL WIND TUNNEL (Completed in 1963)
 FLUID DYNAMICS & DIFFUSION LABORATORY
 COLORADO STATE UNIVERSITY

Figure 3.1-1. The Meteorological Wind Tunnel

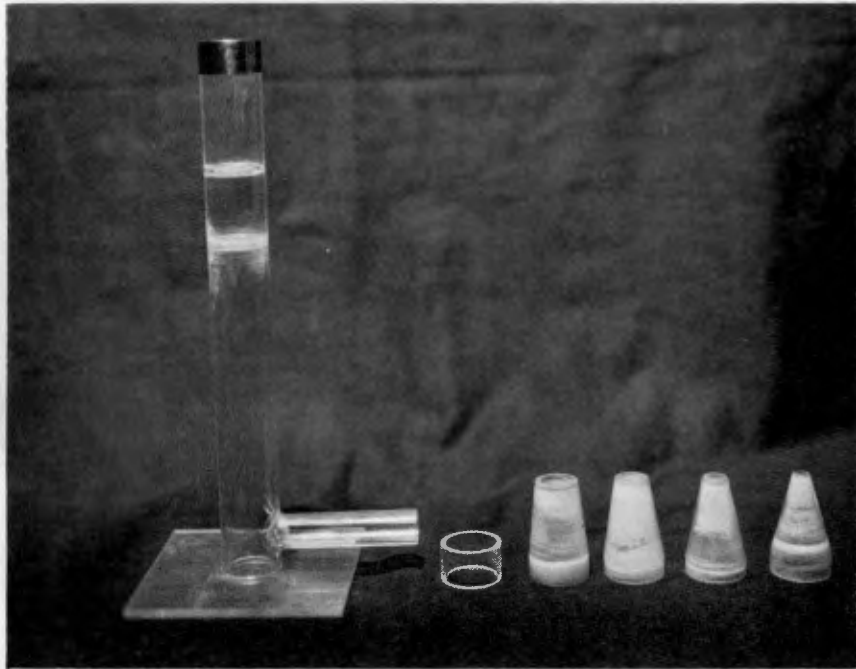


Figure 3.2-1. Photograph of model stack with the five nozzle attachments.

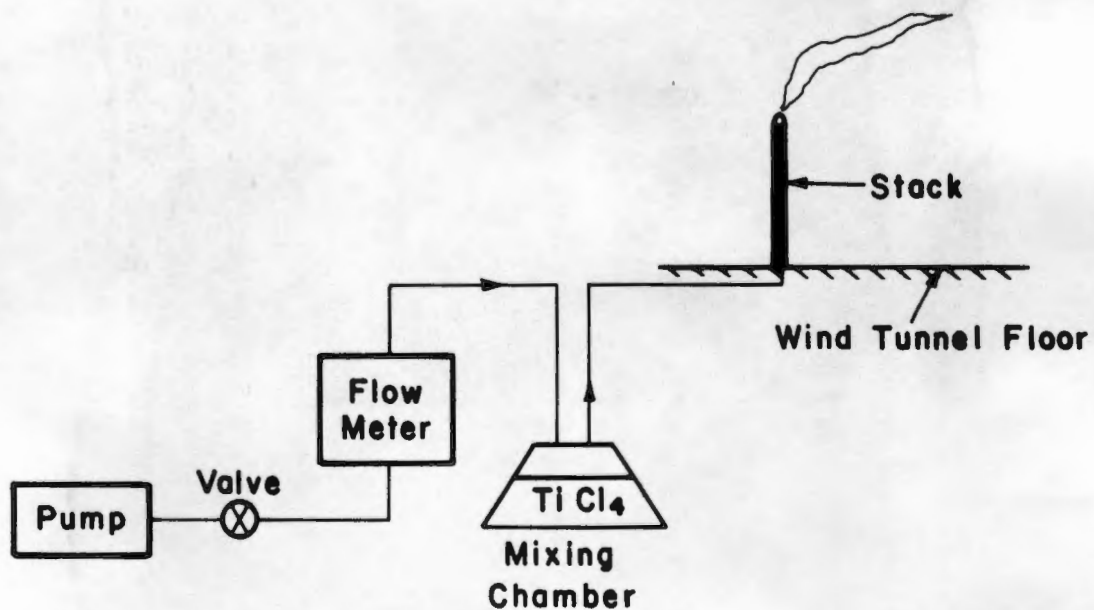


Figure 3.3-1. Schematic of Plume Visualization System

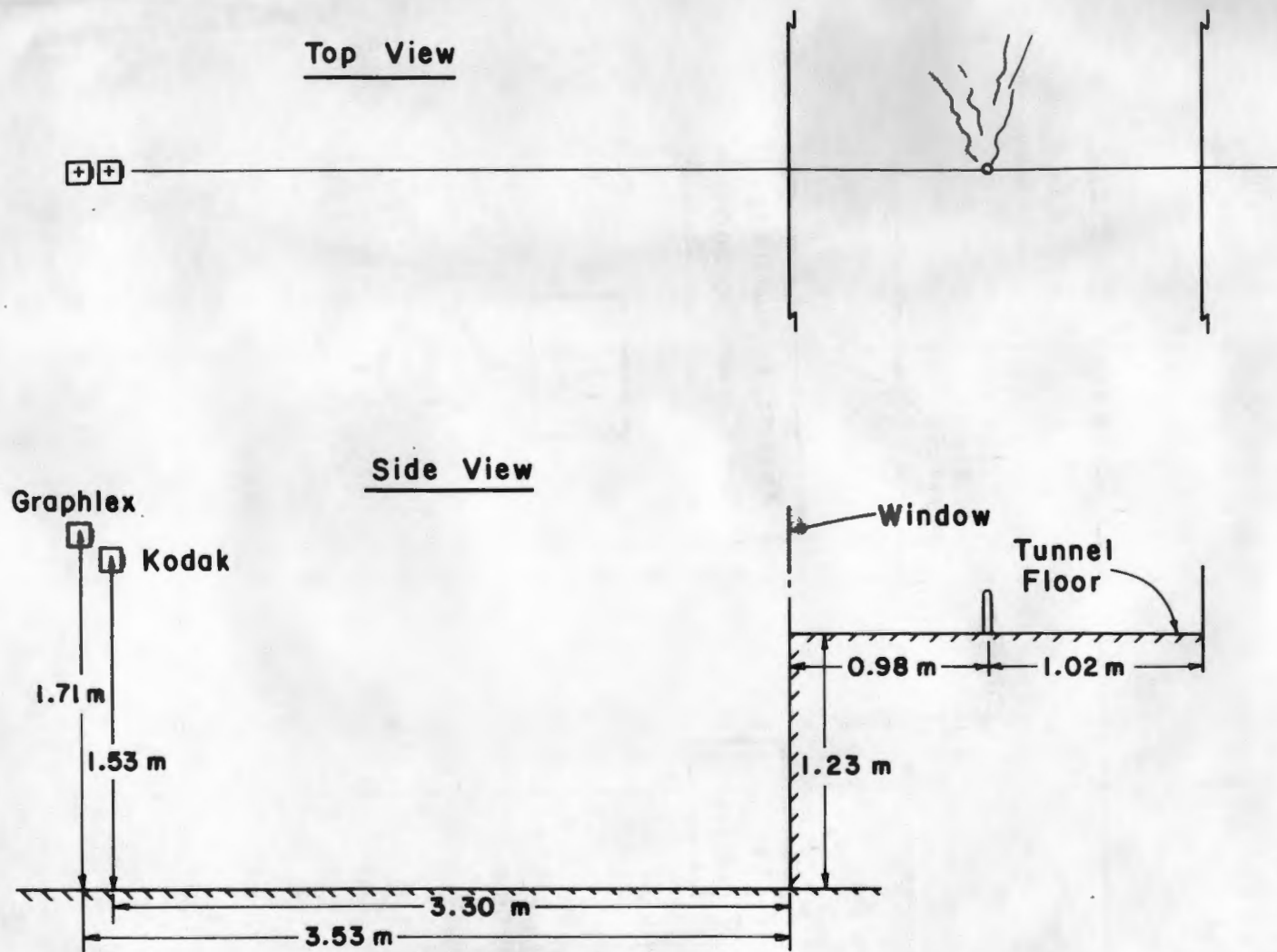


Figure 3.3-2. Plan and Top View of Camera Set-up for Photographing the Wind Tunnel Plumes

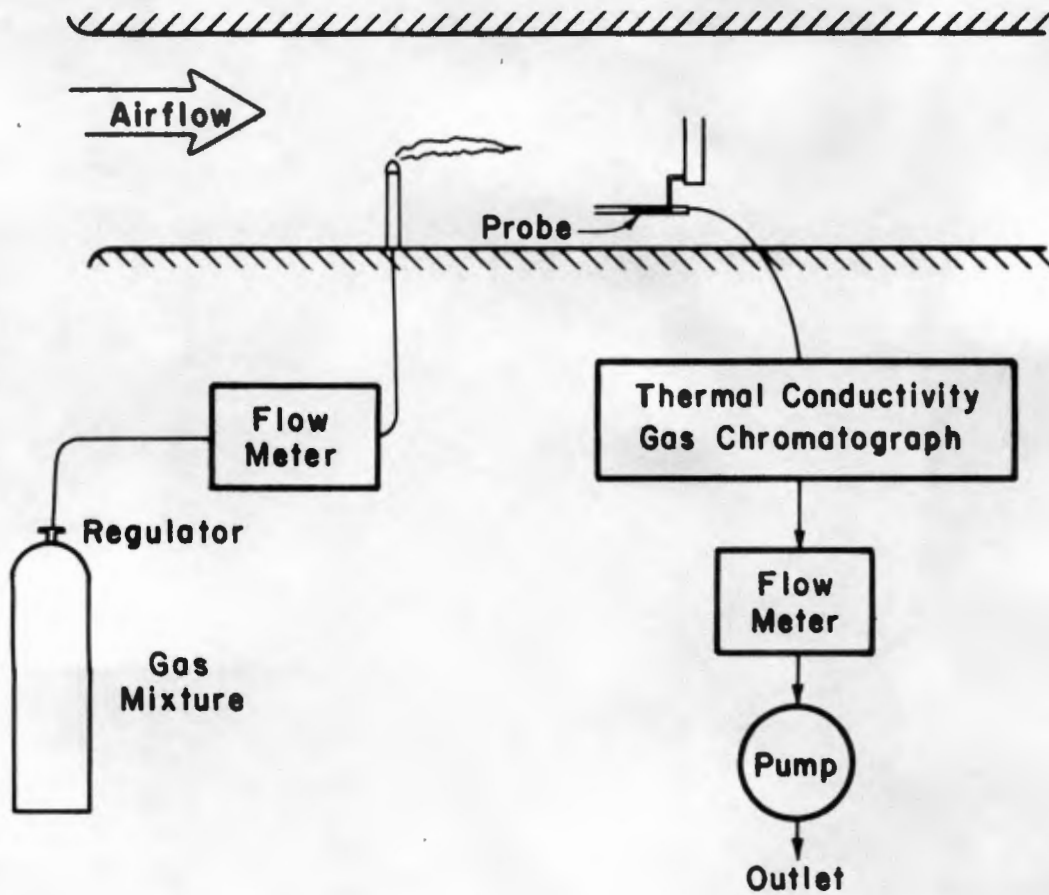


Figure 3.4-1. Schematic of Gas Sampling System

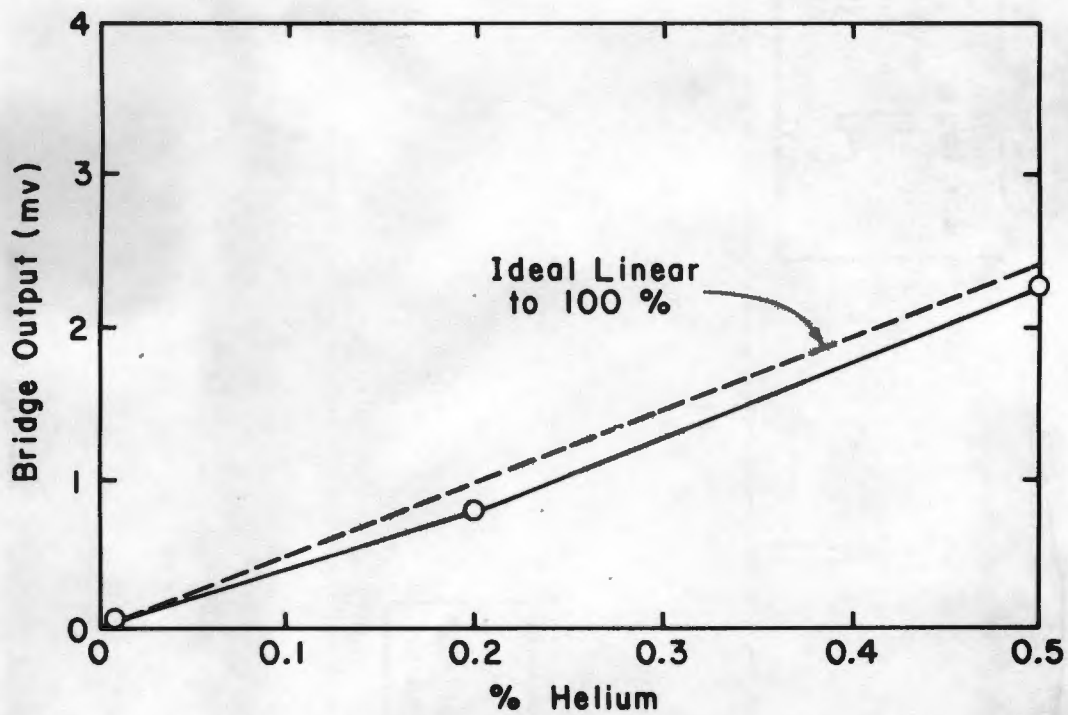


Figure 3.4-2. Gas Chromatograph Calibration Curve

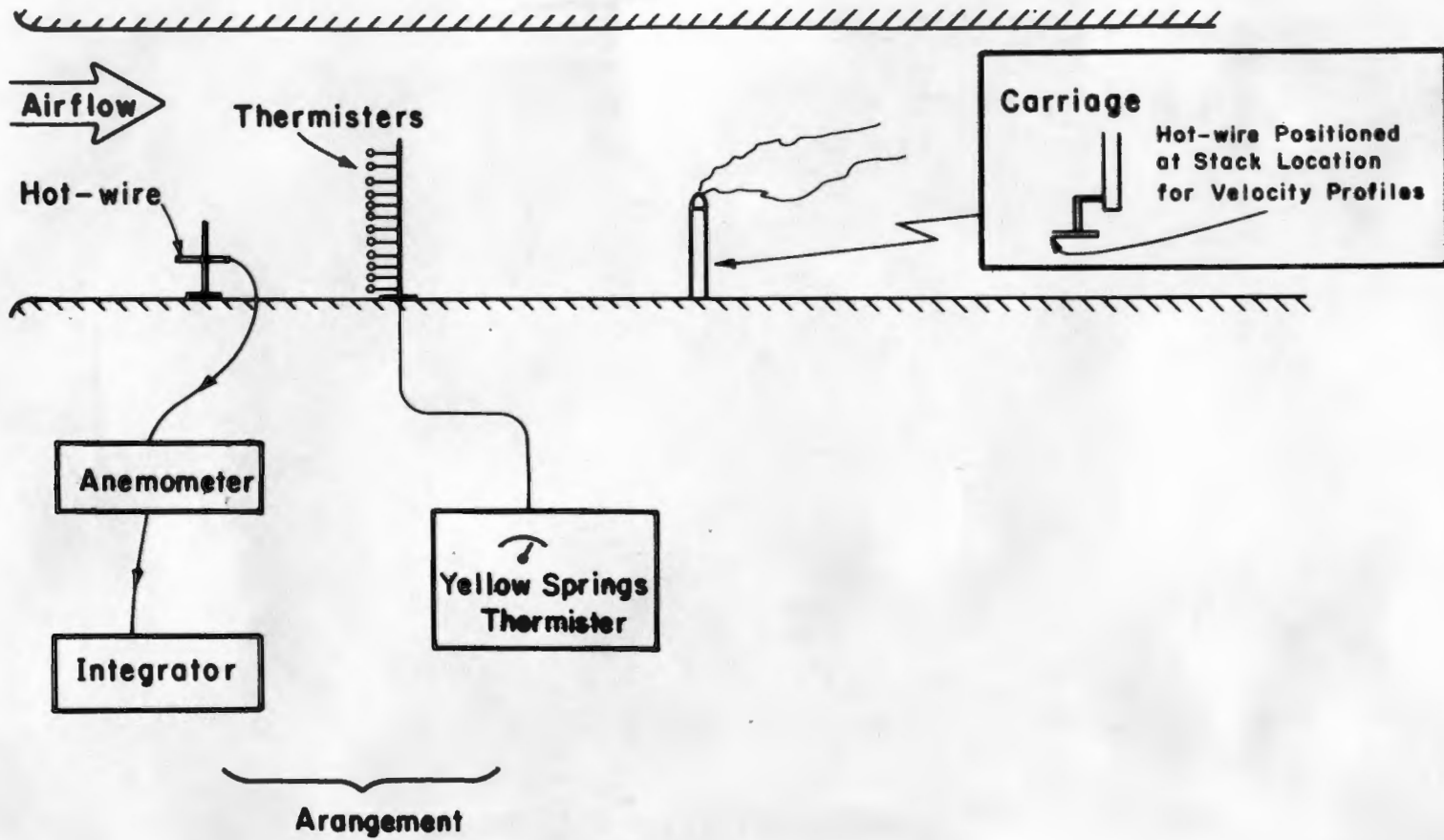


Figure 3.5-1. Schematic of Velocity and Temperature Measurement System

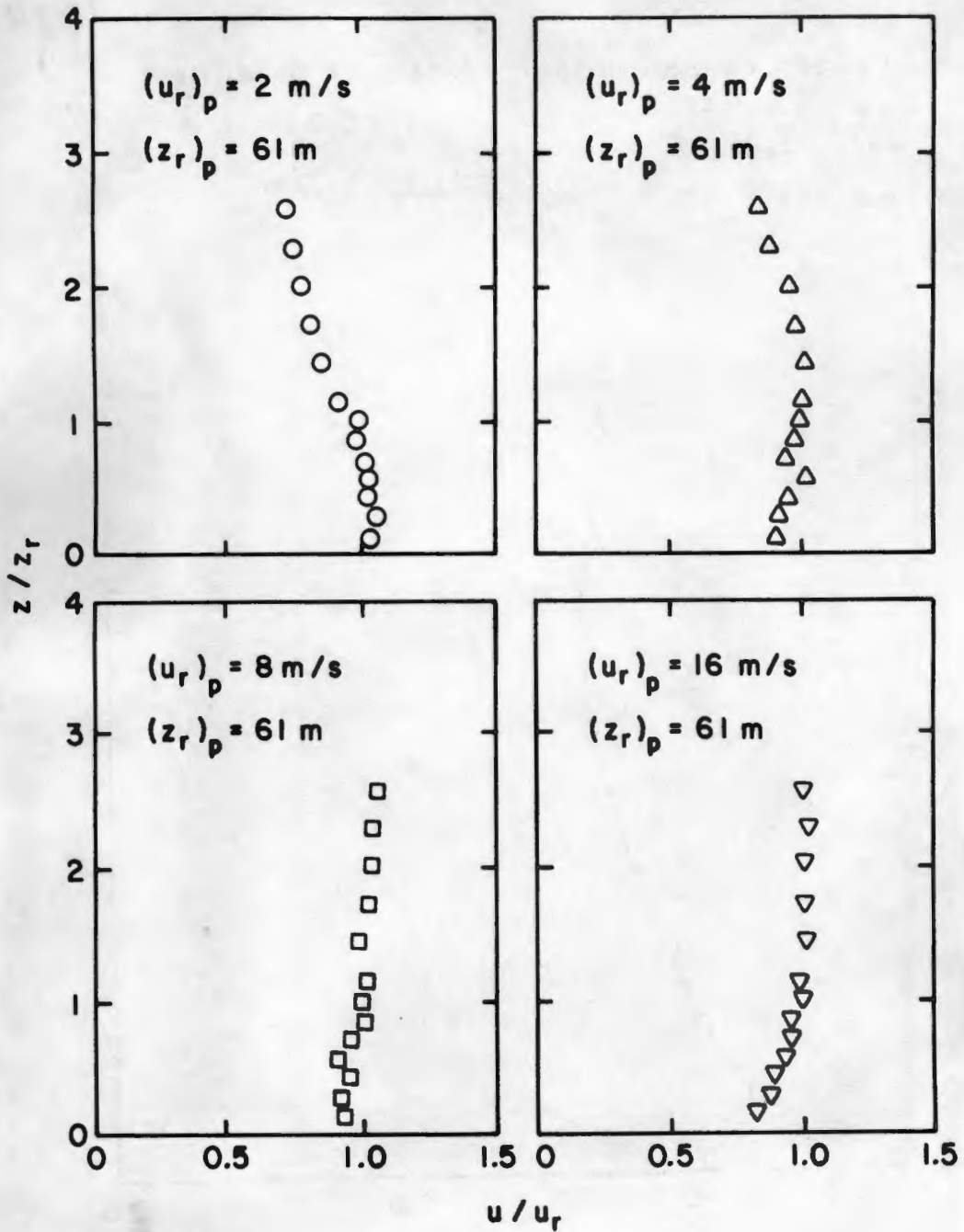


Figure 3.5-2. Velocity Profiles for Neutral Conditions

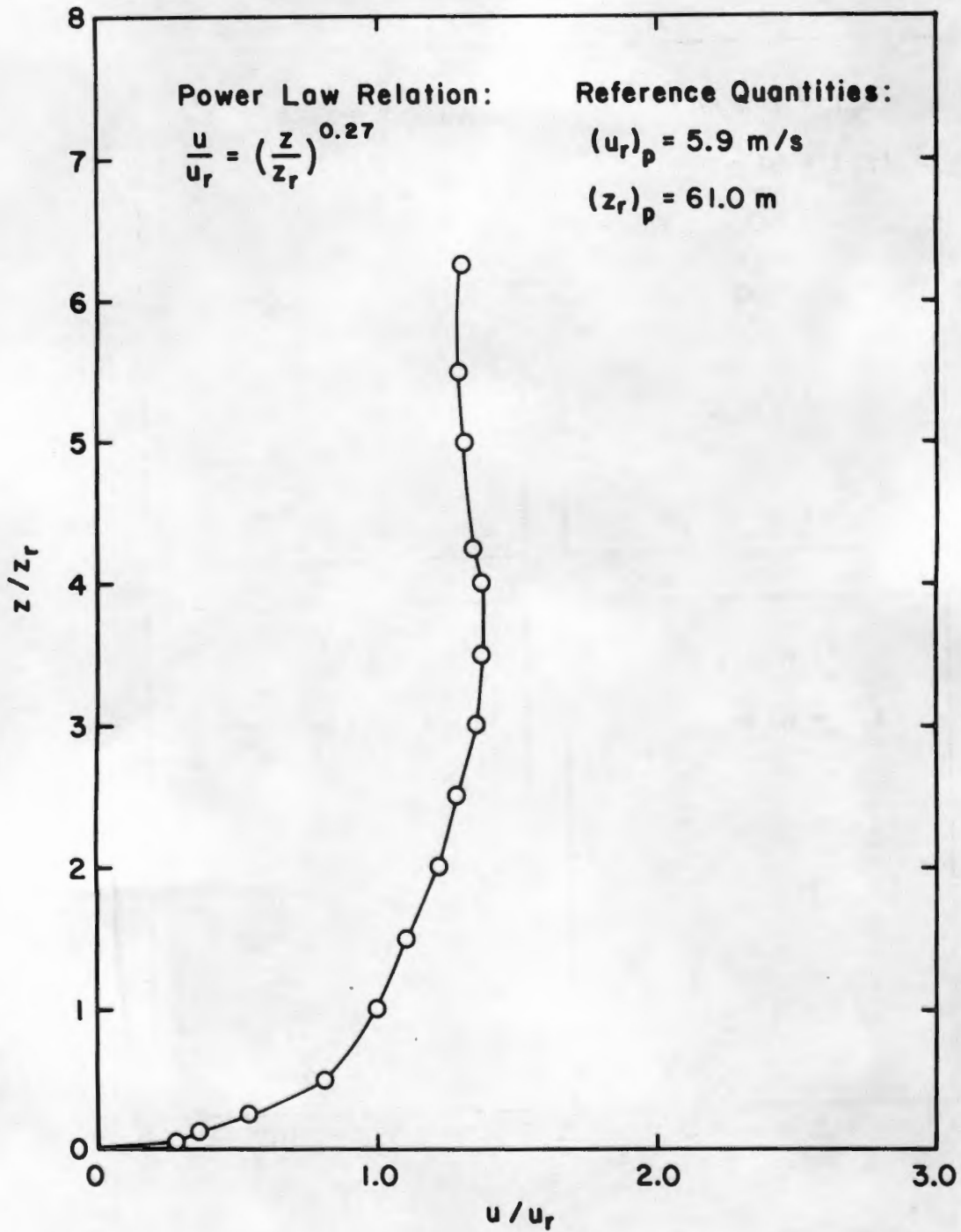


Figure 3.5-3. Velocity Profiles for E-stability

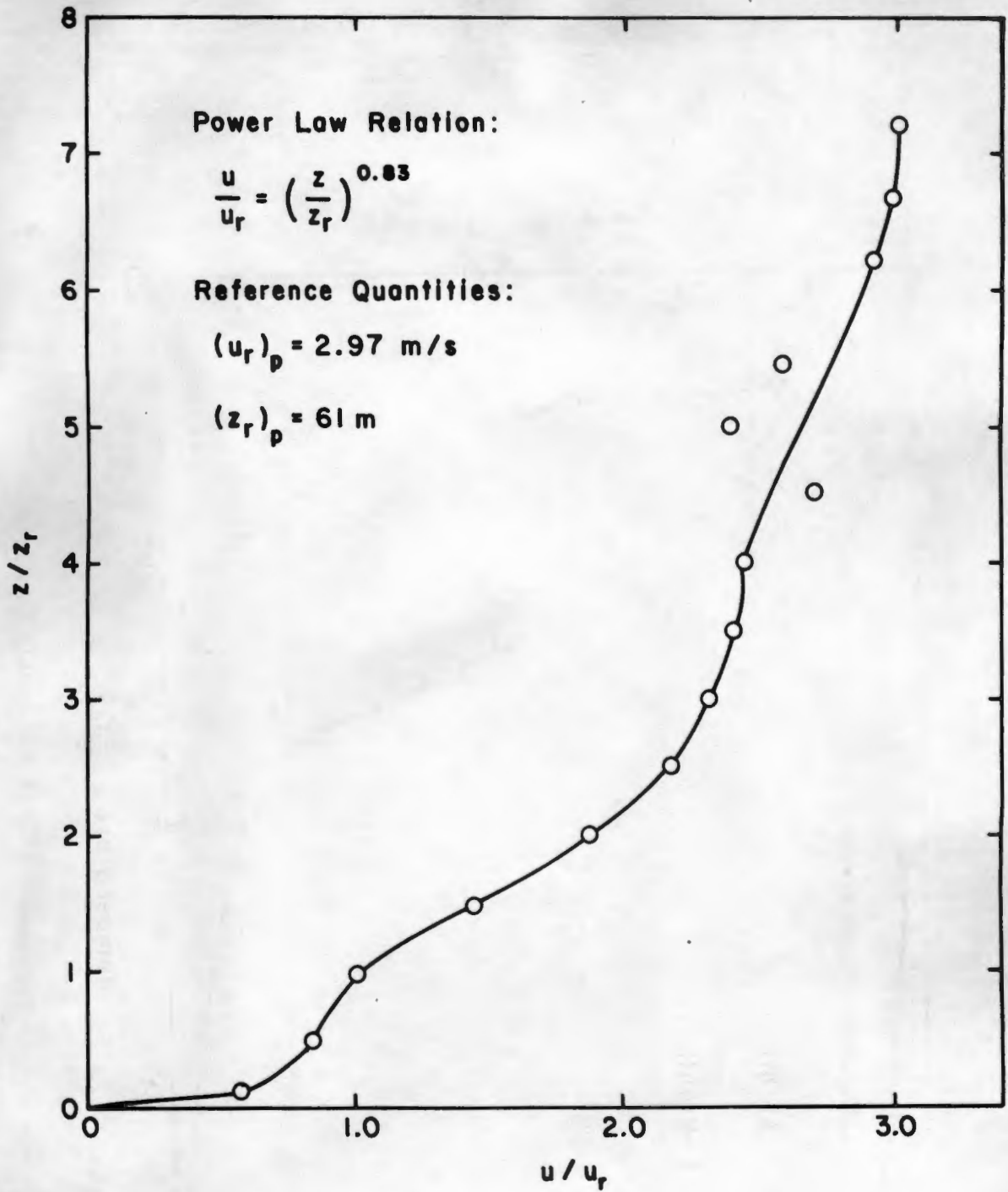


Figure 3.5-4. Velocity Profiles for F-stability

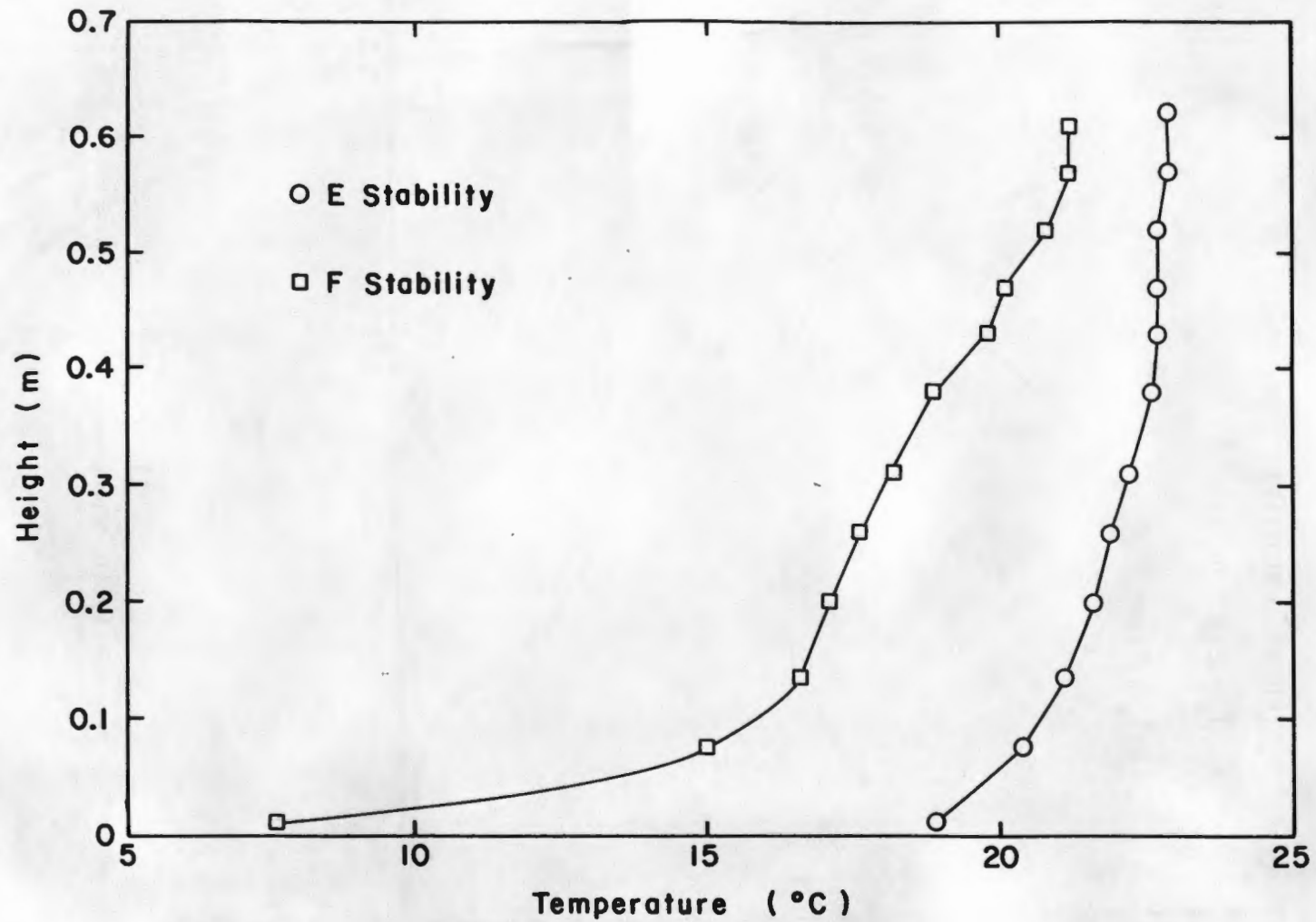


Figure 3.5-5. Temperature Profiles for Stable Conditions

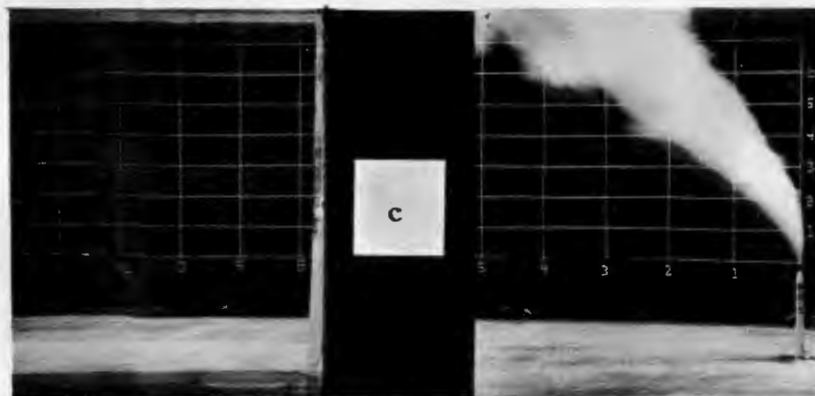
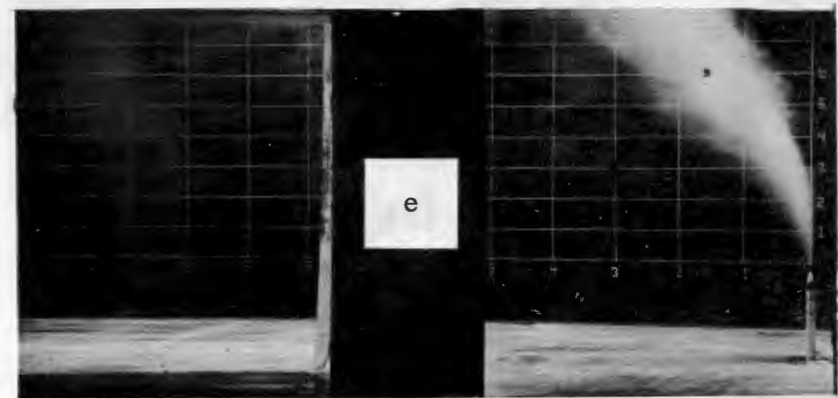
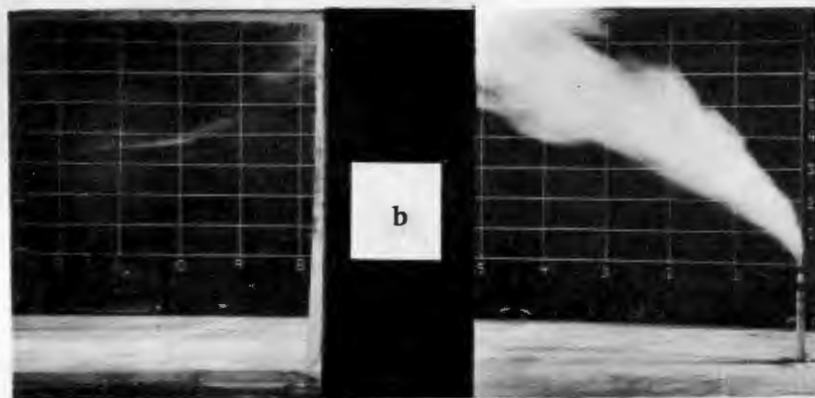
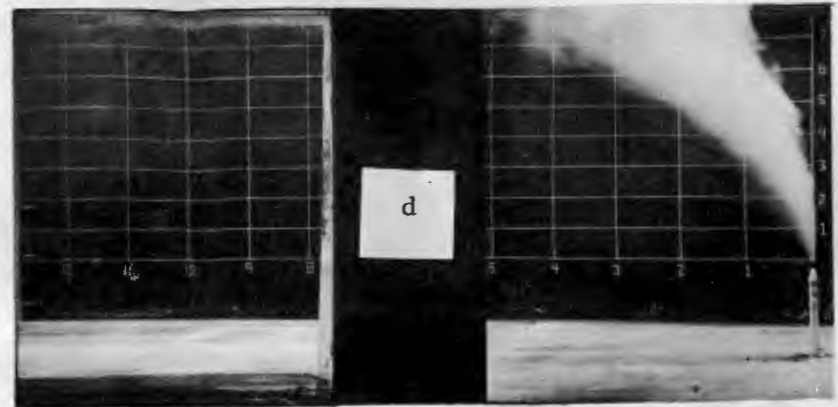


Figure 4.1-1. Plume visualization for neutral stability, a stack height wind speed of 2 m/s, a 388°K exit temperature, and exit velocities of a) 12.5 m/s, b) 30 m/s, c) 60 m/s, d) 120 m/s and e) 240 m/s.

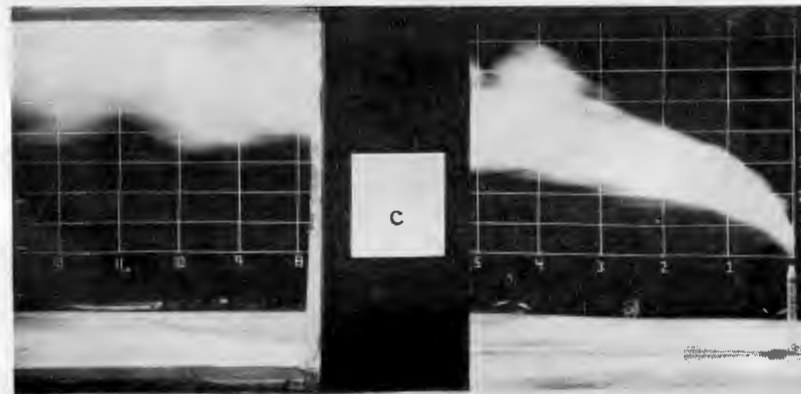
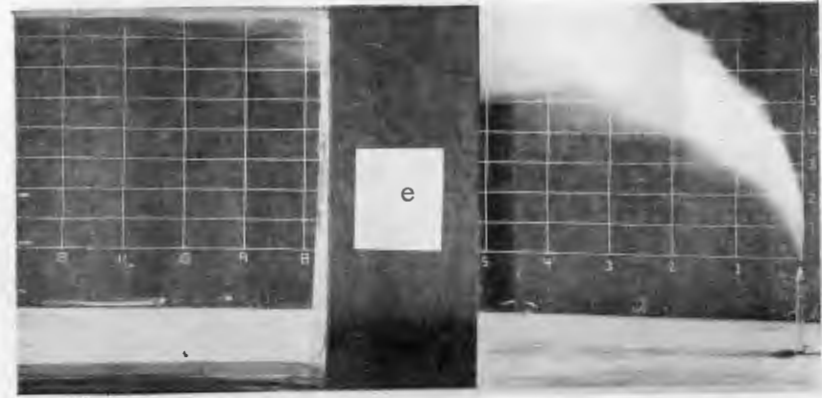
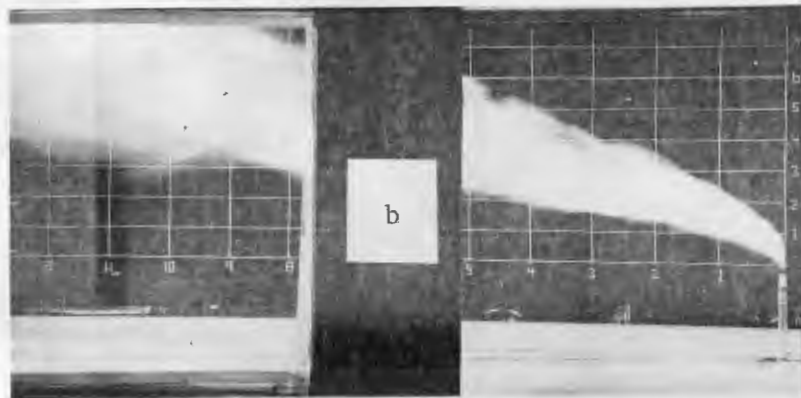
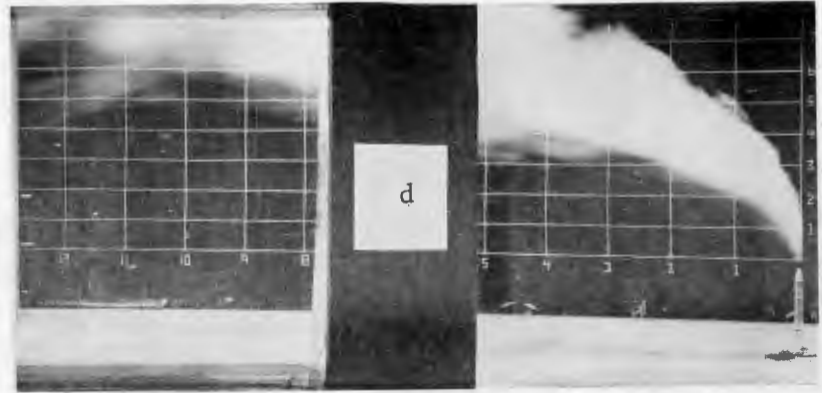
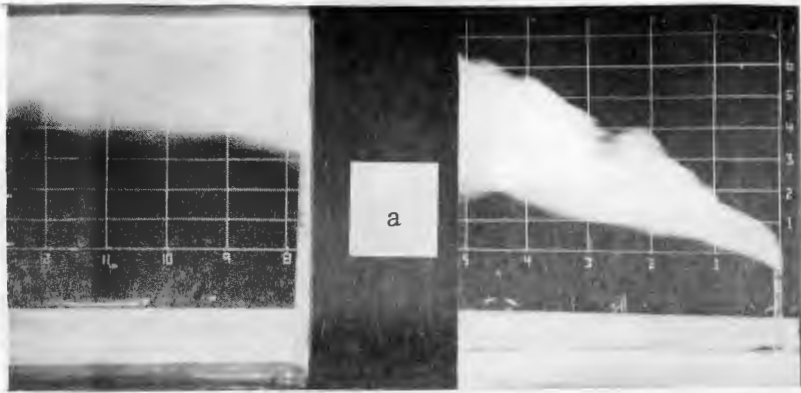


Figure 4.1-2. Plume visualization for neutral stability, a stack height wind speed of 4 m/s, a 388°K exit temperature, and exit velocities of a) 12.5 m/s, b) 30 m/s, c) 60 m/s, d) 120 m/s and e) 240 m/s.

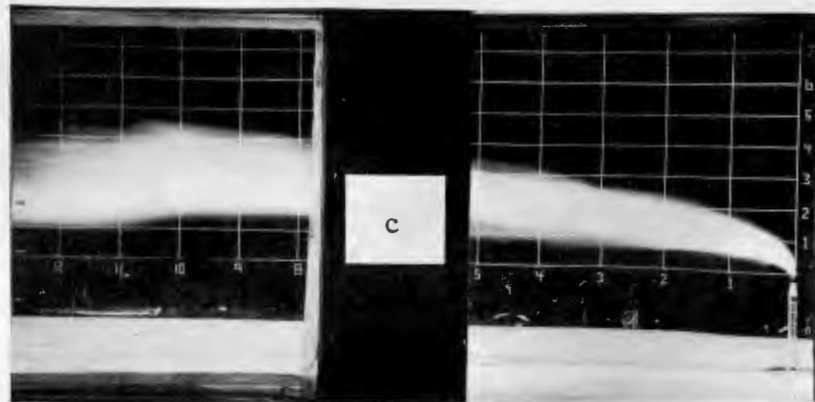
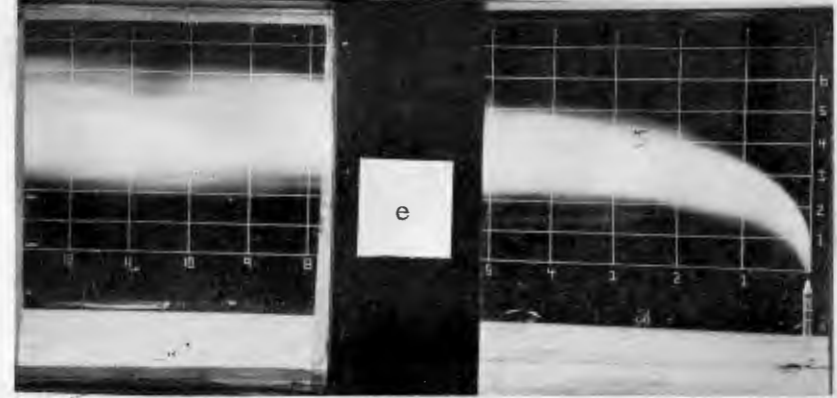
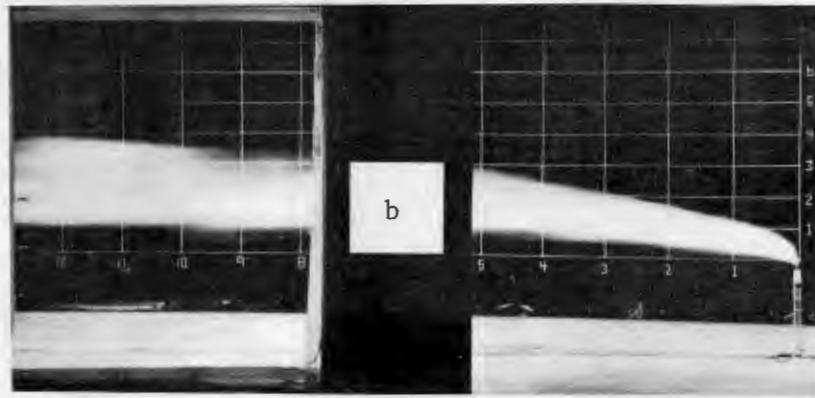
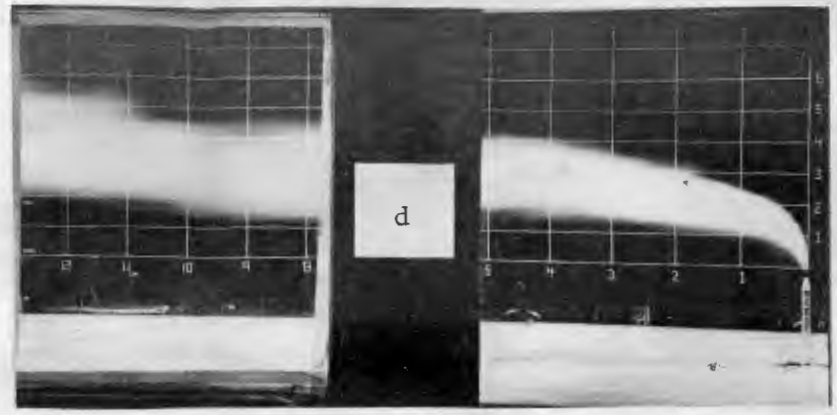
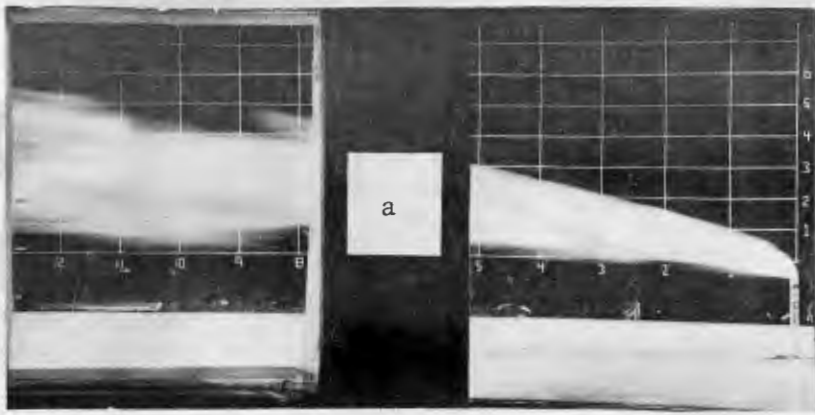


Figure 4.1-3. Plume visualization for neutral stability, a stack height wind speed of 8 m/s, a 388°K exit temperature, and exit velocities of a) 12.5 m/s, b) 30 m/s, c) 60 m/s, d) 120 m/s and e) 240 m/s.

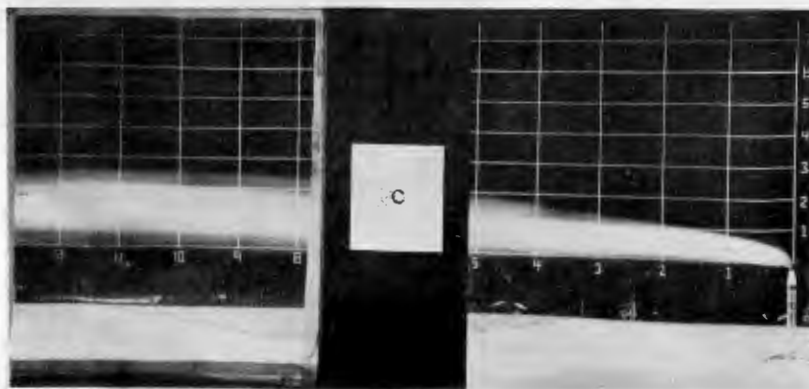
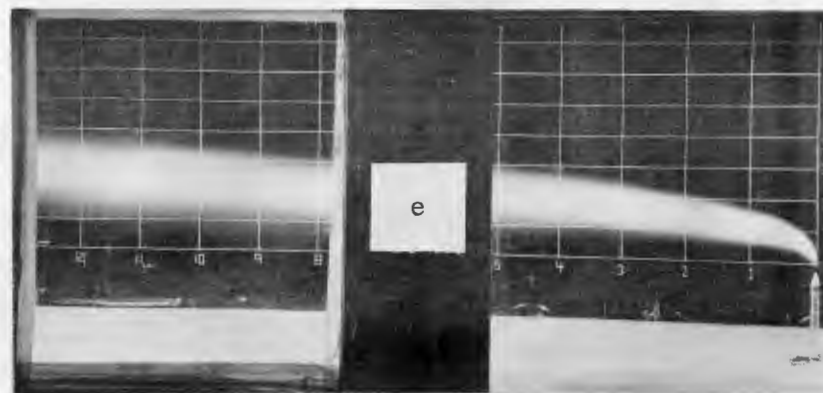
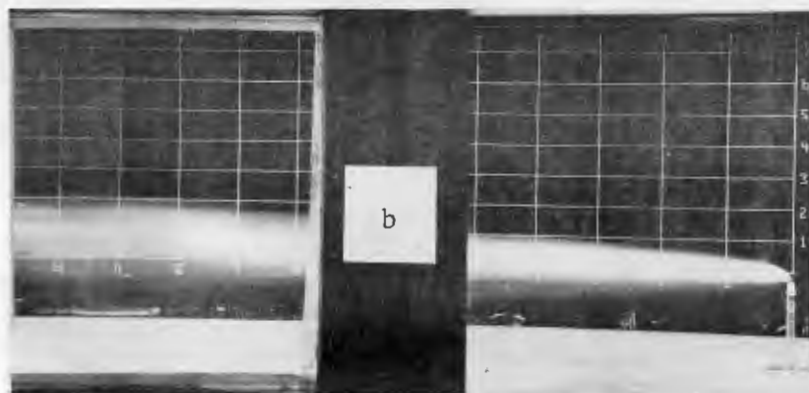
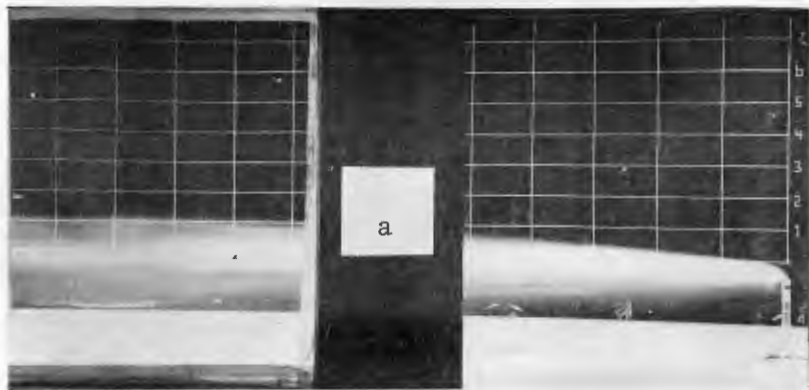


Figure 4.1-4. Plume visualization for neutral stability, a stack height wind speed of 16 m/s, a 388°K exit temperature, and exit velocities of a) 12.5 m/s, b) 30 m/s, c) 60 m/s, d) 120 m/s and e) 240 m/s.

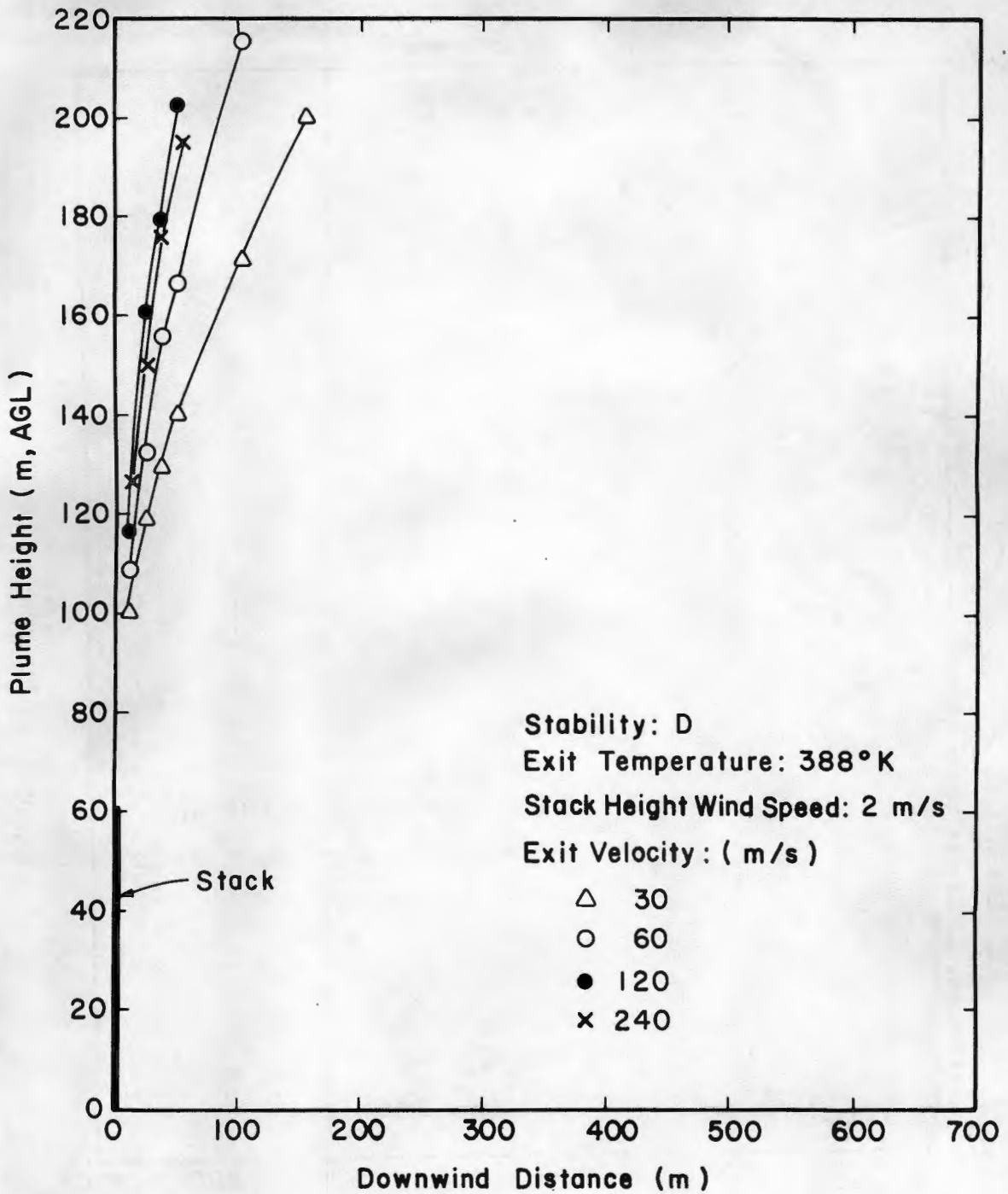


Figure 4.1-5a. Plume Centerline Trajectories for D-stability, a 388°K Exit Temperature, Various Exit Velocities and a Stack Height Wind Speed of 2 m/s

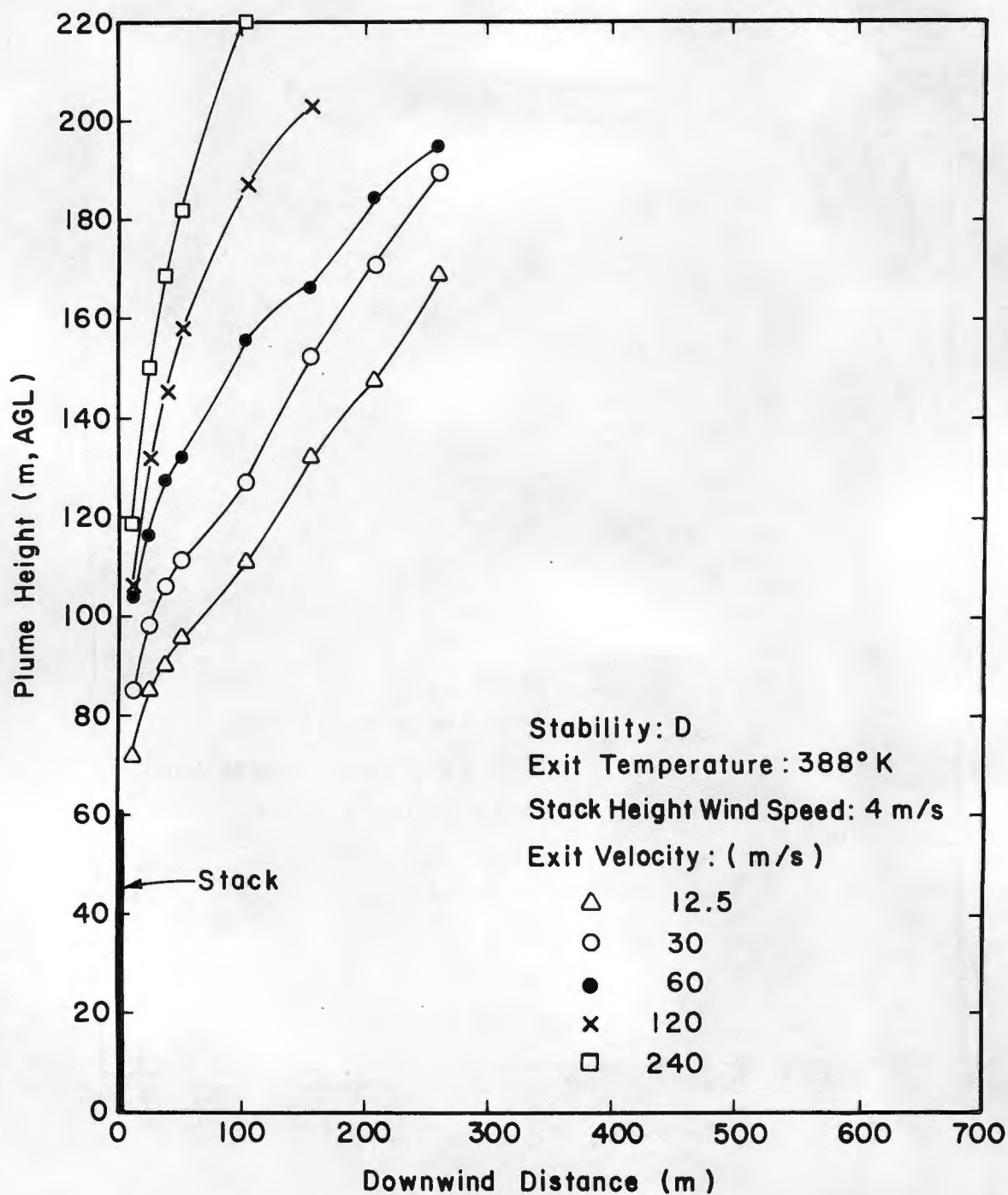


Figure 4.1-5b. Plume Centerline Trajectories for D-stability, a 388°K Exit Temperature, Various Exit Velocities and a Stack Height Wind Speed of 4 m/s

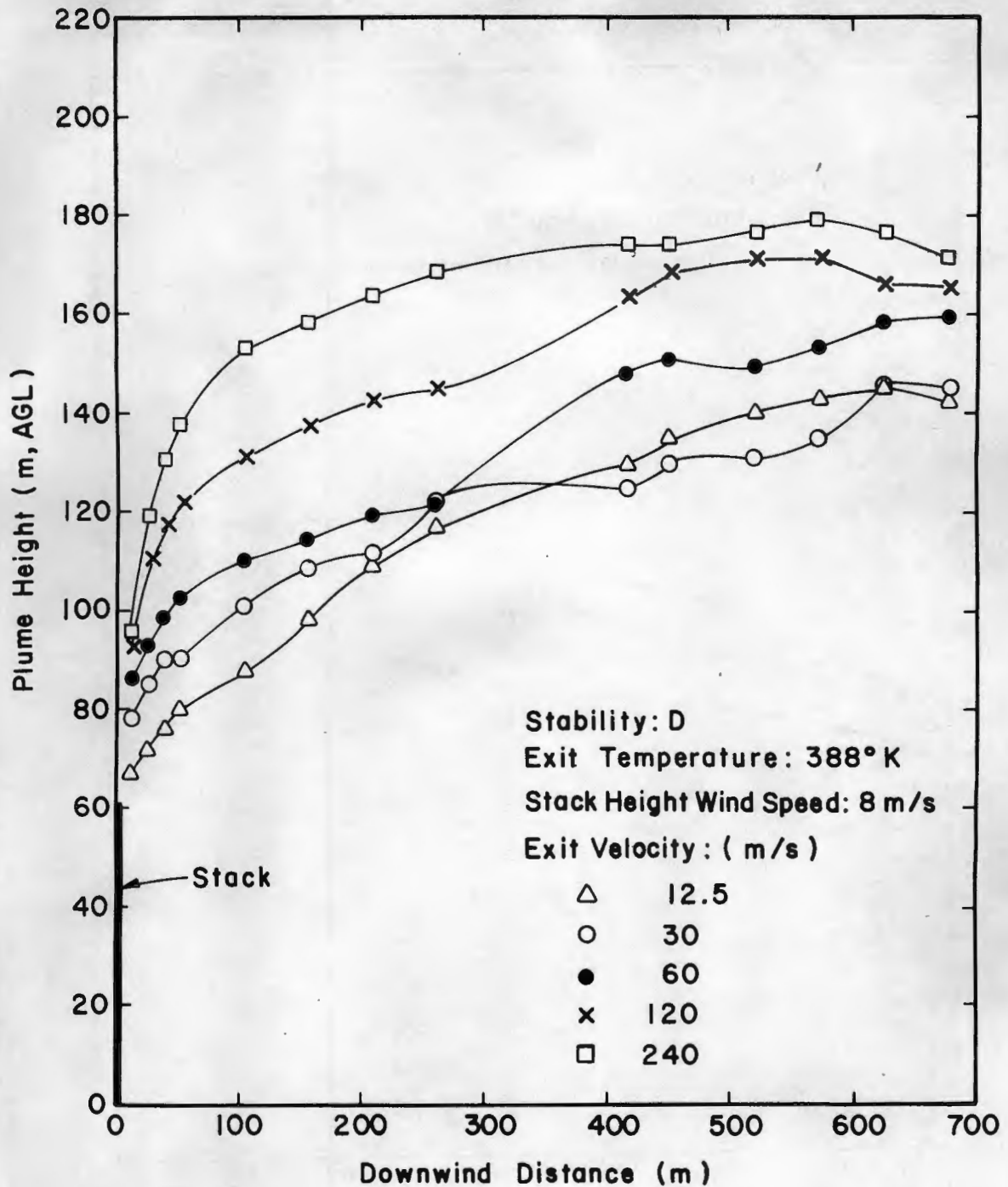


Figure 4.1-5c. Plume Centerline Trajectories for D-stability, a 388°K Exit Temperature, Various Exit Velocities and a Stack Height Wind Speed of 8 m/s

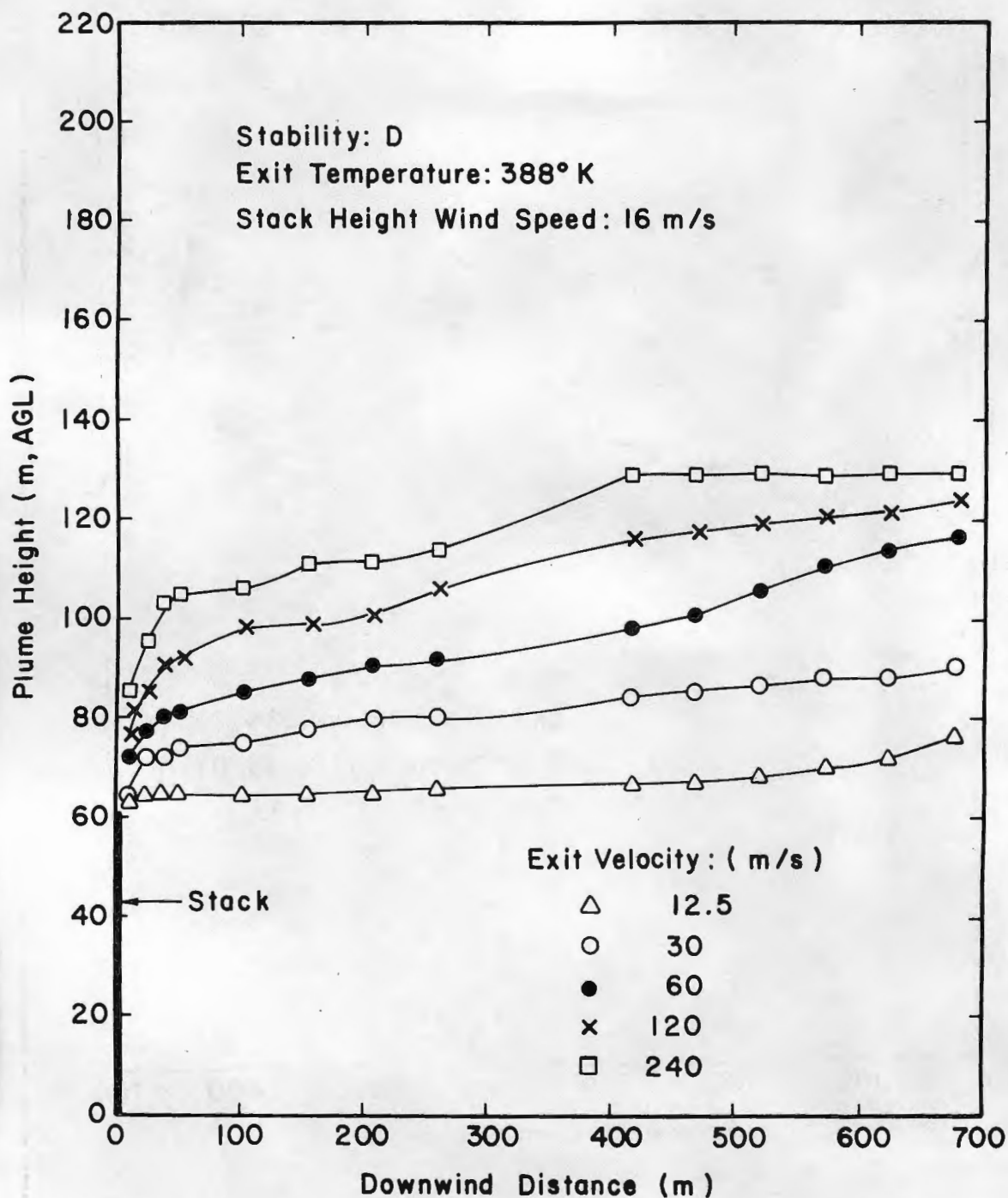


Figure 4.1-5d. Plume Centerline Trajectories for D-stability, a 388°K Exit Temperature Various Exit Velocities and a Stack Height Wind Speed of 8 m/s

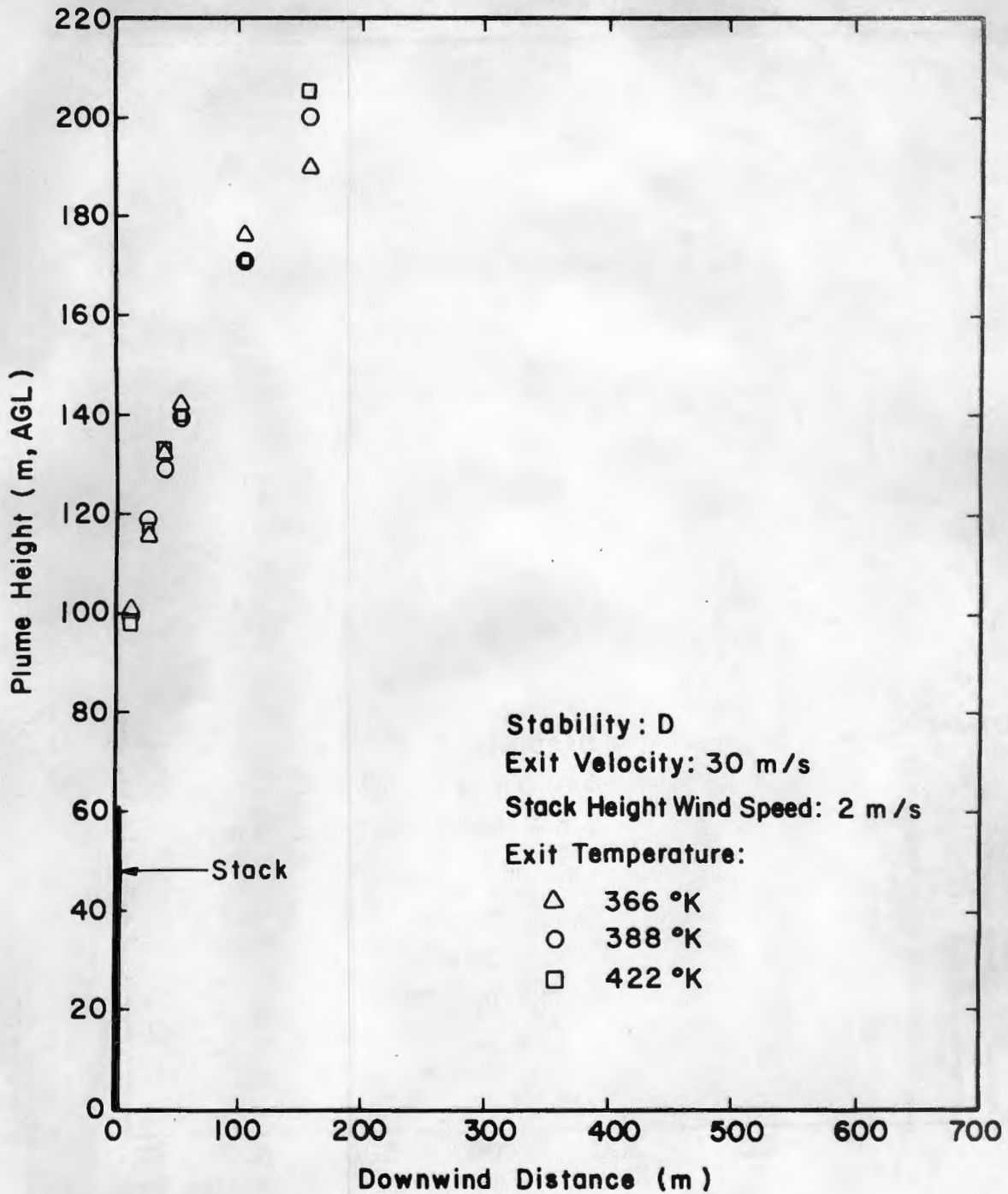


Figure 4.1-6a. Plume Centerline Trajectories for D-stability, a 30 m/s Exit Velocity, Three Exit Temperatures and a Stack Height Wind Speed of 2 m/s

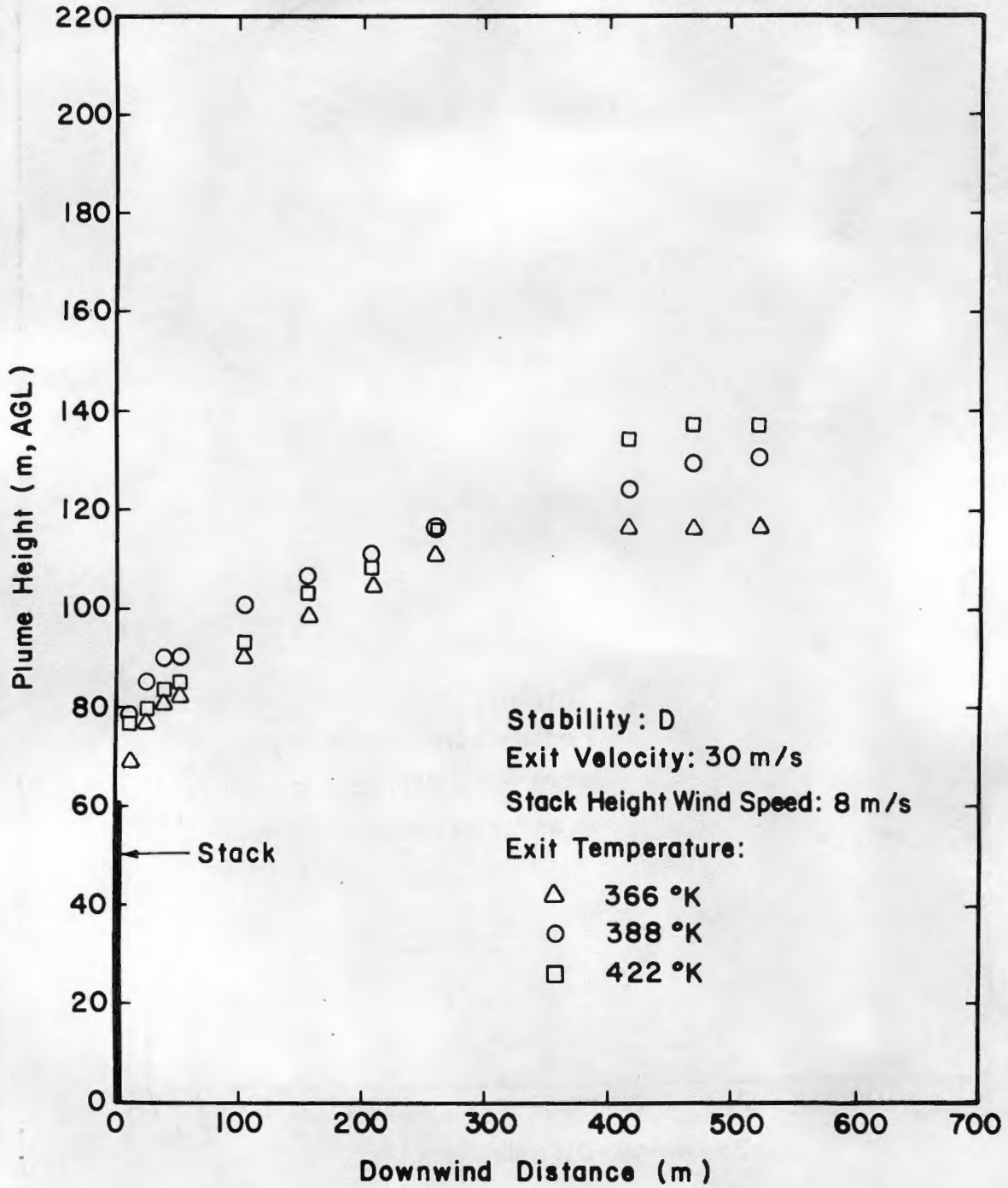


Figure 4.1-6b. Plume Centerline Trajectories for D-stability, a 30 m/s Exit Velocity, Three Exit Temperatures and a Stack Height Wind Speed of 8 m/s

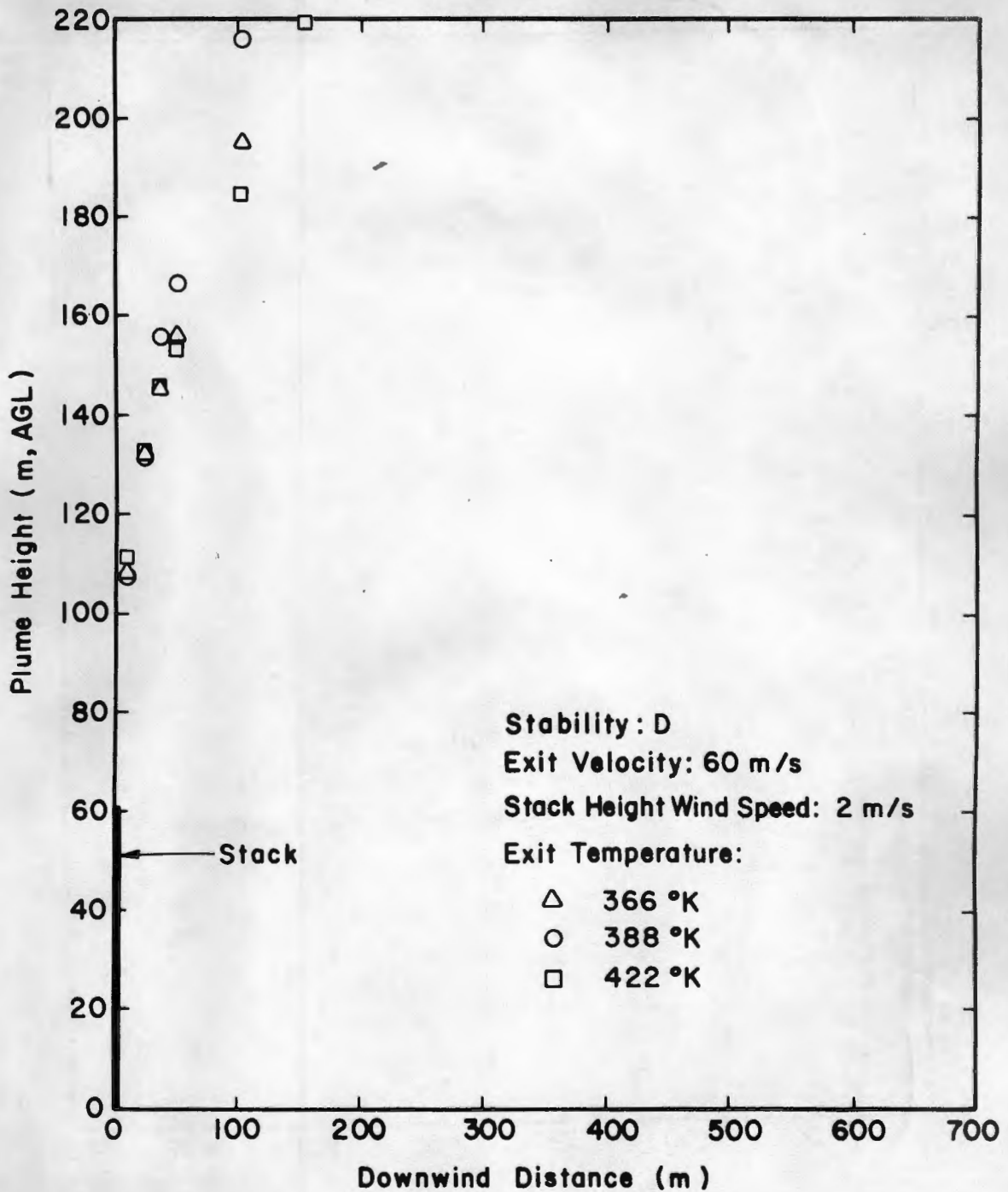


Figure 4.1-7a. Plume Centerline Trajectories for D-stability, a 60 m/s Exit Velocity, Three Exit Temperatures and a Stack Height Wind Speed of 2 m/s

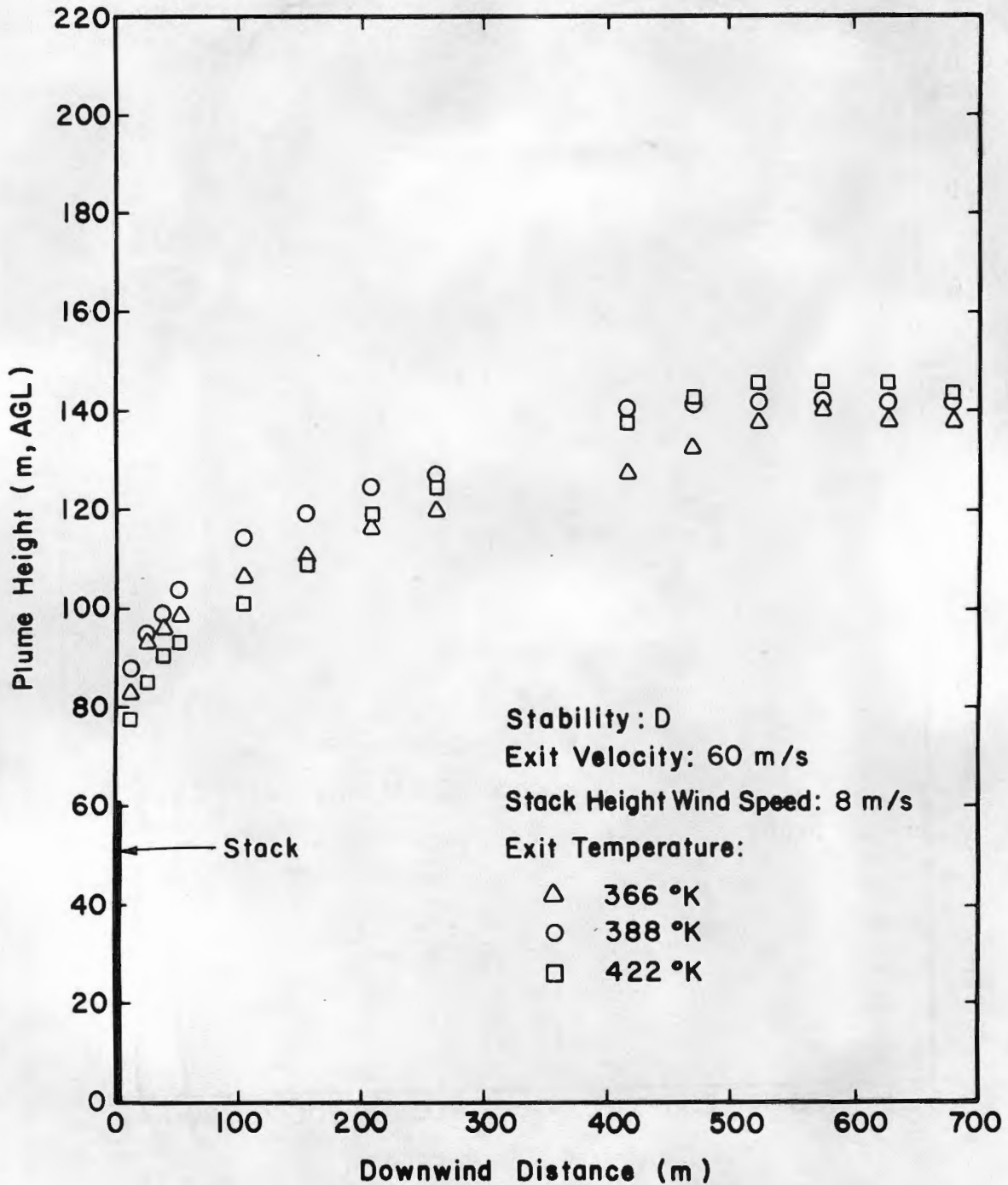


Figure 4.1-7b. Plume Centerline Trajectories for D-stability, a 60 m/s Exit Velocity, Three Exit Temperatures and a Stack Height Wind Speed of 8 m/s

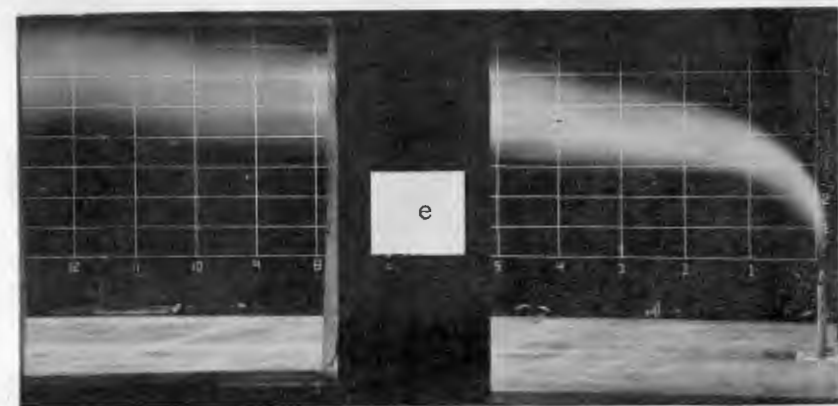
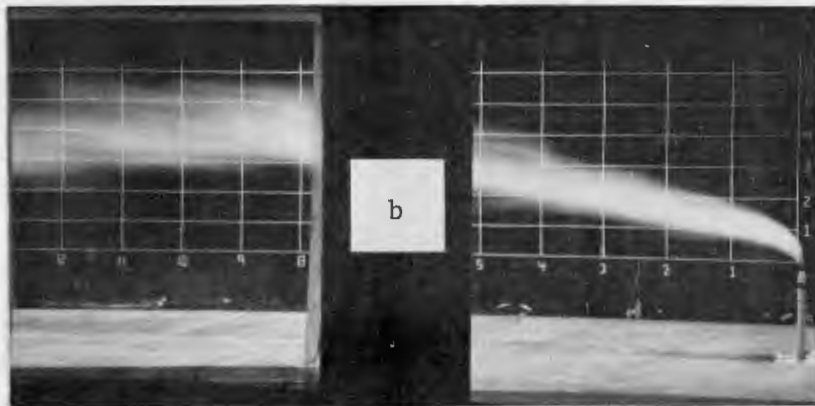
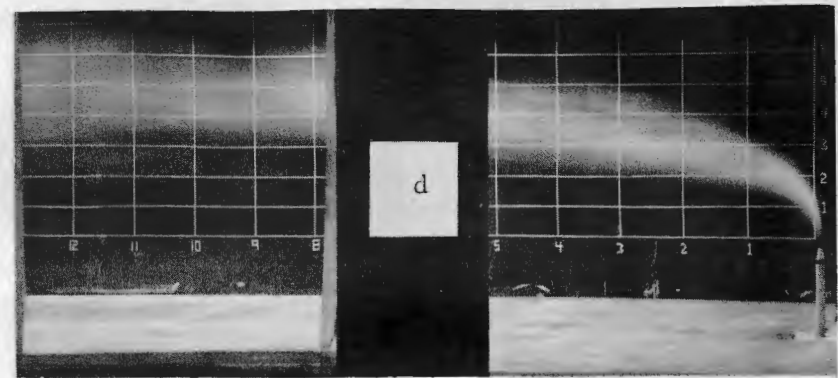


Figure 4.1-8. Plume visualization for E-stability, a stack height wind speed of 5.9 m/s, a 366°K exit temperature, and exit velocities of a) 12.5 m/s, b) 30 m/s, c) 60 m/s, d) 120 m/s and e) 240 m/s.

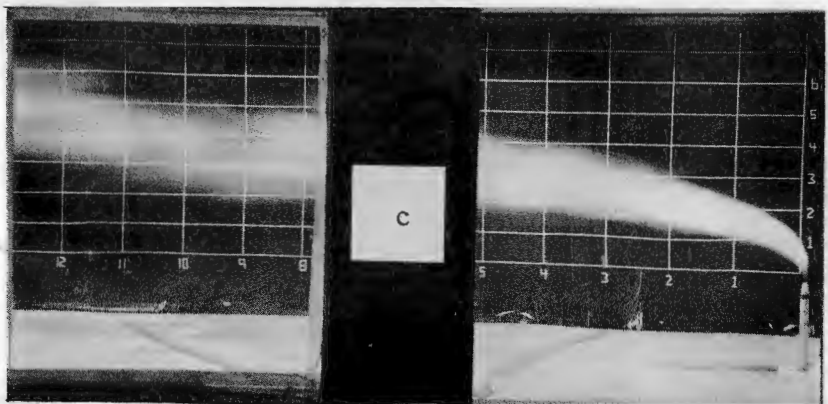
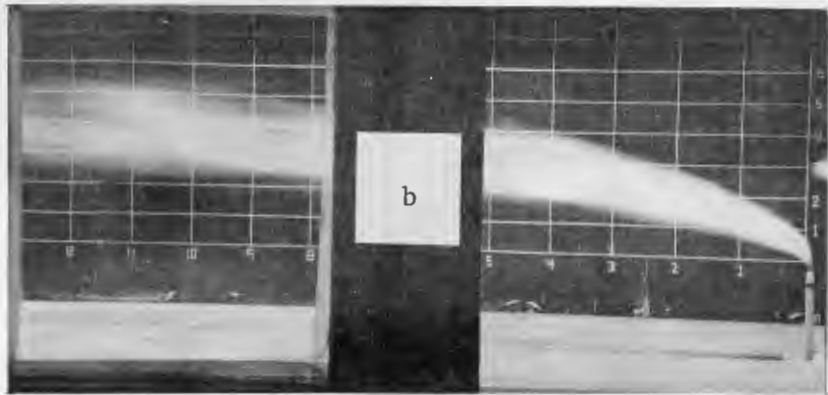
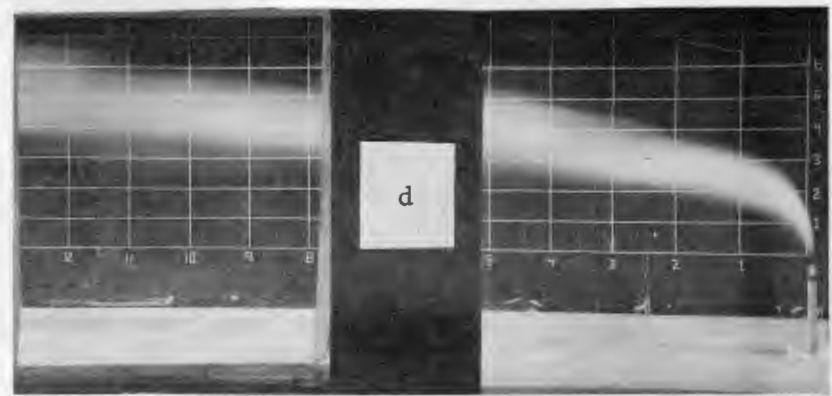


Figure 4.1-9. Plume visualization for E-stability, a stack height wind speed of 5.9 m/s, a 388°K exit temperature, and exit velocities of a) 12.5 m/s, b) 30 m/s, c) 60 m/s, d) 120 m/s and e) 240 m/s.

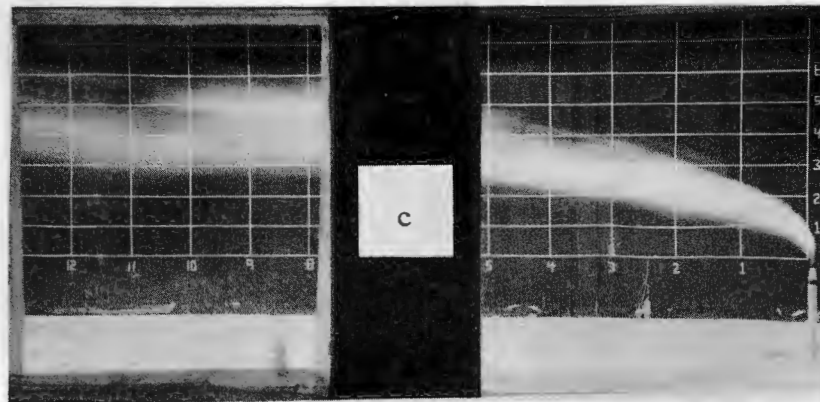
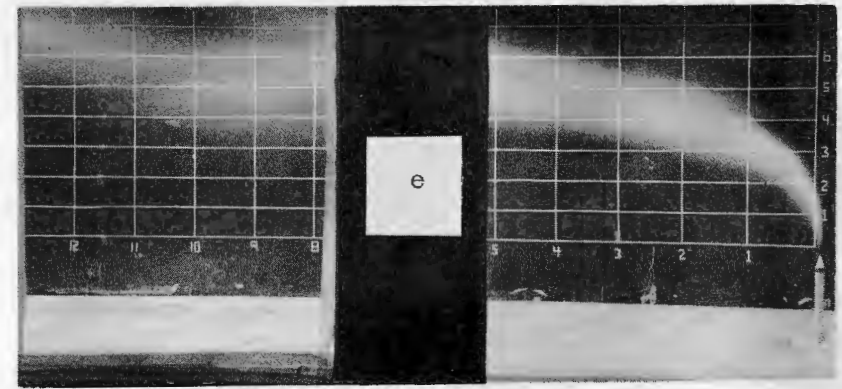
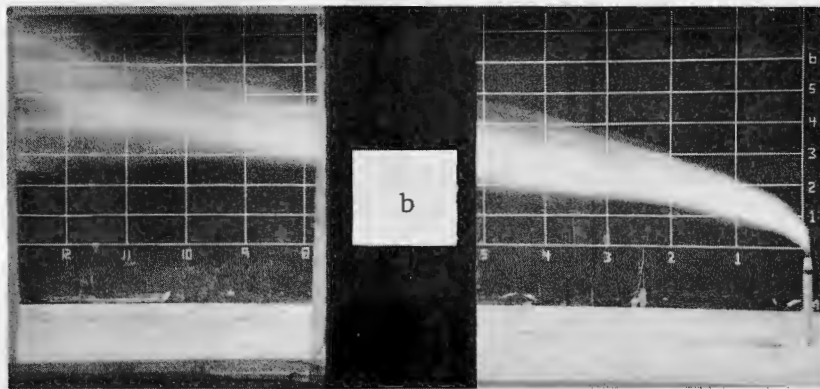
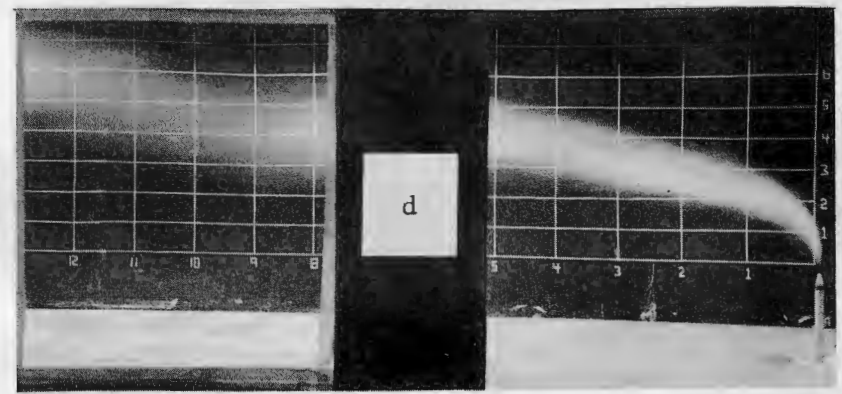
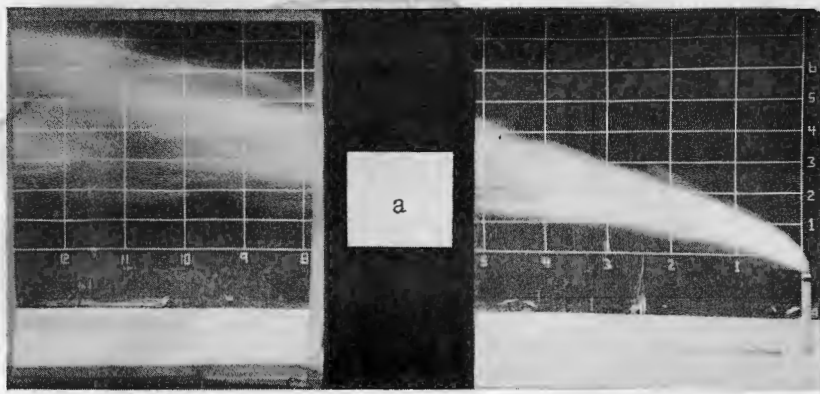


Figure 4.1-10. Plume visualization for E-stability, a stack height wind speed of 5.9 m/s, a 422°K exit temperature, and exit velocities of a) 12.5 m/s, b) 30 m/s, c) 60 m/s, d) 120 m/s and e) 240 m/s.

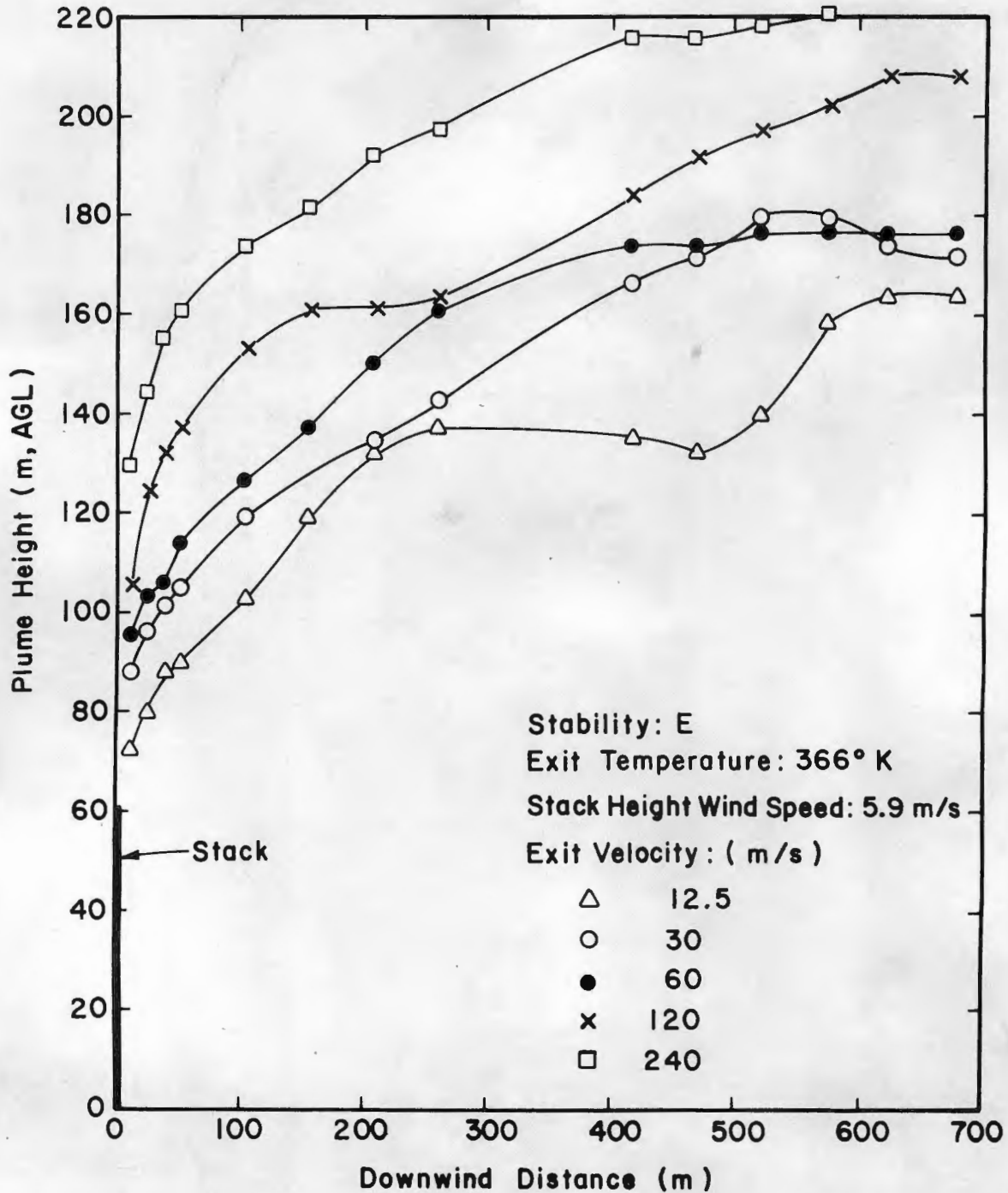


Figure 4.1-11a. Plume Centerline Trajectories for E-stability, a Stack Height Wind Speed of 5.9 m/s, Various Exit Velocities and an Exit Temperature of 366°K

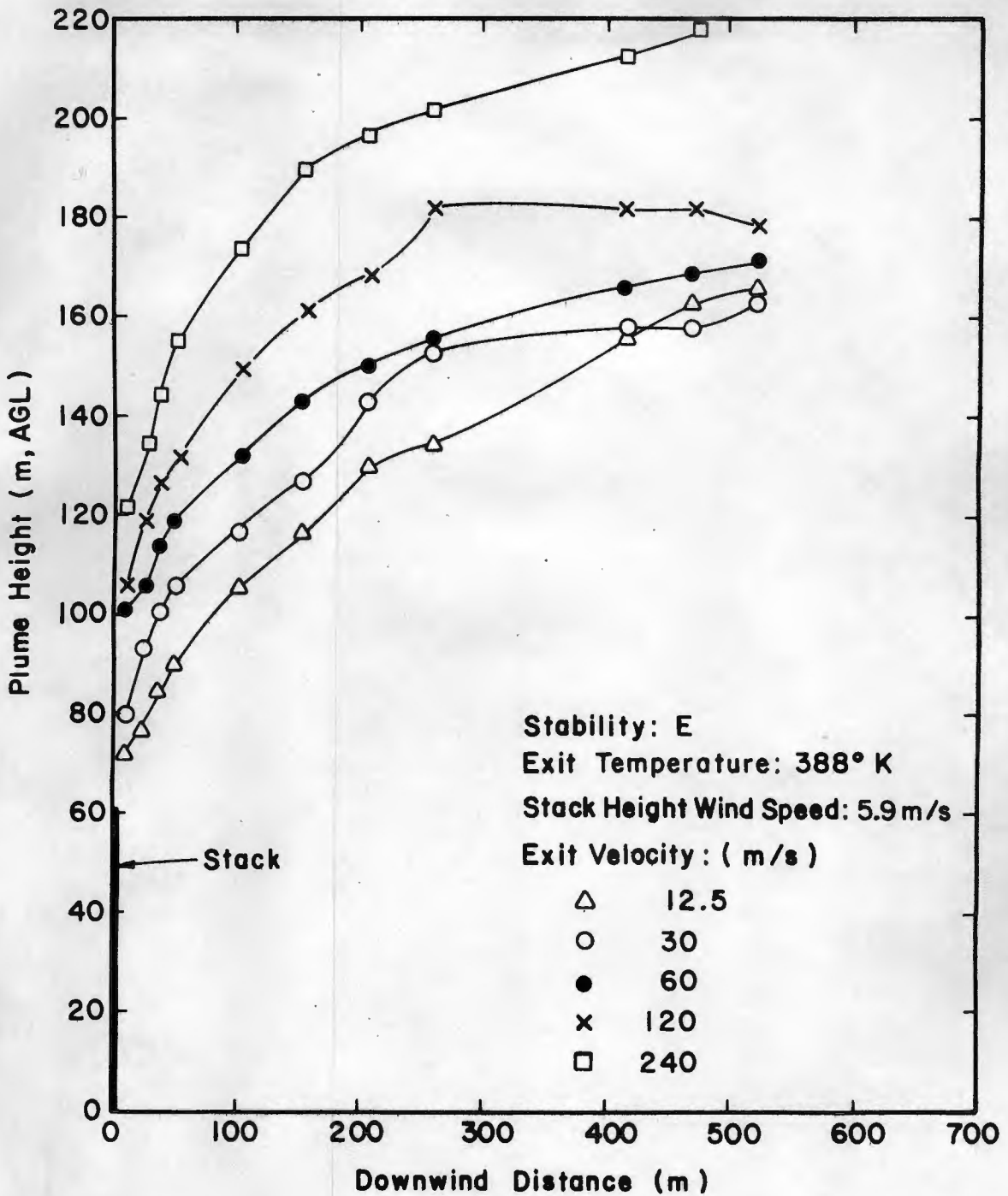


Figure 4.1-11b. Plume Centerline Trajectories for E-stability, a Stack Height Wind Speed of 5.9 m/s, Various Exit Velocities and an Exit Temperature of 388°K

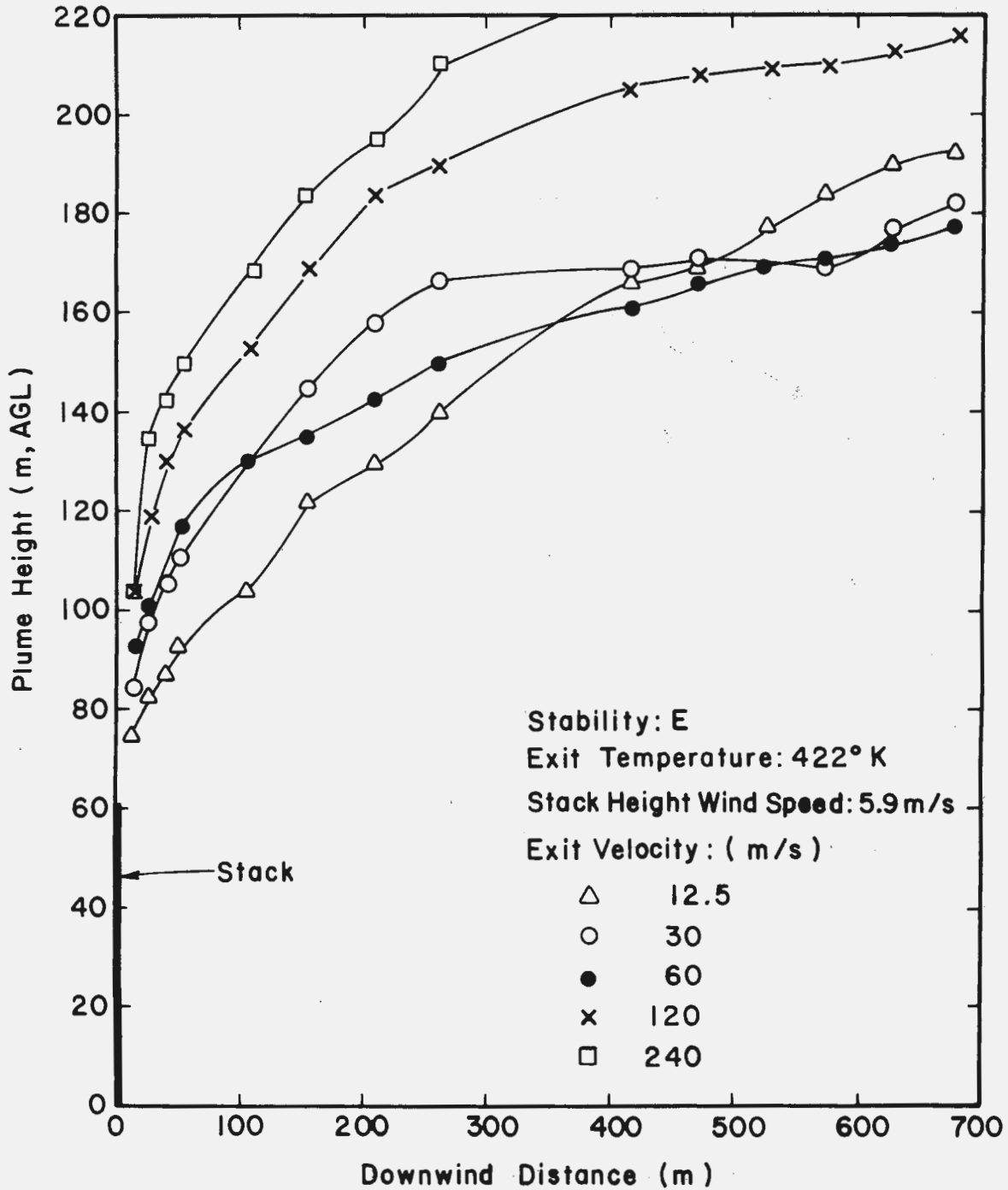


Figure 4.1-11c. Plume Centerline Trajectories for E-stability, a Stack Height Wind Speed of 5.9 m/s, Various Exit Velocities and an Exit Temperature of 422°K

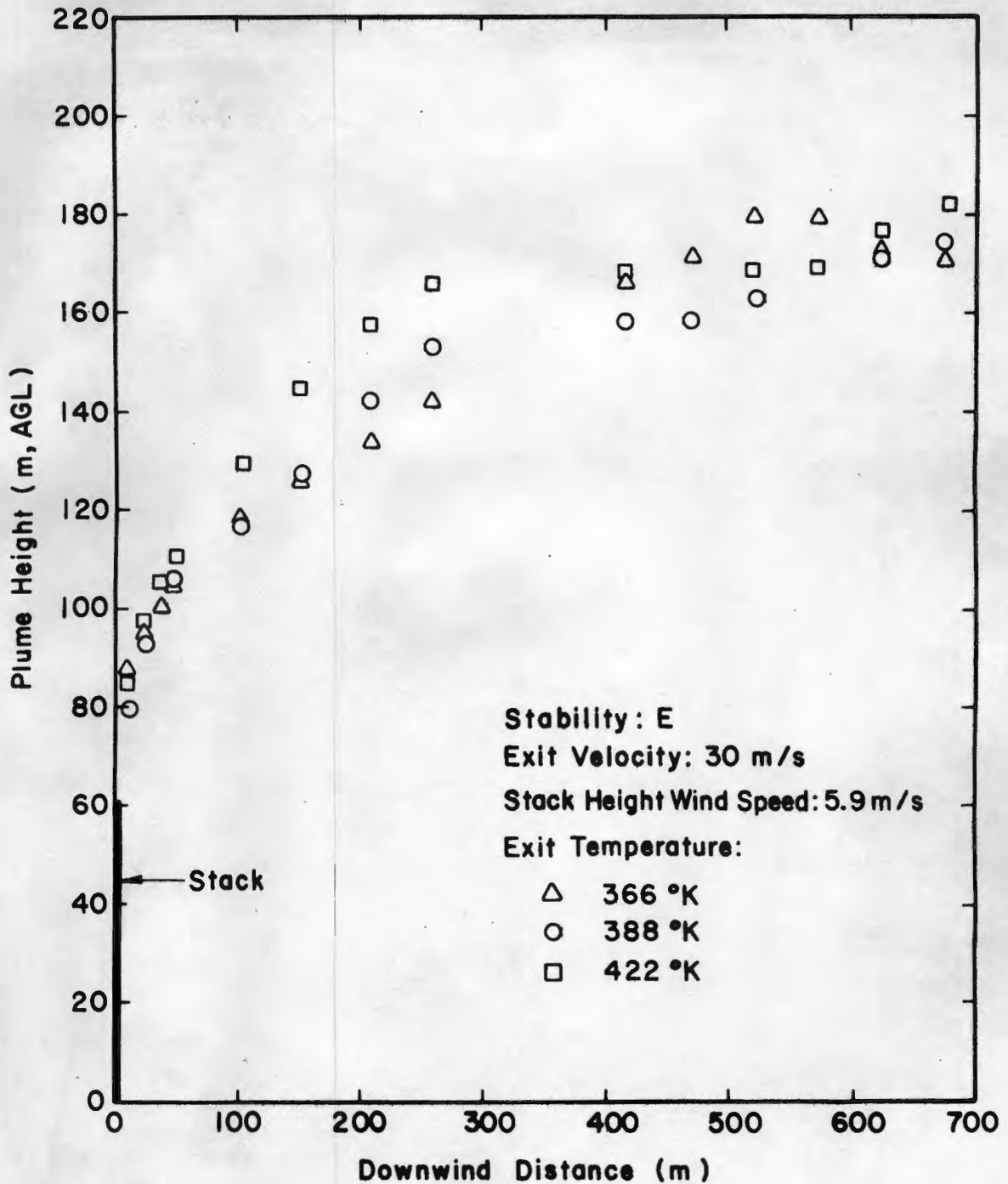


Figure 4.1-12a. Plume Centerline Trajectories for E-stability, a Stack Height Wind Speed of 5.9 m/s, Three Exit Temperatures and an Exit Velocity of 30 m/s.

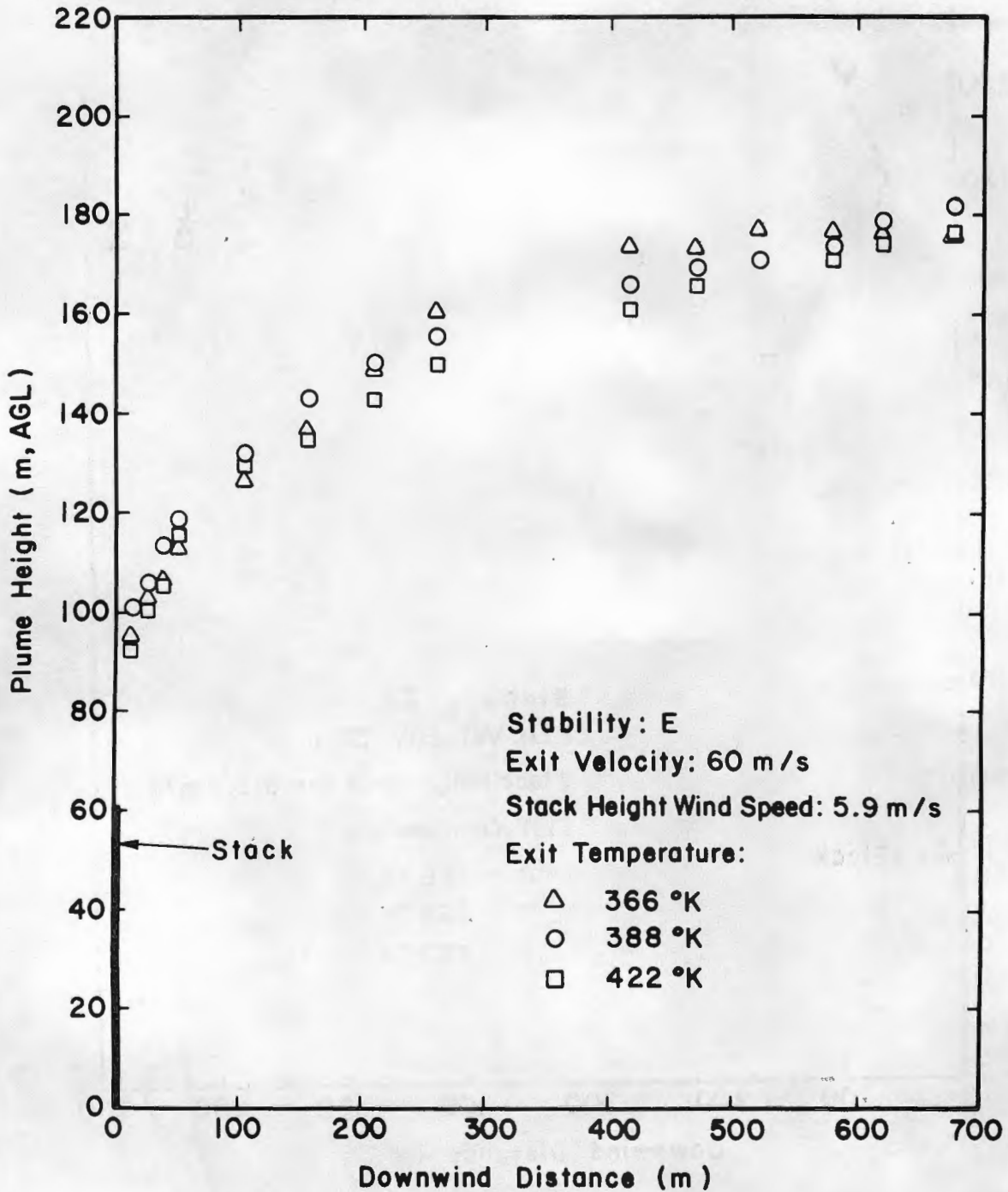
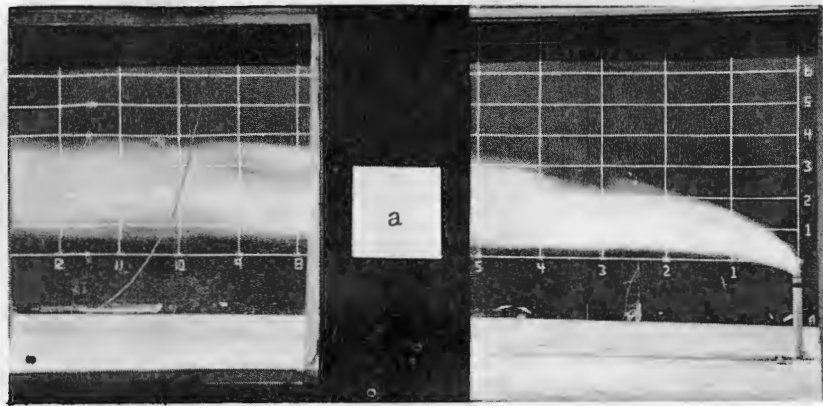
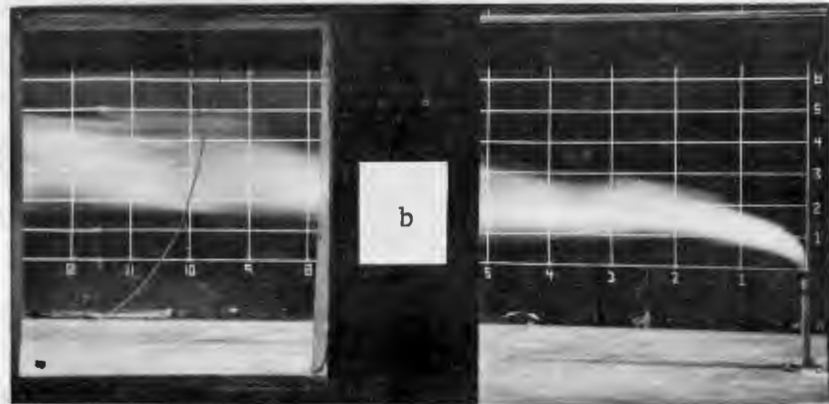


Figure 4.1-12b. Plume Centerline Trajectories for E-stability, a Stack Height Wind Speed of 5.9 m/s, Three Exit Temperatures and an Exit Velocity of 60 m/s



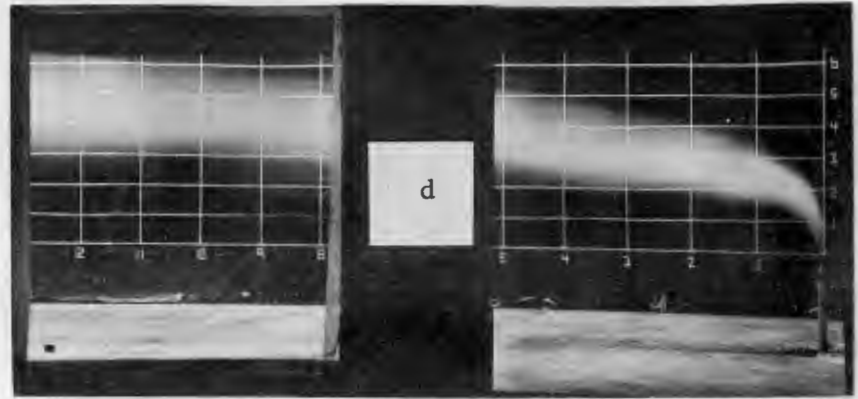
a



b



c



d



e

Figure 4.1-13. Plume visualization for F-stability, a stack height wind speed of 3.0 m/s, a 366°K exit temperature, and exit velocities of a) 12.5 m/s, b) 30 m/s, c) 60 m/s, d) 120 m/s and e) 240 m/s.

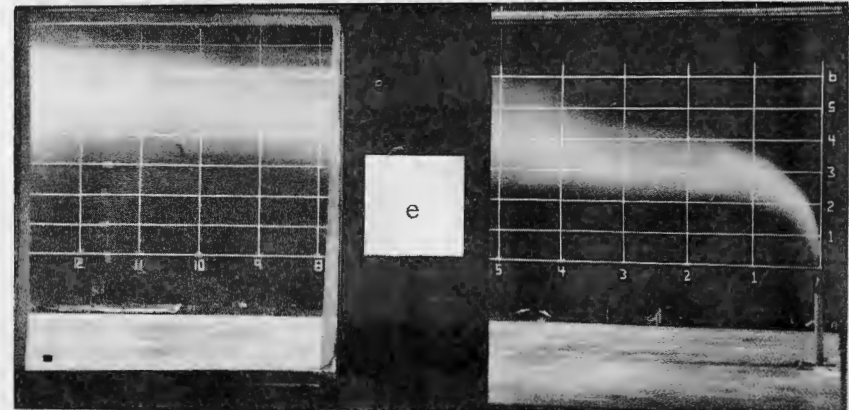
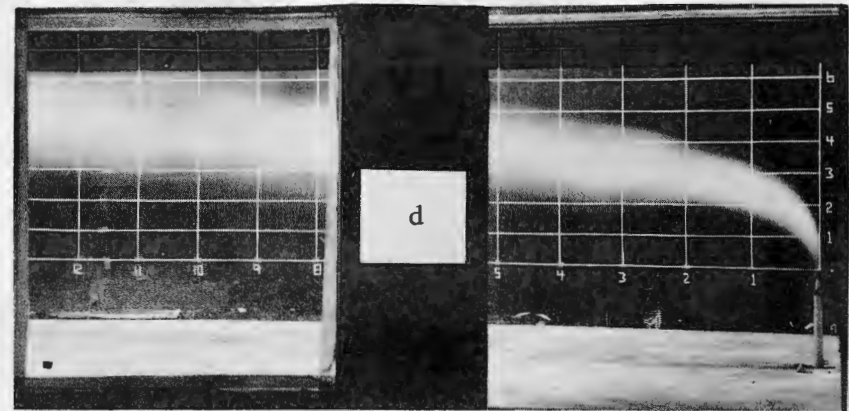
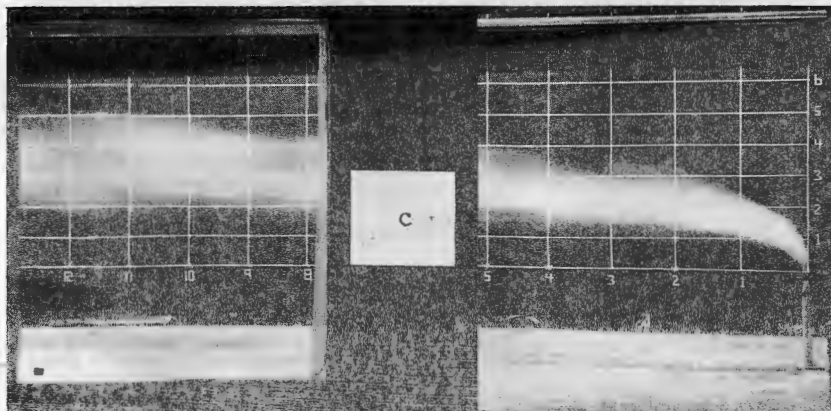
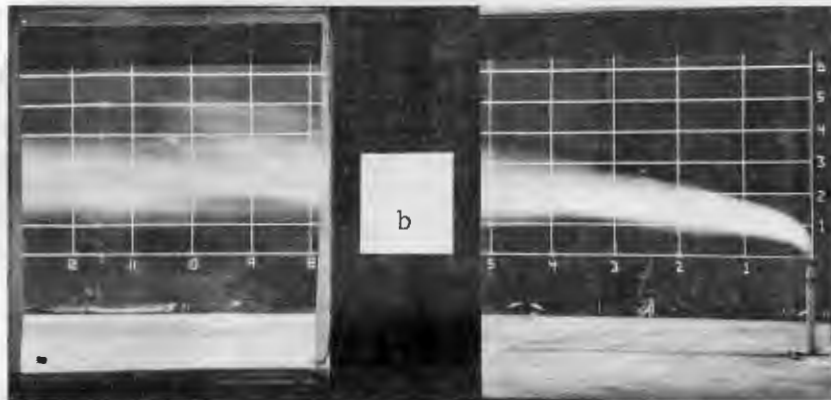
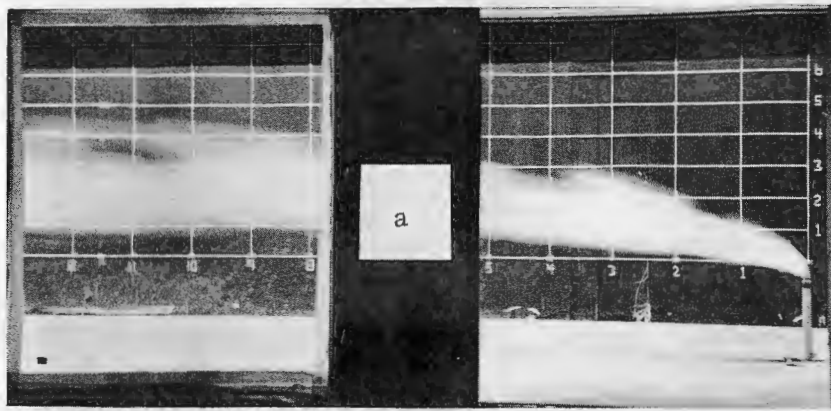


Figure 4.1-14. Plume visualization for F-stability, a stack height wind speed of 3.0 m/s, a 388°K exit temperature, and exit velocities of a) 12.5 m/s, b) 30 m/s, c) 60 m/s, d) 120 m/s and e) 240 m/s.

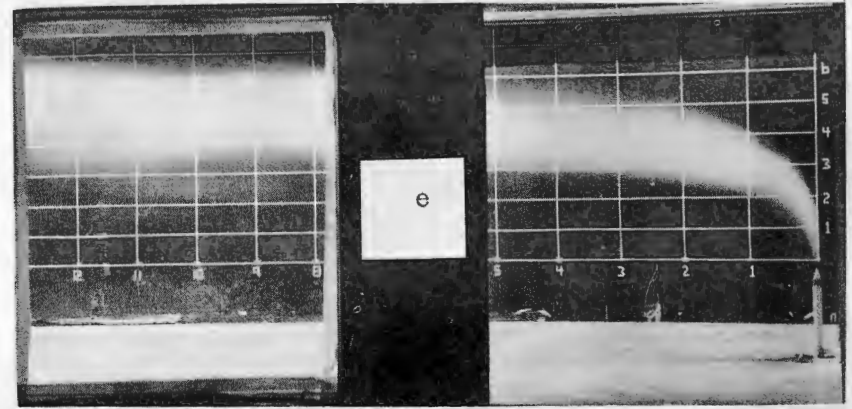
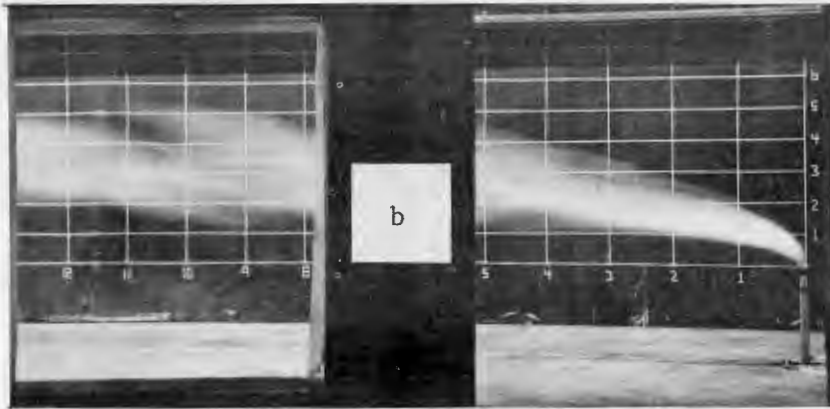
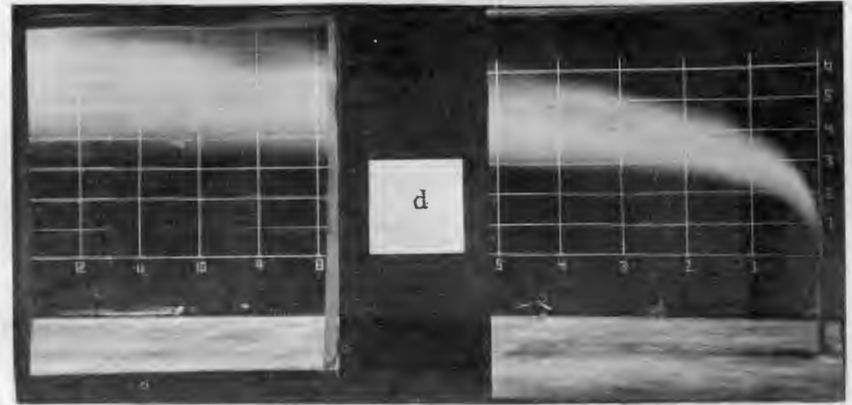


Figure 4.1-15. Plume visualization for F-stability, a stack height wind speed of 3.0 m/s, a 422°K exit temperature, and exit velocities of a) 12.5 m/s, b) 30 m/s, c) 60 m/s, d) 120 m/s and e) 240 m/s.

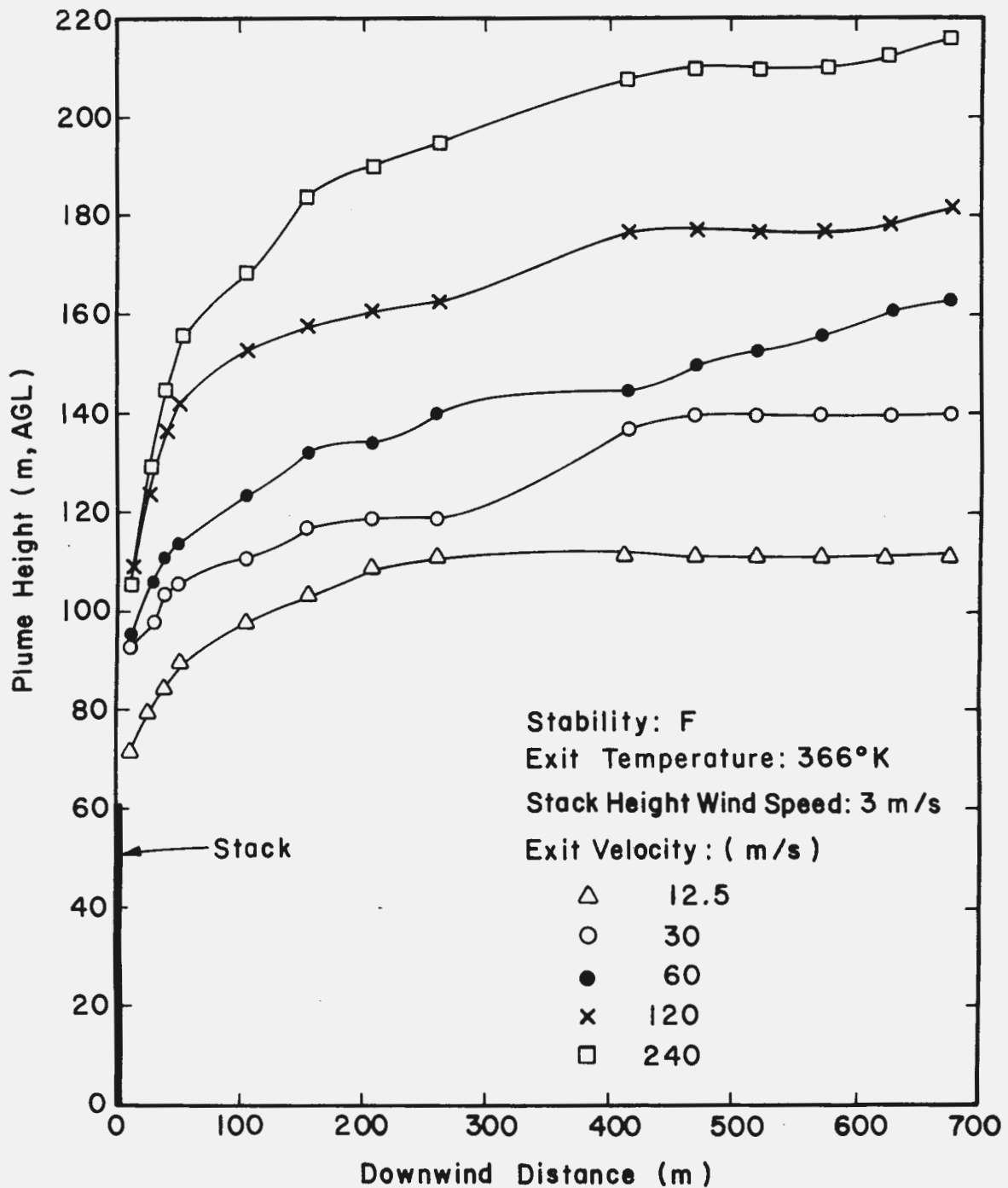


Figure 4.1-16a. Plume Centerline Trajectories for F-stability, a Stack Height Wind Speed of 3.0 m/s, Various Exit Velocities and an Exit Temperature of 366°K

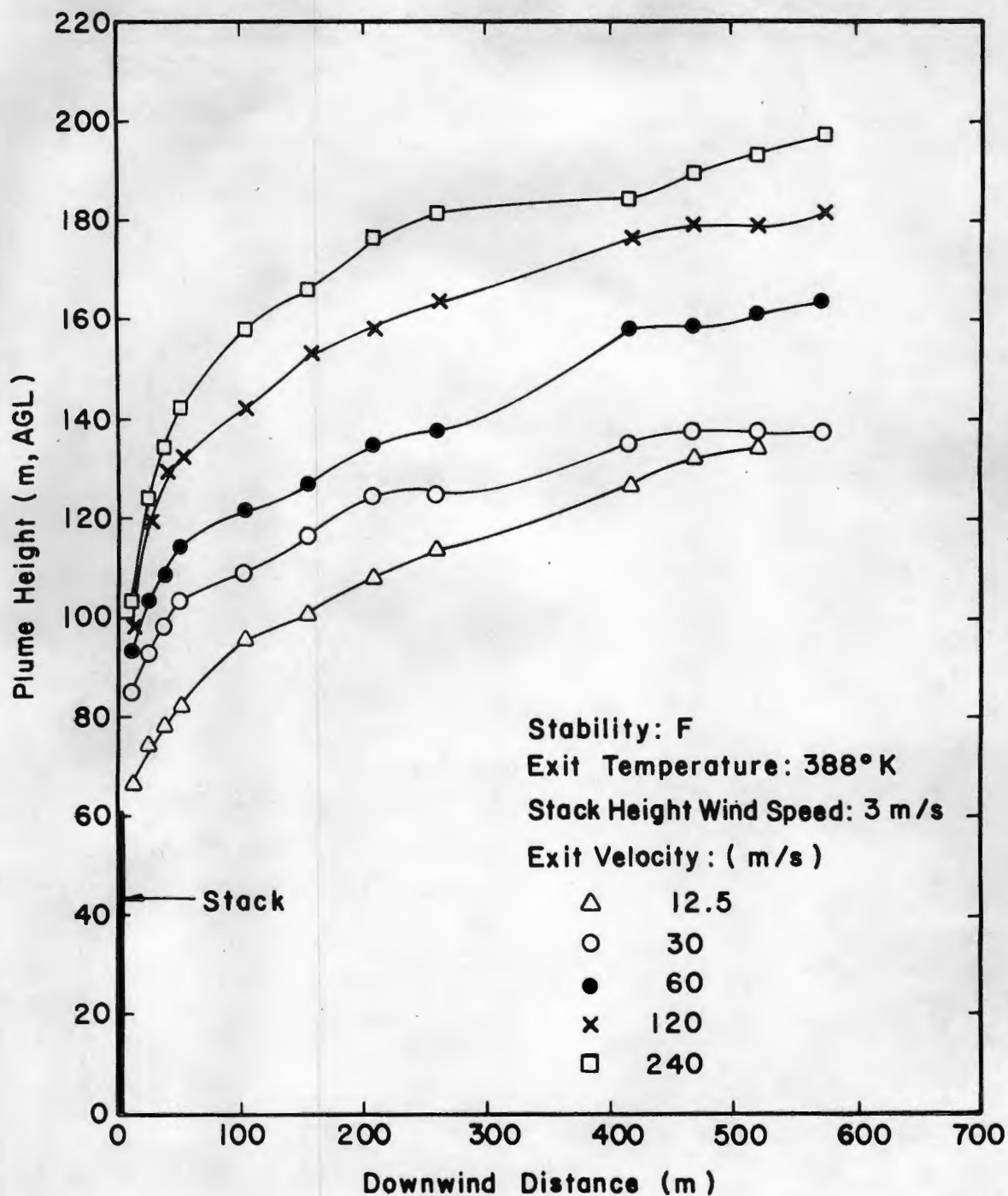


Figure 4.1-16b. Plume Centerline Trajectories for F-stability, a Stack Height Wind Speed of 3.0 m/s, Various Exit Velocities and an Exit Temperature of 388°K

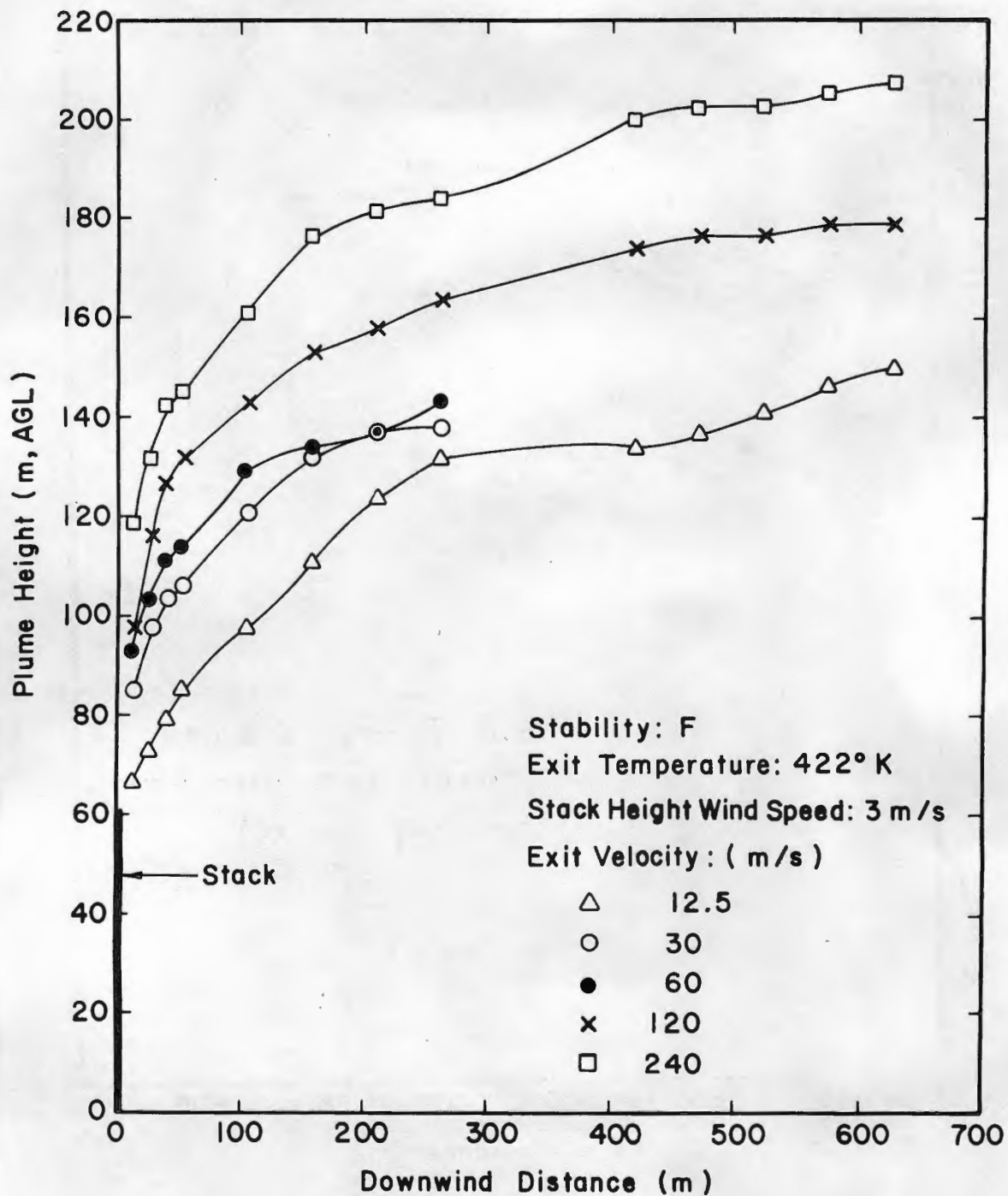


Figure 4.1-16c. Plume Centerline Trajectories for F-stability, a Stack Height Wind Speed of 3.0 m/s, Various Exit Velocities and an Exit Temperature of 422°K

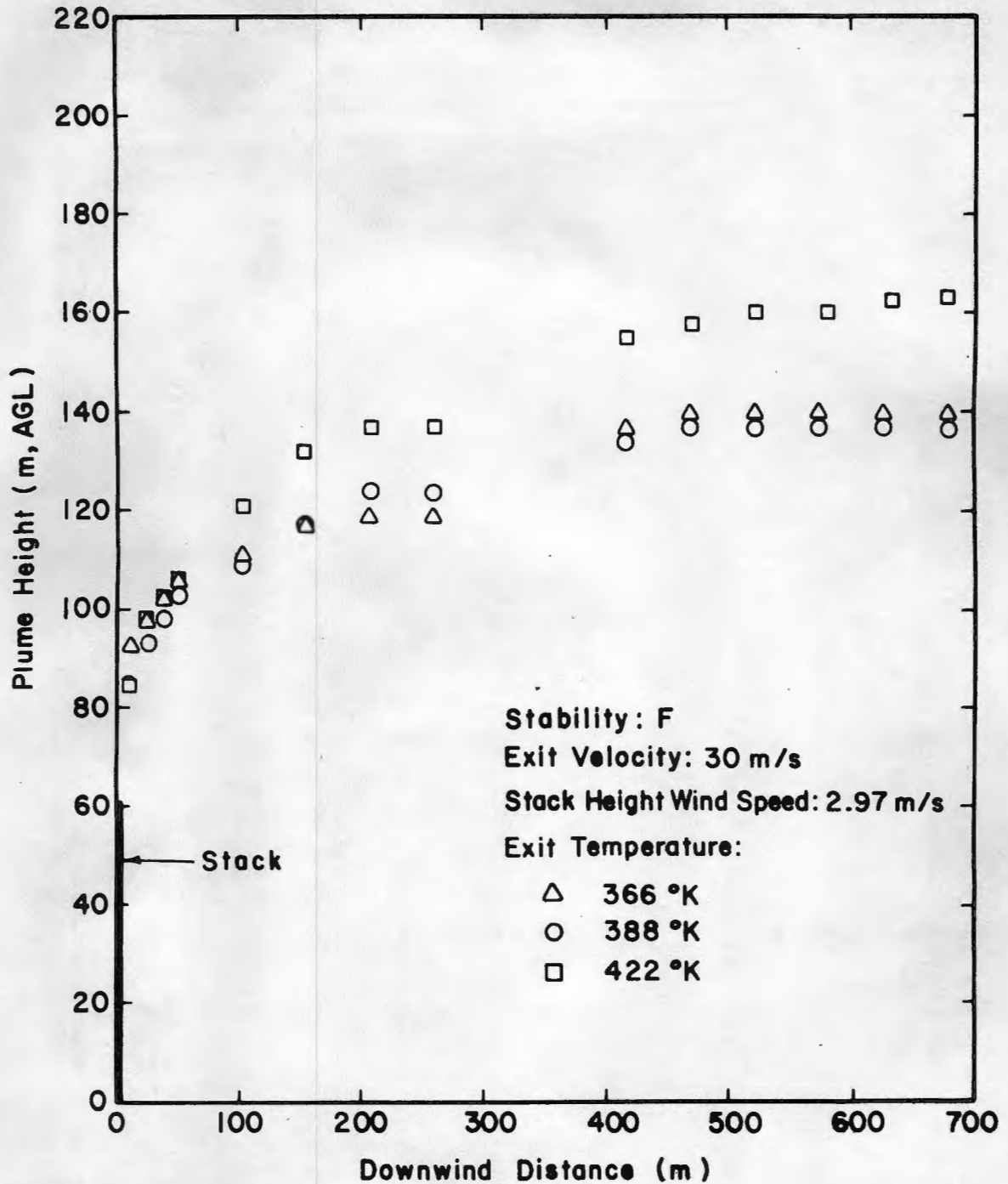


Figure 4.1-17a. Plume Centerline Trajectories for F-stability, a Stack Height Wind Speed of 3.0 m/s, Three Exit Temperatures and an Exit Velocity of 30 m/s

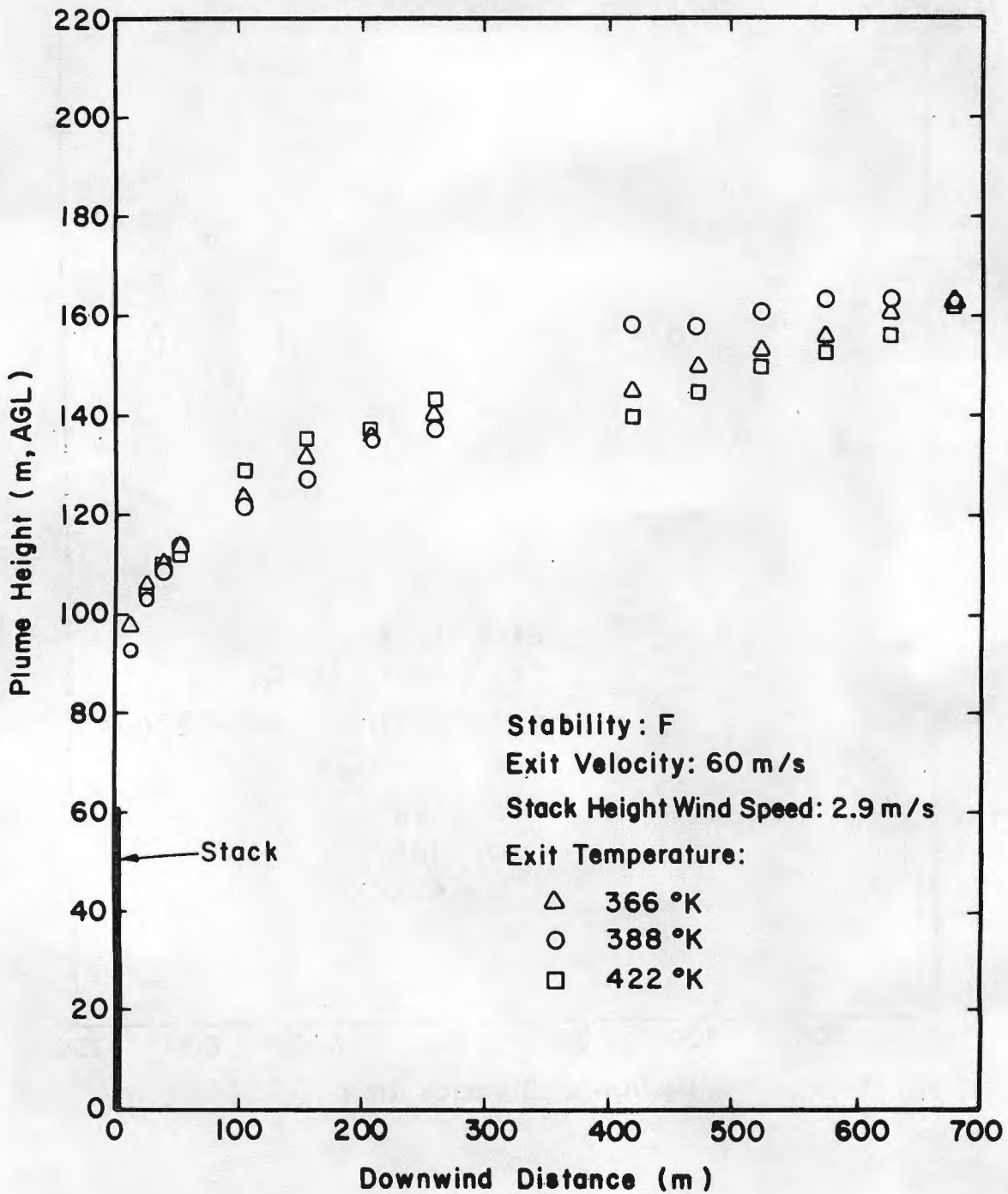


Figure 4.1-17b. Plume Centerline Trajectories for F-stability, a Stack Height Wind Speed of 3.0 m/s, Three Exit Temperatures and an Exit Velocity of 60 m/s

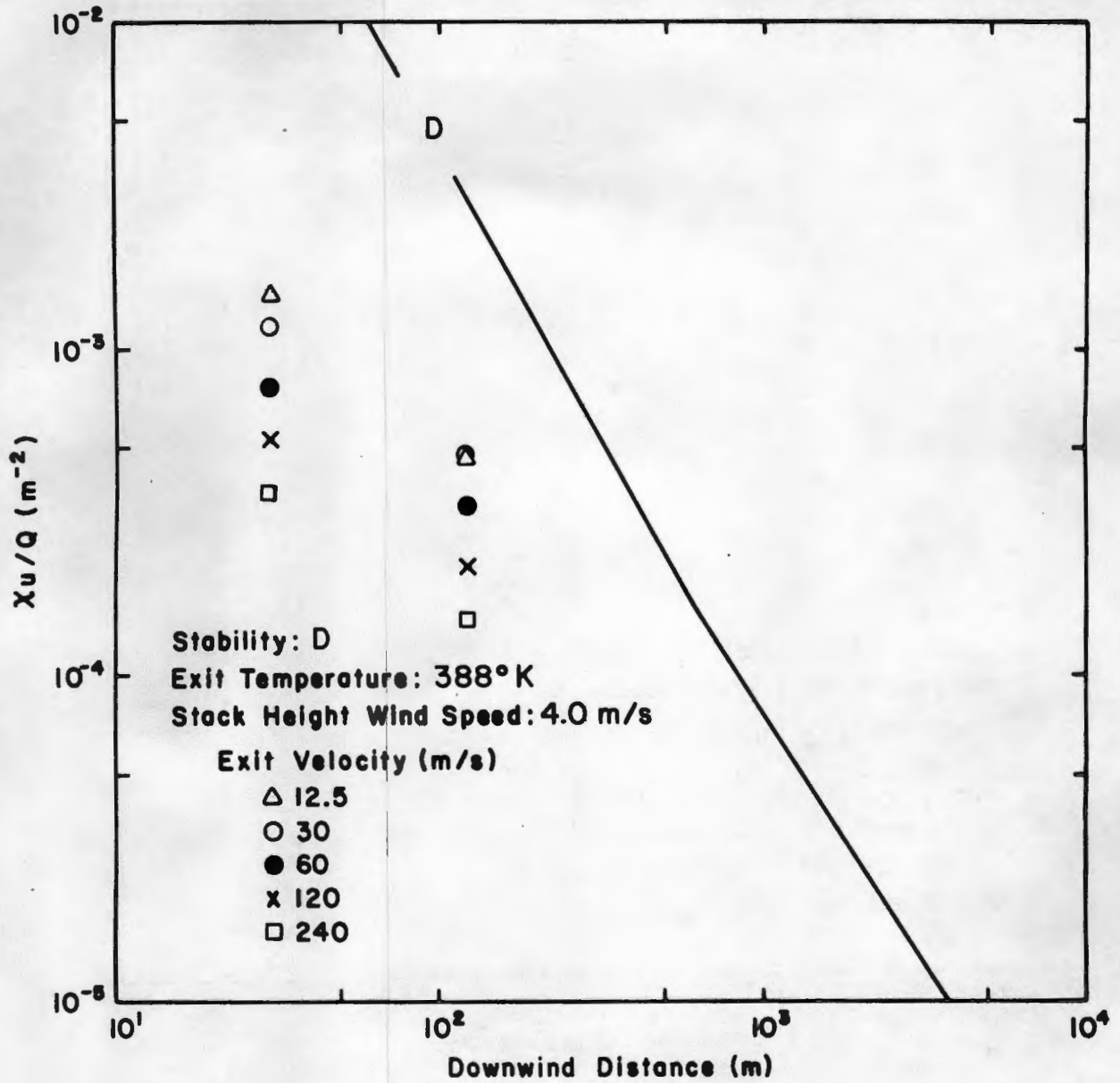


Figure 4.2-1a. Plume Dilution ($\chi u/Q$) versus Downwind Distance for D-stability, at 388°K Exit Temperature, Various Exit Speeds and a Stack Top Wind Speed of 4 m/s

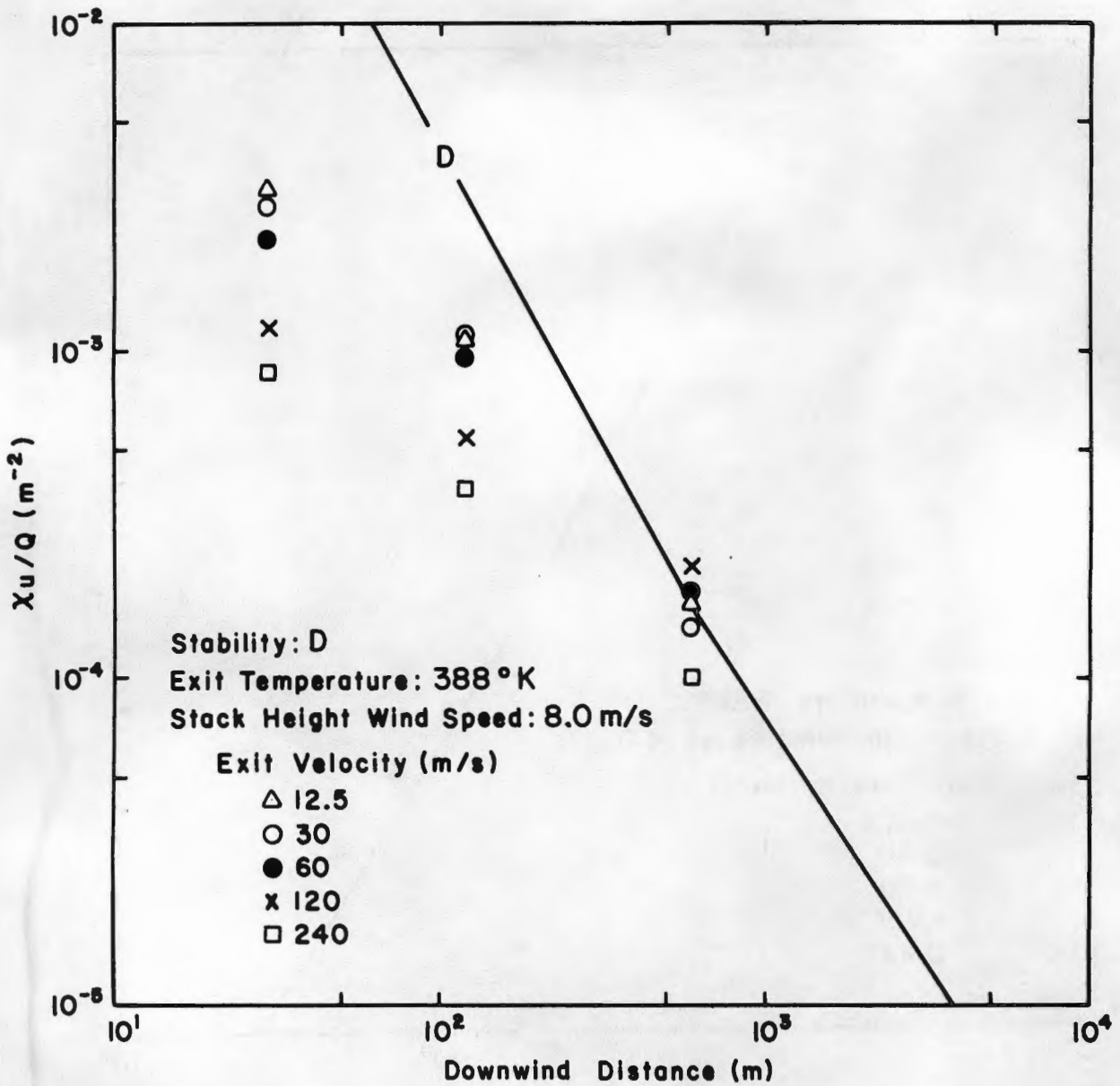


Figure 4.2-1b. Plume Dilution ($\chi u/Q$) versus Downwind Distance for D-stability, a 388°K Exit Temperature, Various Exit Speeds and a Stack Top Wind Speed of 4 m/s

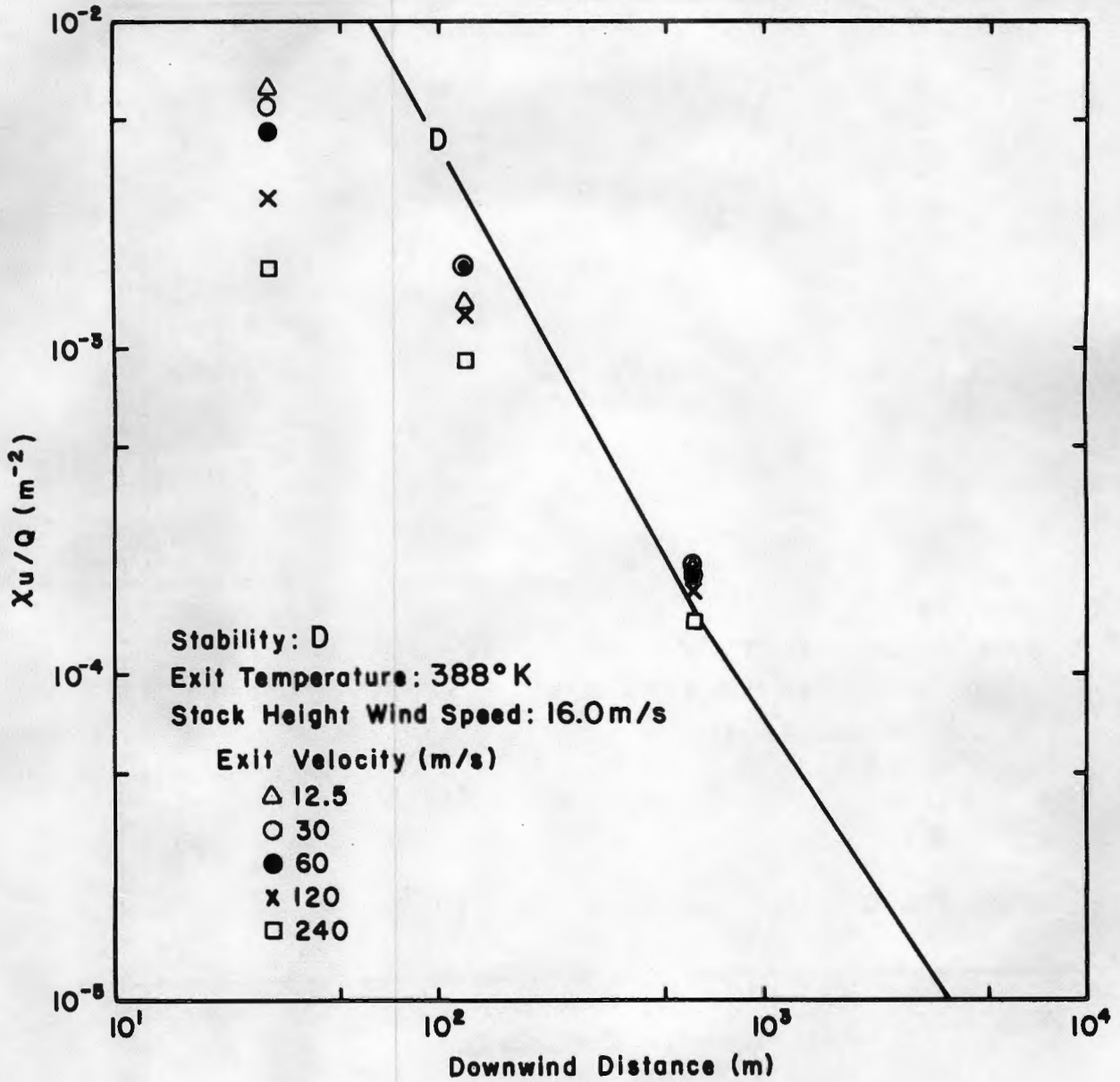


Figure 4.2-1c. Plume Dilution ($\chi u/Q$) versus Downwind Distance for D-stability, a 388°K Exit Temperature, Various Exit Speeds and a Stack Top Wind Speed of 16 m/s

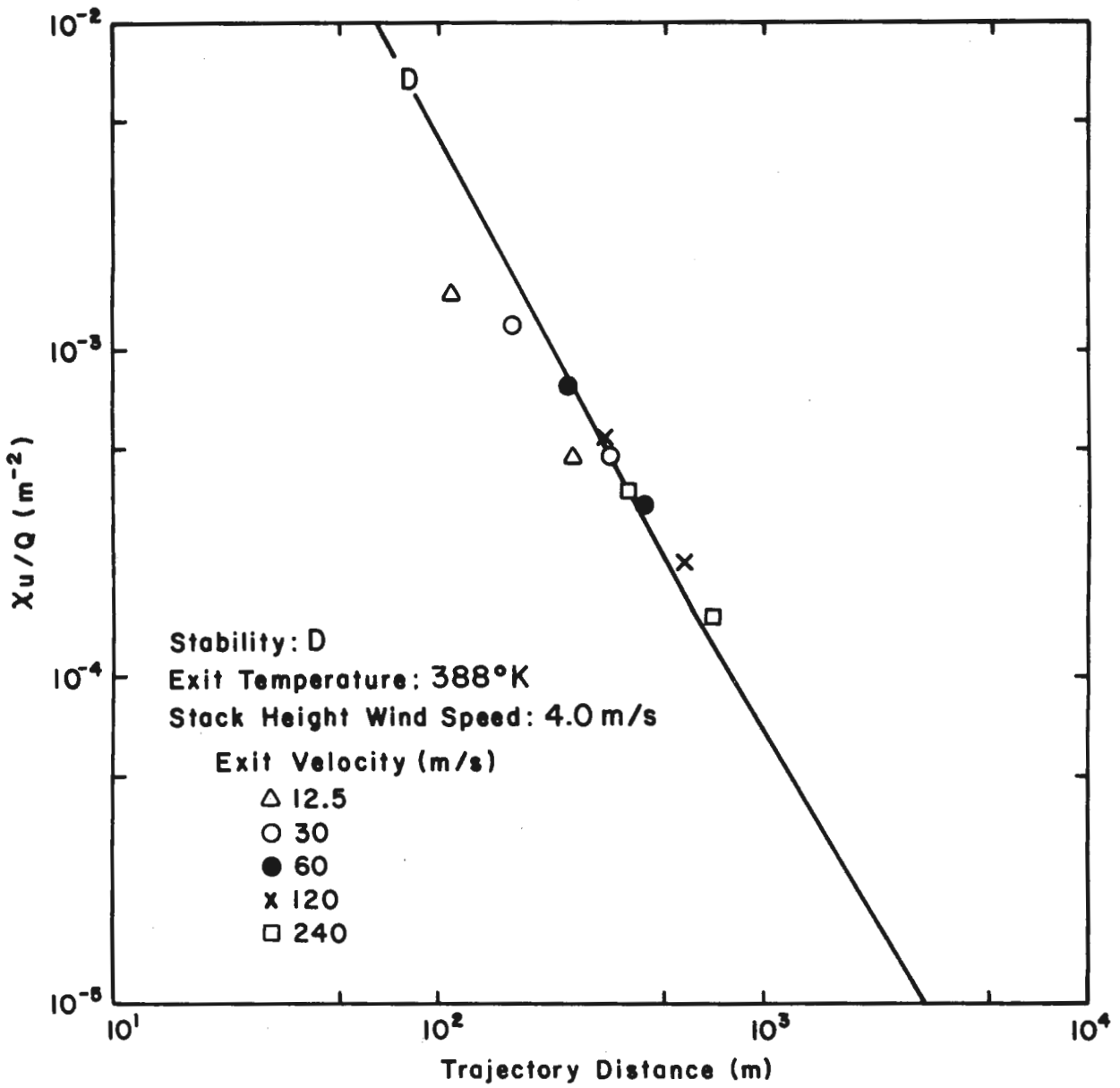


Figure 4.2-2a. Plume Dilution ($\chi u/Q$) versus Trajectory Distance for D-stability, a 388°K Exit Temperature, Various Exit Speeds and a Stack Top Wind Speed of 4 m/s

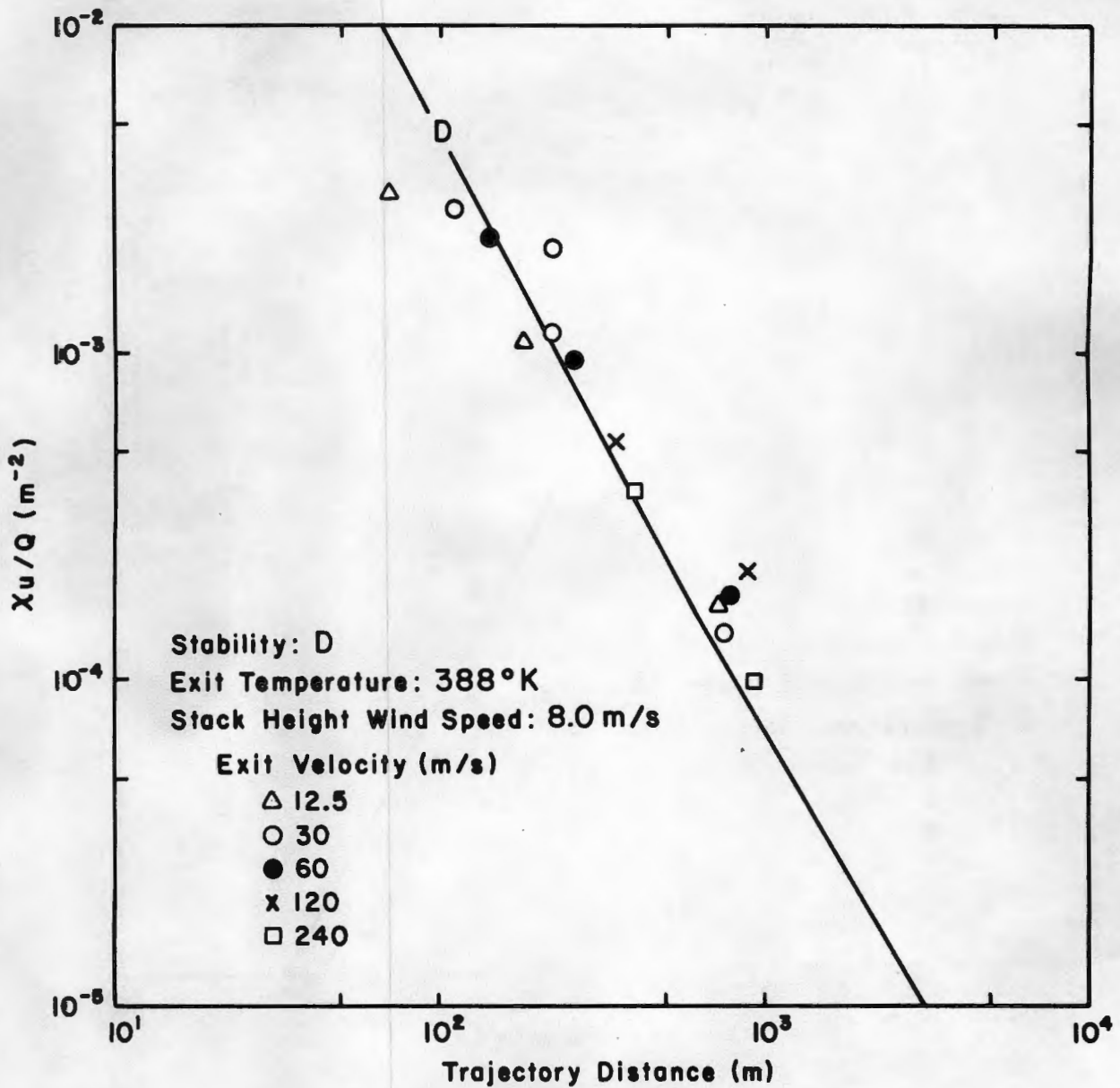


Figure 4.2-2b. Plume Dilution ($\chi u/Q$) versus Trajectory Distance for D-stability, a 388°K Exit Temperature, Various Exit Speeds and a Stack Top Wind Speed of 8 m/s

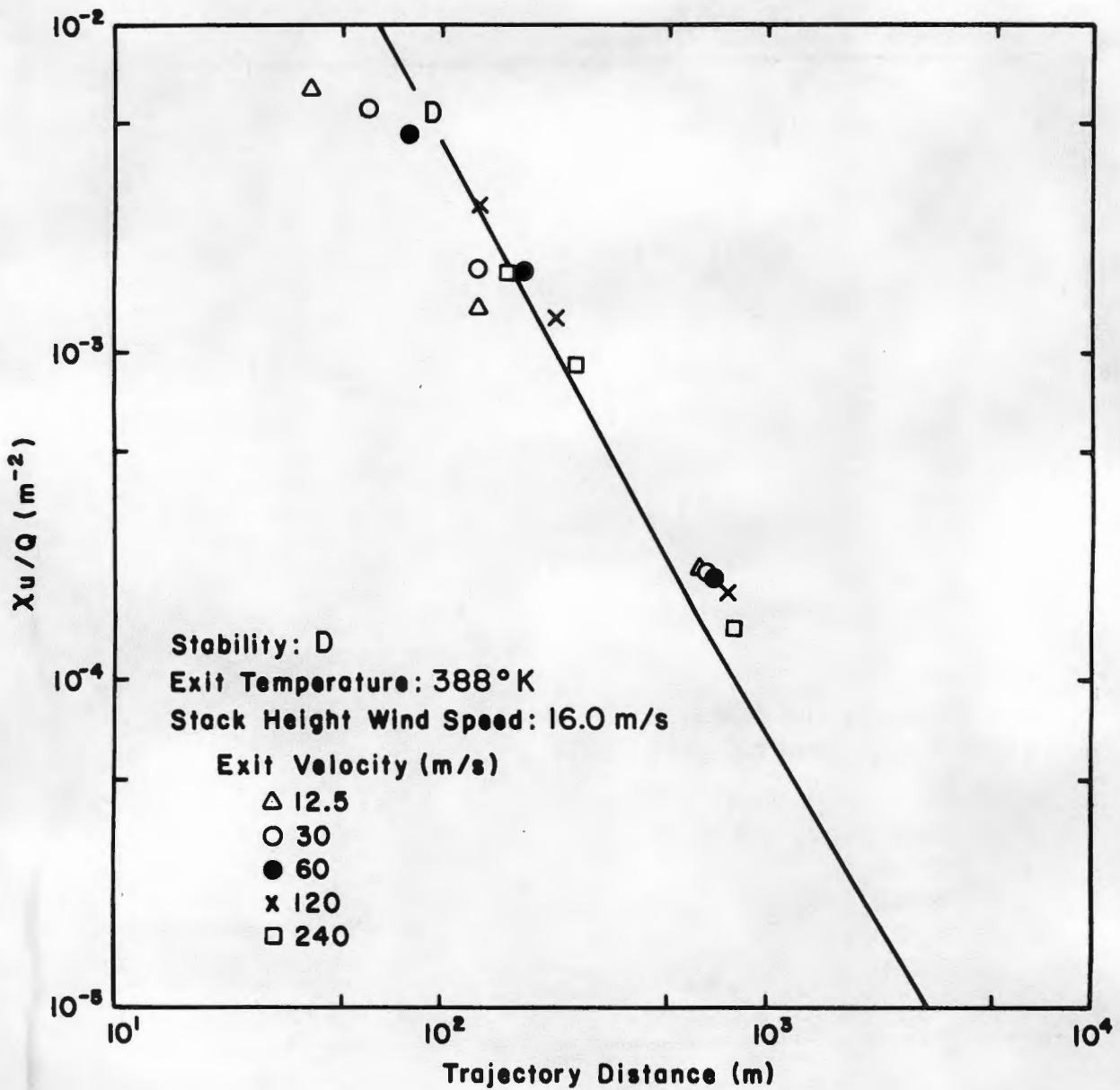


Figure 4.2-2c. Plume Dilution ($\chi u/Q$) versus Trajectory Distance for D-stability, a 388°K Exit Temperature, Various Exit Speeds and a Stack Top Wind Speed of 16 m/s

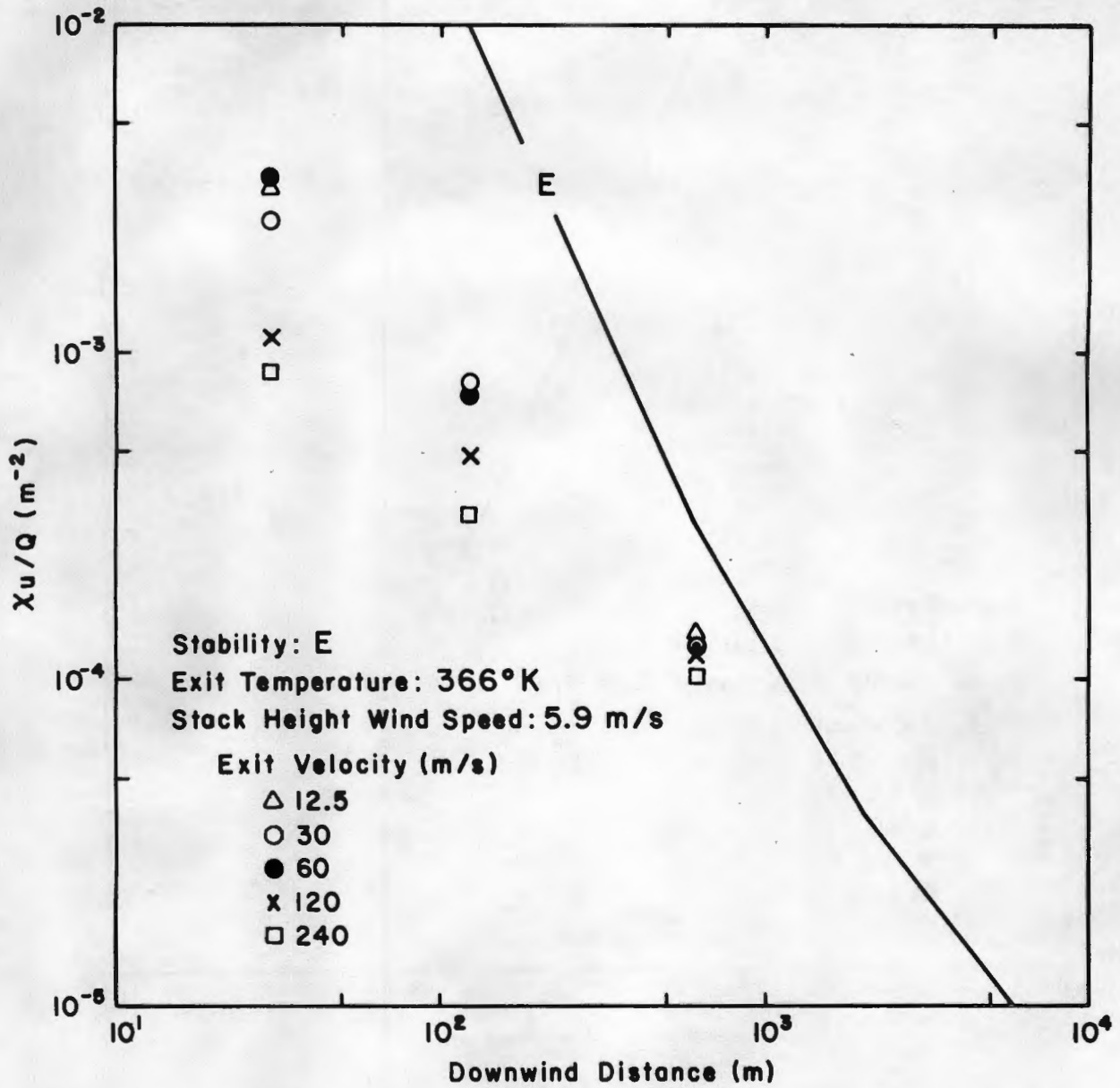


Figure 4.2-3a. Plume Dilution ($\chi u/Q$) versus Downwind Distance for E-stability, a Stack Top Wind Speed of 5.9 m/s, Various Exit Velocities and Exit Temperature of 366°K

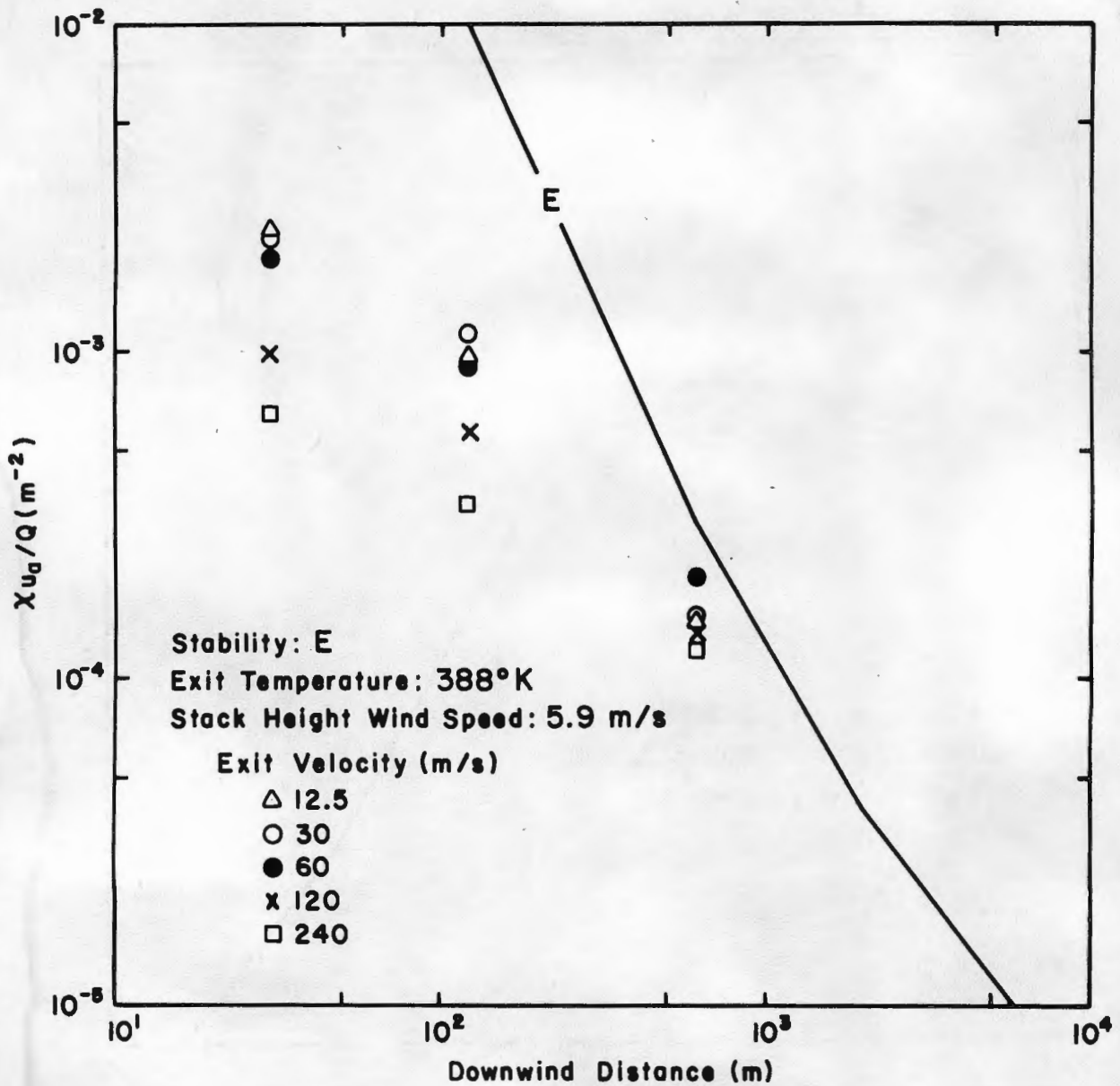


Figure 4.2-3b. Plume Dilution ($\chi u/Q$) versus Downwind Distance for $Ri = 0.57$

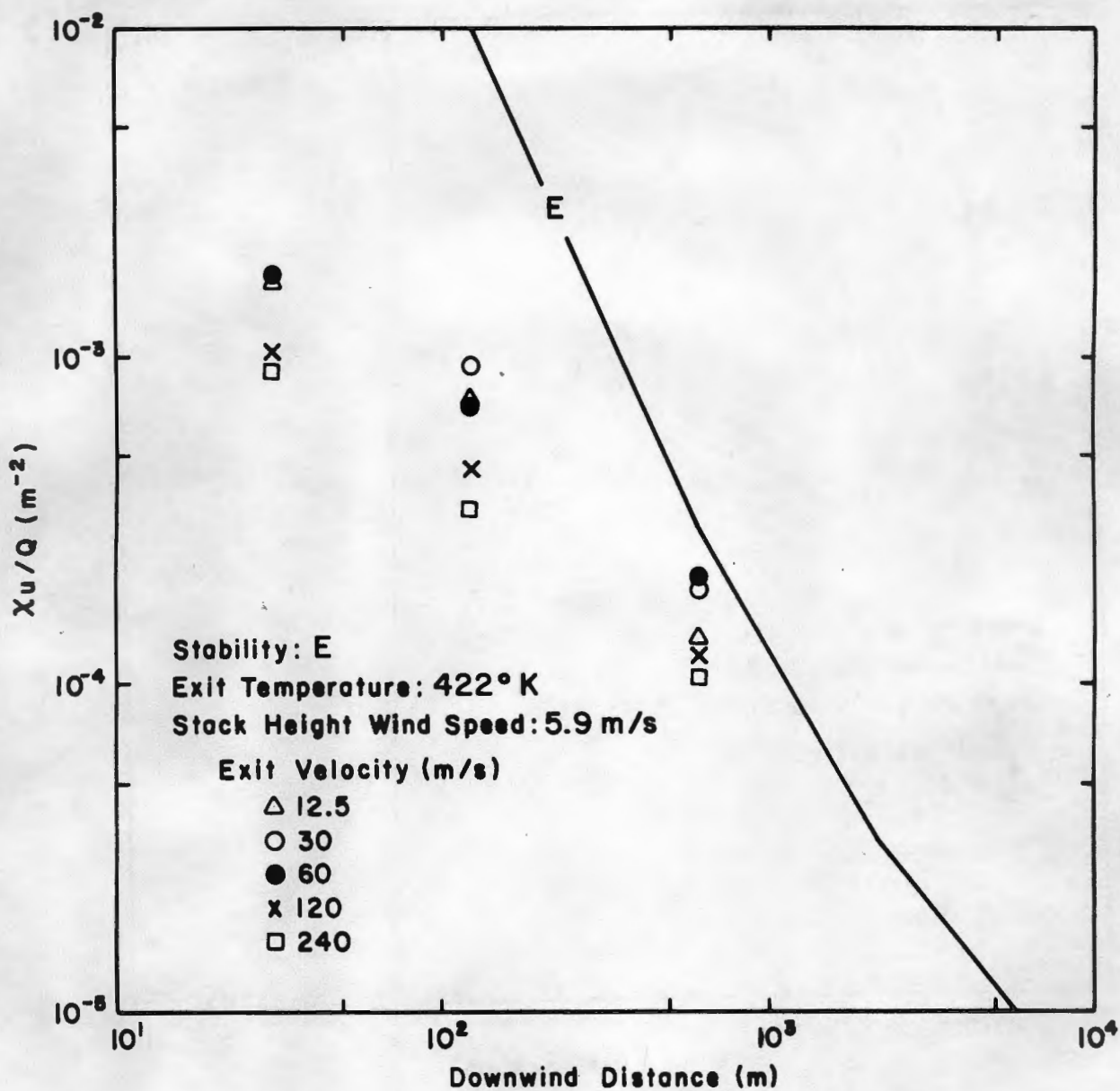


Figure 4.2-3c. Plume Dilution ($\chi u/Q$) versus Downwind Distance for E-stability, a Stack Top Wind Speed of 5.9 m/s, Various Exit Velocities and Exit Temperature of 422°K

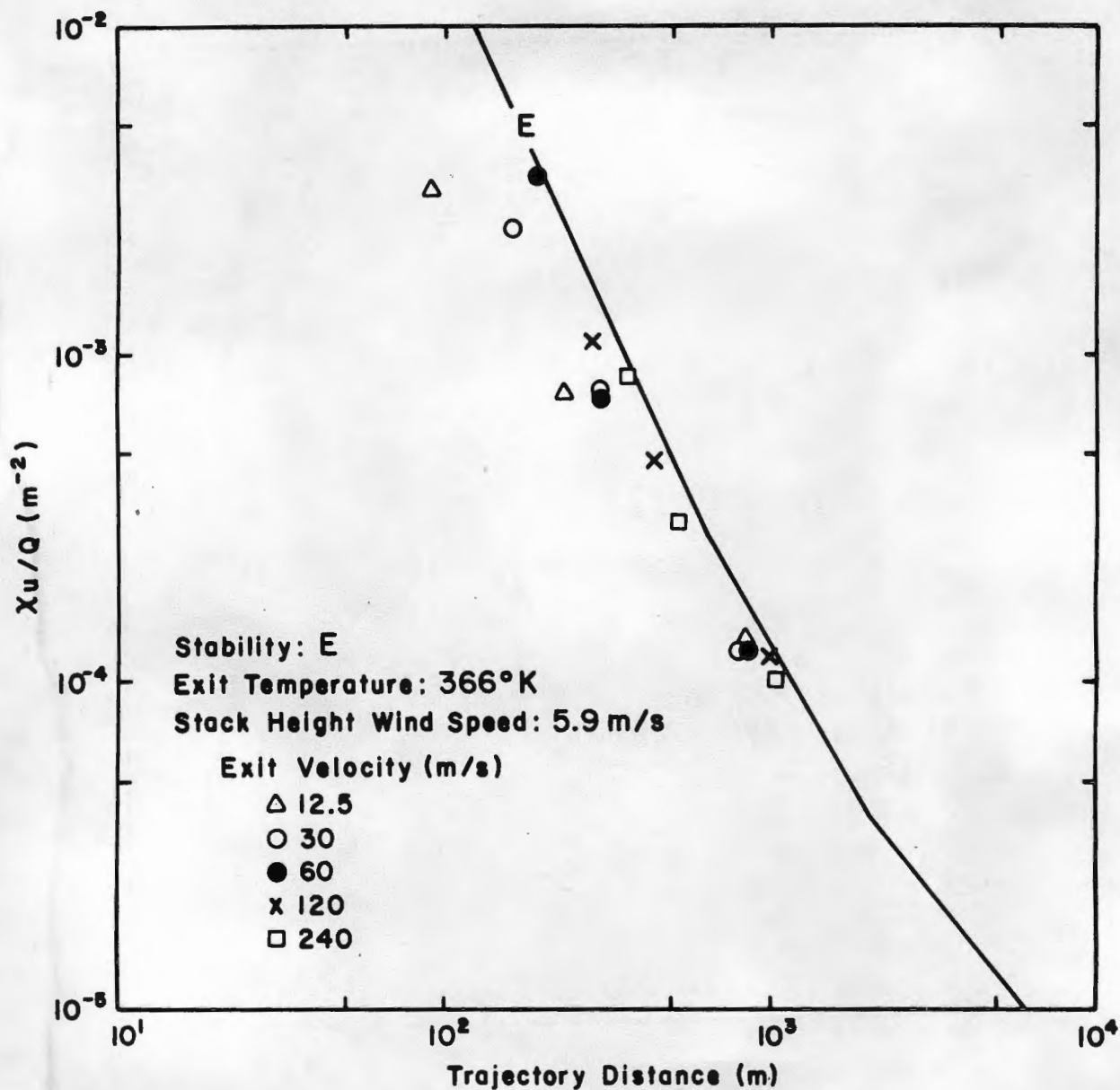


Figure 4.2-4a. Plume Dilution ($\chi u/Q$) versus Trajectory Distance for E-stability, a Stack Top Wind Speed of 5.9 m/s, Various Exit Velocities and Exit Temperature of 366°K

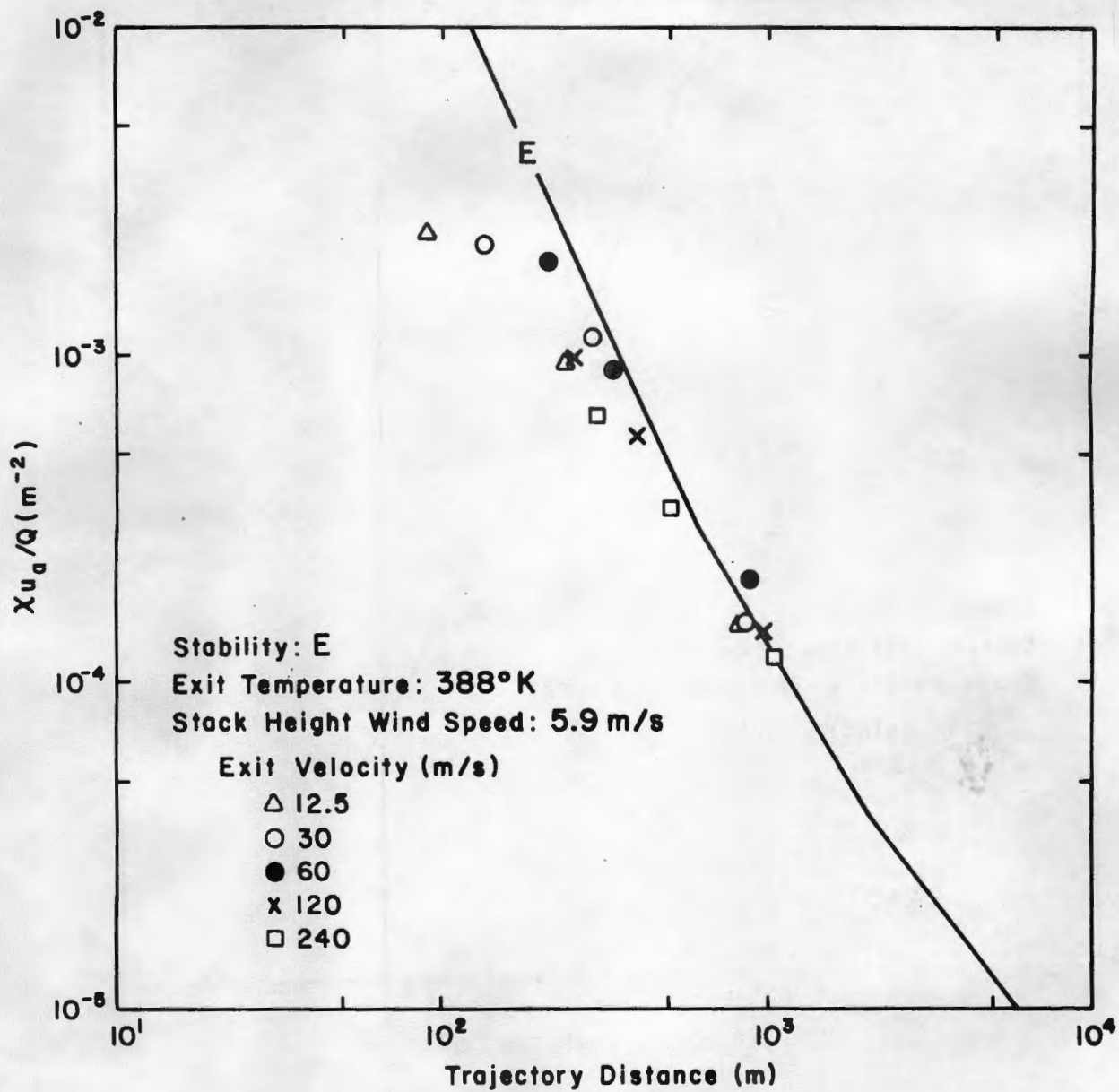


Figure 4.2-4b. Plume Dilution ($\chi u/Q$) versus Trajectory Distance for $Ri = 0.57$

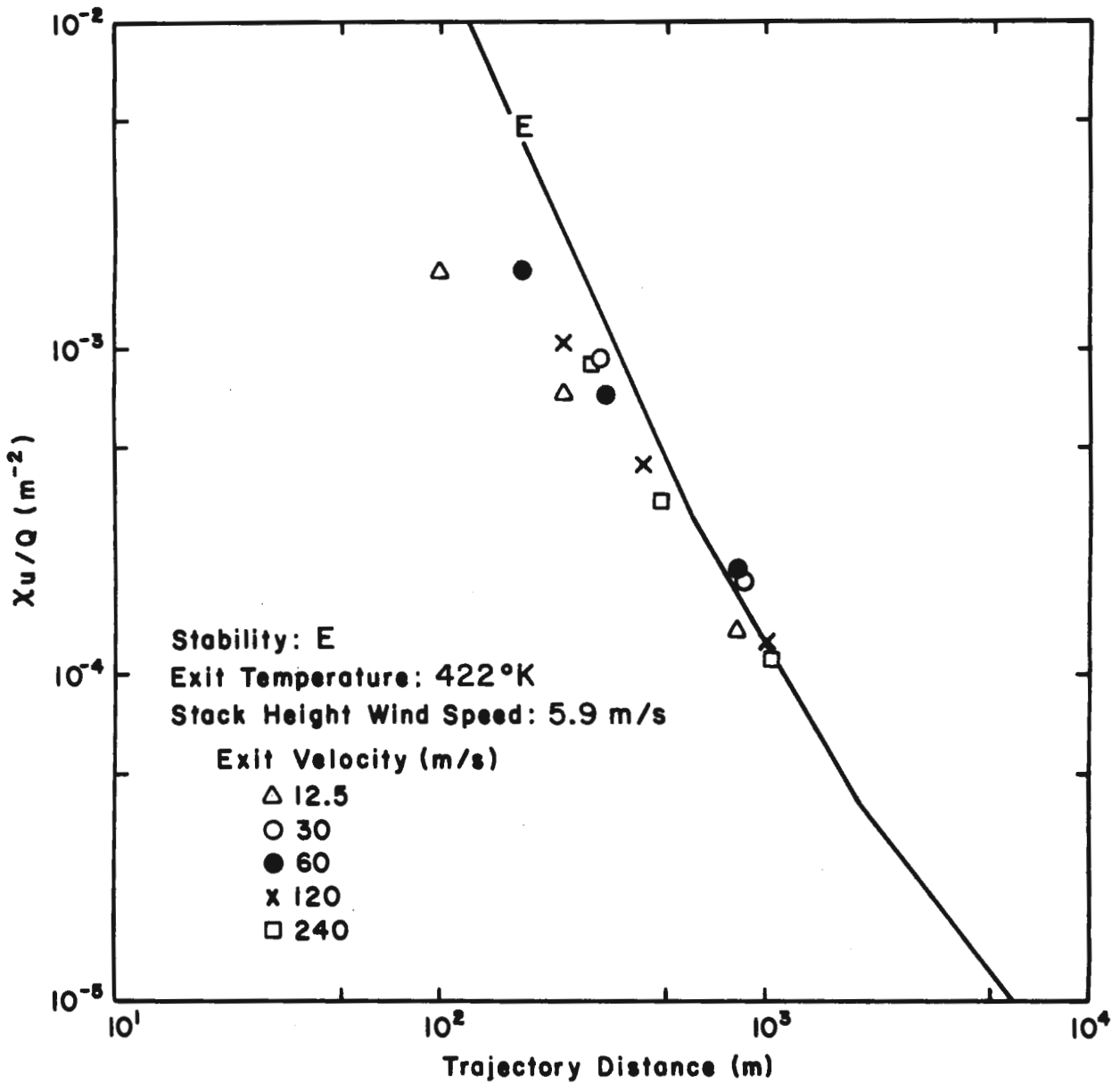


Figure 4.2-4c. Plume Dilution ($\chi u/Q$) versus Trajectory Distance for E-stability, a Stack Top Wind Speed of 5.9 m/s, Various Exit Velocities and Exit Temperature of 422°K

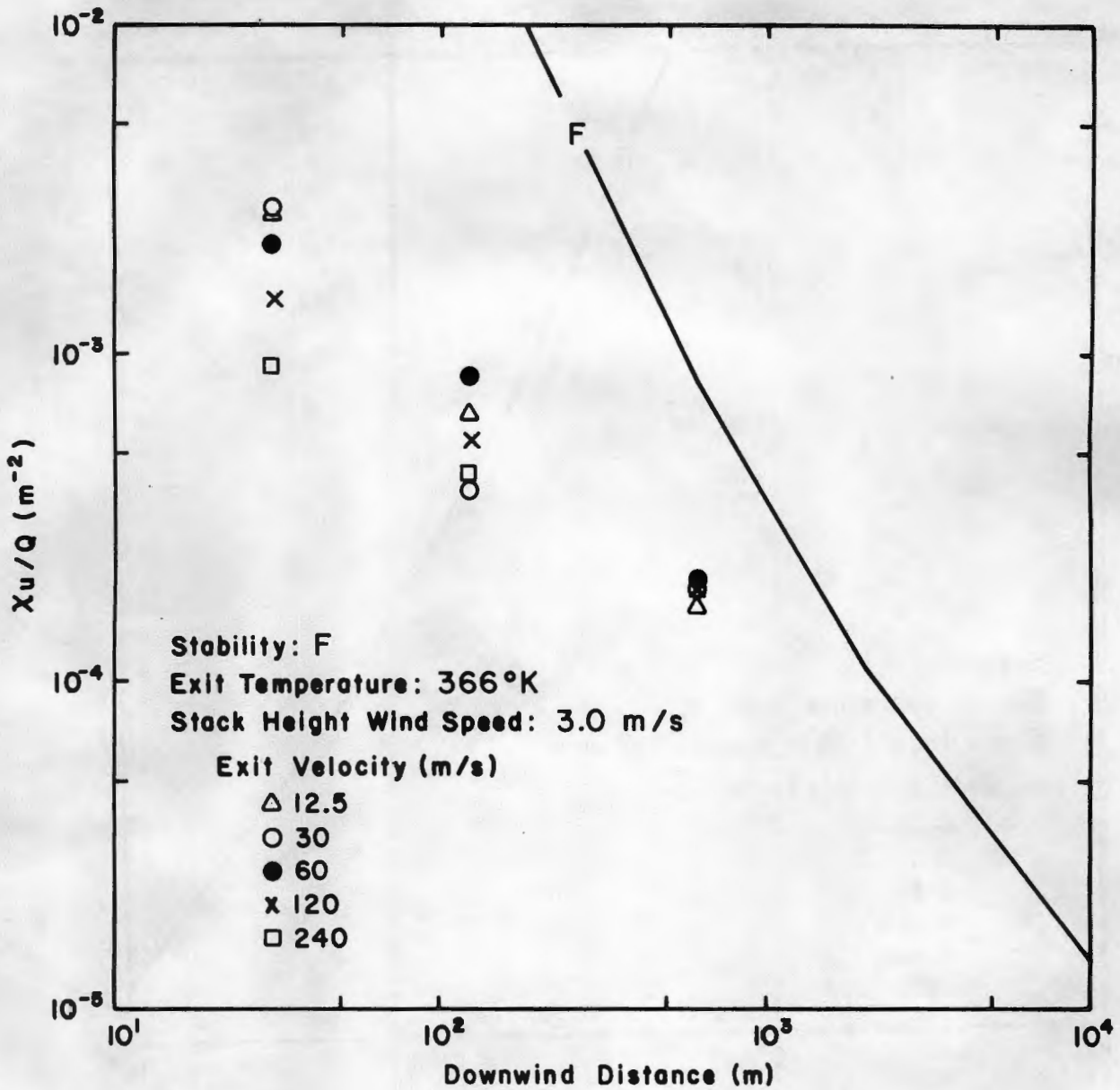


Figure 4.2-5a. Plume Dilution (xu/Q) versus Downwind Distance for F-stability, a Stack Top Wind Speed of 3.0 m/s, Various Exit Velocities and Exit Temperature of 366°K

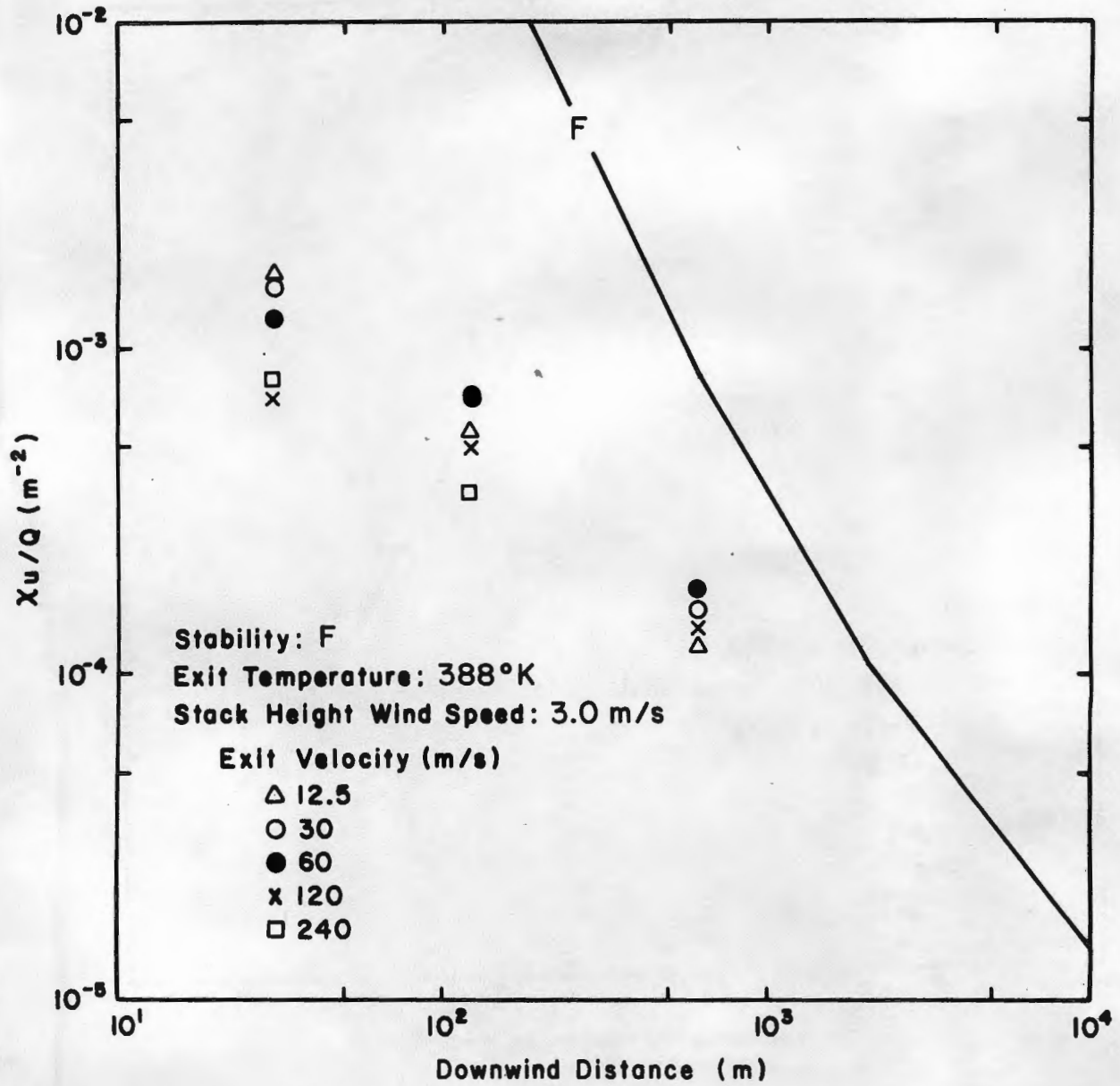


Figure 4.2-5b. Plume Dilution ($\chi u/Q$) versus Downwind Distance for F-stability, a Stack Top Wind Speed of 3.0 m/s, Various Exit Velocities and Exit Temperature of 388°K

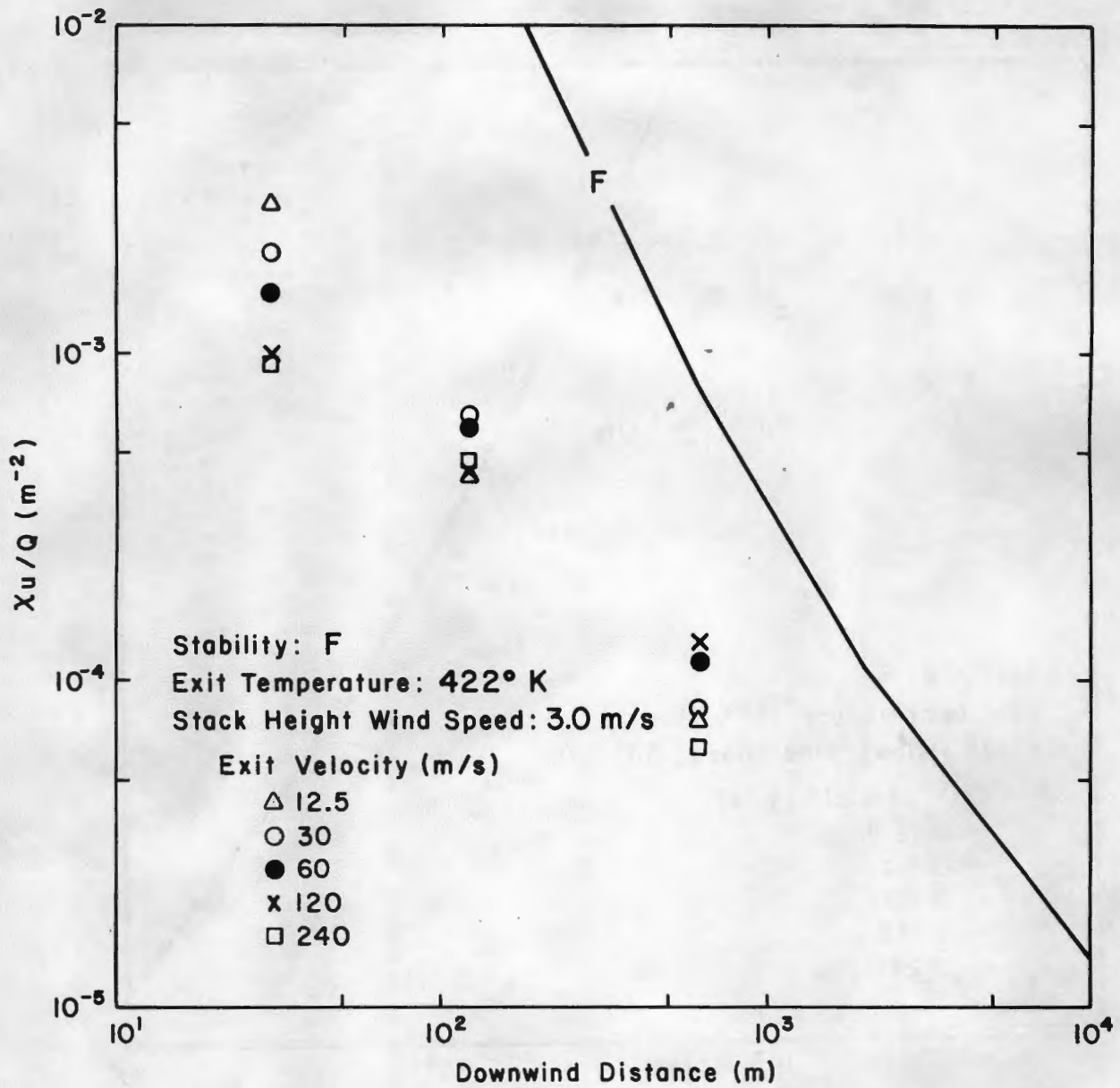


Figure 4.2-5c. Plume Dilution ($\chi u/Q$) versus Downwind Distance for F-stability, a Stack Top Wind Speed of 3.0 m/s, Various Exit Velocities and Exit Temperature of 422°K

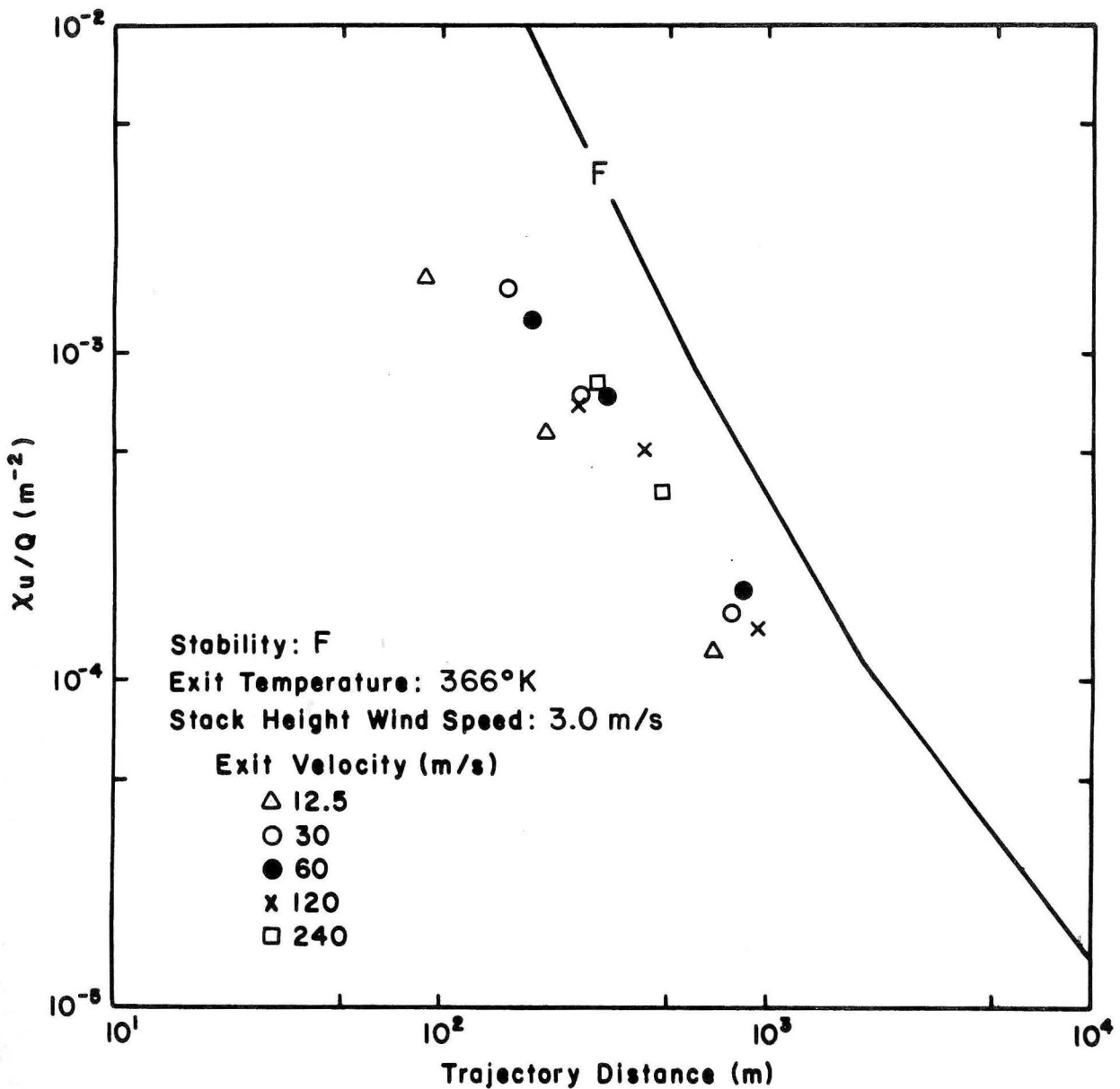


Figure 4.2-6a. Plume Dilution ($\chi u/Q$) versus Trajectory Distance for F-stability, a Stack Top Wind Speed of 3.0 m/s, Various Exit Velocities and Exit Temperature of 366°K

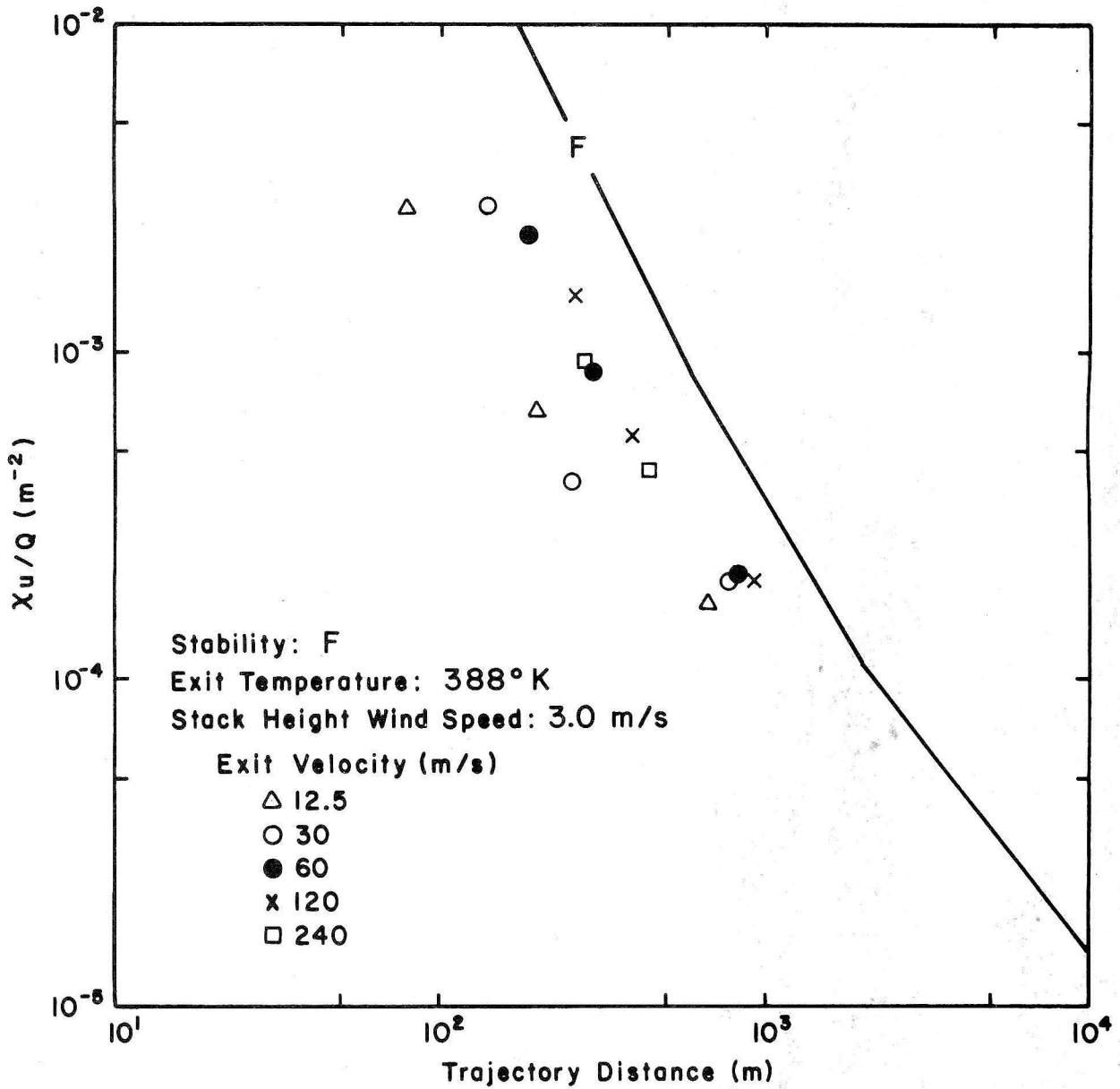


Figure 4.2-6b. Plume Dilution (X_u/Q) versus Trajectory Distance for F-stability, a Stack Top Wind Speed of 3.0 m/s, Various Exit Velocities and Exit Temperature of 388°K

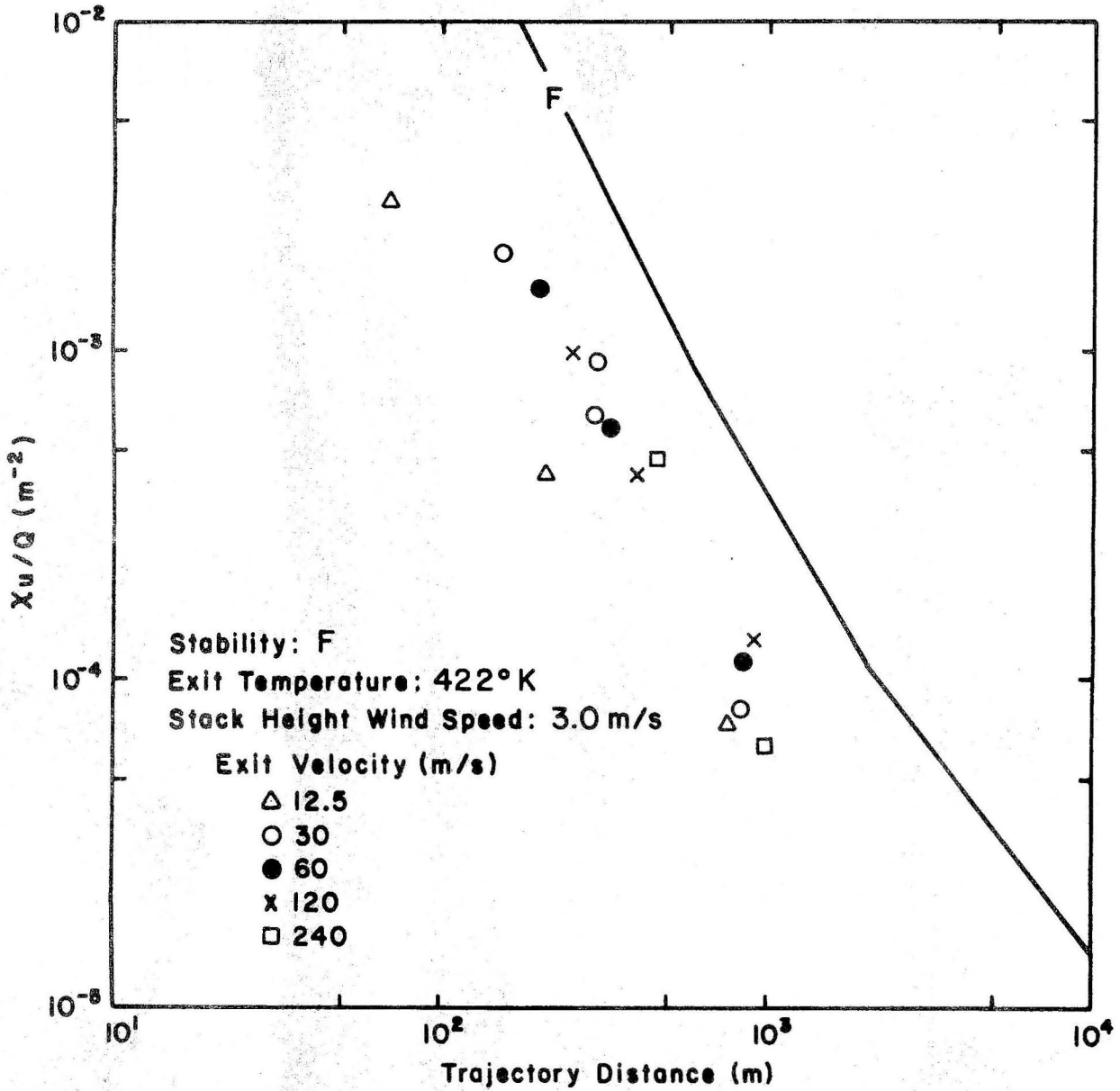


Figure 4.2-6c. Plume Dilution ($\chi u/Q$) versus Trajectory Distance for F-stability, a Stack Top Wind Speed of 3.0 m/s, Various Exit Velocities and Exit Temperature of 422°K

410000